Design Studies for Tapered Transmission Line Matching Circuits

by

Raymond Sprungle

B.E., Youngstown State University, 1997

M.S., The Ohio State University, 2008

A thesis submitted to the

Faculty of the Graduate School of the

University of Colorado in partial fulfillment

of the requirements for the degree of

Doctor of Philosophy

Department of Electrical, Computer & Energy Engineering

2023

Committee Members:

Edward Kuester, Chair

Dejan Filipović

Taylor Barton

Cody Scarborough

Michael Buck

Christopher Holloway

Sprungle, Raymond (Ph.D., Electrical Engineering)

Design Studies for Tapered Transmission Line Matching Circuits

Thesis directed by Prof. Edward Kuester

When two RF circuits or devices are connected, there is often an impedance mismatch causing unwanted reflection if not corrected. Impedance matching can be realized using lumped or distributed circuit elements. When considering transmission line segments, the length of the line with respect to the wavelength of the matched frequency is significant. It has been empirically observed [1] while designing short transmission line matching circuits, that there is a lower limit to the segment length that can provide a perfect match when constraints are placed on the possible values of characteristic impedance. However, this limit has not been extensively studied.

In this dissertation, lengths limits for zero reflection are derived. The length limits are a function of the characteristic impedances used along the non-uniform transmission line. Discontinuities along the transmission line can be used in impedance matching. A study of complex reflection using global and local reflection coefficients is developed to understand the contributions of line length, taper, and impedance discontinuities.

A special case of a nonuniform transmission line that can be used for impedance matching is the exponential line. While past studies of exponential transmission lines have concentrated on the case where there are no discontinuities at the load and input ends of the line, this dissertation allows for an infinite number of exponential lines with various discontinuities at the load and source end of the line. For this case, a closed form solution for the reflection coefficient as a function of distance along the line can be computed. A one-parameter family of designs for an exponentially tapered transmission line needed to match a given resistive load to a real input impedance is derived. Consideration is also given to frequency bandwidth, ripple height, and length of the matching section. Several of these transmission lines have been fabricated and measured.

Dedication

To Lucia, Tereza, Kristina, and Natalia.

Acknowledgements

I am deeply grateful to my advisor, Edward F. Kuester. Several of my colleagues and professors at the university suggested that I ask for his support as a PhD advisor. The recommendations all described Professor Kuester as an excellent teacher who would give me the challenge, the time, and the instruction necessary to understand each detail of the work I was completing. The recommendations were correct, he has been a wonderful teacher and also a mentor and role model. His patience with my questions and my schedule over the years have been critical to allowing me to bring this journey to completion.

I am thankful for my committee. Dejan Filipović was the first professor I met while studying at the University of Colorado; his interest and energy in electromagnetics create a desire to find out something new at every opportunity. Michael Buck has been a great help navigating my professional and academic career.

I will never be able to adequately express my gratitude to my wife, Lucia Sprungle, for her unwavering support and belief in me. When I felt I was at my strongest as a PhD student, I know my feelings of contentment were supported by her selfless desire to see me succeed. When I felt overwhelmed by the thought that the end was not in reach; she provided assistance without being asked in ways I did not expect at just the right time. Her words of encouragement have always helped and her actions to support my dream were the reinforcement that made it possible.

Special thanks to Tereza, Kristina, and Natalia. They are a part of every facet of my life. I would like to thank each of you for sacrifice of time spent with Dad. You have expressed your support for my desire to spend time working on myself as a student, and you have expressed your concern for me whenever I cut short a night of sleep to complete another task. I am grateful for each of you for the way you are as individuals and am encouraged and amazed at what kind of people you have become in the time since I started this PhD program until now. I can't wait to see what each of you does with the talents you have. Your accomplishments mean the world to me and your support brings me joy and humility.

I am grateful for my parents, Richard and Theresa Sprungle for providing me so many opportunities to be curious and insisting that I discover many new experiences. My siblings have been, and continue to be, my role models in many ways. Thank you to Robert, Richard, Ann Marie, and Ronald.

I am very thankful for friends and colleagues that supported the fabrication of the hardware necessary to complete this study. Material for the construction of the stripline circuits was provided by Rogers Corporation. Special thanks to Jeremy Chapman for material selection and procurement. The etch of the circuits was completed by Timothy May at the University of Colorado Integrated Teaching and Learning Laboratory. Test fixture and testing support was provided by Steve Clark and R. J. Smith at Ball Aerospace.

Through my course of my study I have been employed at Ball Aerospace and Battelle Memorial Institute. I am not able to thank all of the colleagues I have been proud to work alongside, but I would like to thank those helped in the completion of this thesis; Richard Higgins, Douglas Thornton, Daniel Loesch, Micah Meleski, Ray Welsh, Cesar Garcia, Claude Harton, Madeline Jekot, and Patrick Davenport.

Contents

Tables

Table

Figures

Figure

Chapter 1

Introduction

1.1 Background

When an electromagnetic wave propagates through a medium and encounters a change in the wave impedance, a reflection of some portion of the energy will occur in the direction of the wave's source. Likewise, an electromagnetic wave propagating along a transmission line that encounters a change in the characteristic impedance of the line will also have a portion of its energy reflected toward its source. It is desirable in most RF systems for these reflections of energy to be minimized. Much standard RF equipment is designed with an characteristic impedance of 50Ω or 75Ω. If components could be chosen with the desired impedance in the first place these reflections could be essentially eliminated, but this is not always possible.

When devices such as antennas, amplifiers, directional couplers, and power dividers are used, they typically have characteristic impedances that are not 50Ω or 75Ω. When these load impedances are used in a circuit with unmatched input impedance, there are several techniques by which the source and load impedances can be matched. This can be done with lumped LC elements as shown in Figure 1.1. Transmission lines can also be used to match load impedances to the source characteristic impedance. Nonuniform transmission lines use changes in impedance characteristics and abrupt changes in impedance or "jumps" to match a load to a source impedance.

There are a number of impedance matching techniques that make use of one or more lengths of transmission-line. The quarter-wave transformer (Figures 1.2 and 1.3) uses a single uniform transmission line with a characteristic impedance equal to the geometric mean of the input and

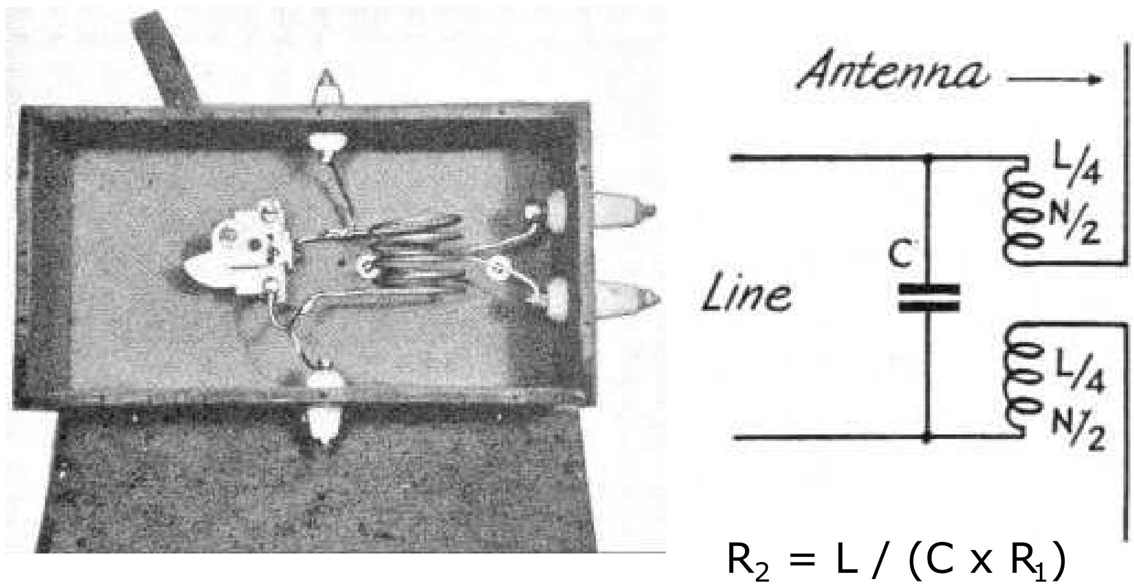

Figure 1.1: Antenna matched with lumped elements.[2]

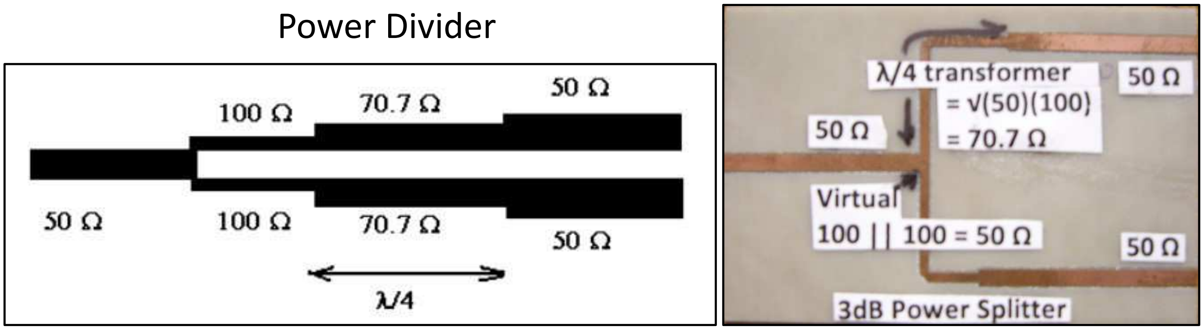

Figure 1.2: Diagram and example picture of a quarter-wave transformer.[3]

the load impedance when both are real. The two discontinuities along with the $\lambda/4$ section of transmission line create an ideal match ($\rho_0 = 0$) at a single frequency and odd harmonics over some limited bandwidth.

Many applications that do not require large bandwidth can make use of impedance transformers shorter than $\lambda/4$ which can conserve space and reduce losses [6]. Even shorter transmission lines can be realized in a similar manner by allowing larger impedance discontinuities [7], [8]. Using this technique, the total electrical length of the coupler can be made arbitrarily small, although parasitic effects are neglected that will probably limit the possible size reduction in practice. On the other hand, at times wide bandwidth, high-pass impedance transformation is needed, such as when testing semiconductors [9], or for use in wide-band amplifier circuits or RF power harvesting [10]. Such matching devices will require longer electrical lengths.

Using nonuniform transmission lines for impedance matching as shown in Figures 1.2, 1.3, and 1.4, the matching characteristics of length and bandwidth are primary considerations. In order to conserve physical space, or minimize loss, it is often favorable to use a short section of transmission line to match a load to a transmission line. It has been empirically observed [1] while designing short transmission line matching circuits, that there is a lower limit to the segment length that will provide a perfect match when constraints are placed on possible values of characteristic impedance. While circuit simulating tools are often used to help find a matching circuit, a priori knowledge of a lower length limit with respect to wavelength can be useful in determining initial

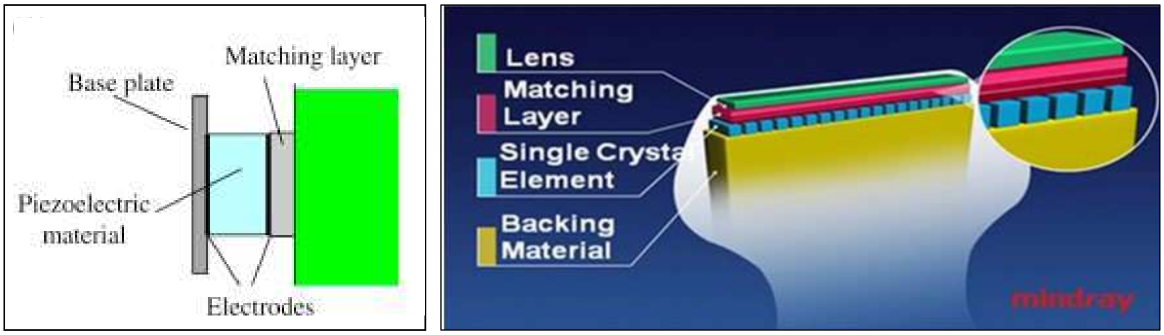

Figure 1.3: Ultrasound quarter-wave matched layer.[4][5]

Figure 1.4: Microstrip non-uniform transmission line example.[1]

design parameters. This length is studied and characterized for any non-uniform transmission line.

To study the overall length of a non-uniform transmission line for impedance transformation, it is useful to plot complex reflection coefficient with respect to position along the line. Choosing the characteristic impedance along that length of line, or a external characteristic impedance as a reference give different insights into how the matching is accomplished. These global and local reflection coefficients are defined and plotted herein.

In order to investigate the length for non-uniform line transformers, a closed form solution example would be "convenient". For the general case, this is not realizable, but for a limited number of cases, a closed form solution can be found. One of these cases is when the non-uniform line follows an exponential taper. The exponential taper is studied mathematically and using the global and local reflection coefficients to compare to the overall length limits and analyze bandwidth. The exponential study is not limited to the classical problem of the exponential transmission line, Chapters 3 and 4 will consider the effects of impedance discontinuities at each end of the line. There has been almost no study of exponential lines with such discontinuities. By allowing for these jumps in characteristic impedance at the input and load end of the taper, a wide range of solutions are available from short (narrow bandwidth) to wider bandwidth but much longer lengths. We will study the trade-offs involved as well as the effects of parasitics by comparing the circuit model with the full-wave electromagnetic solution and measured data.

1.2 Previous Work

While studying various non-uniform transmission lines, it has been observed that there is a fundamental limit to the shortest line which will transform between two impedances with zero reflection [1]. An analytical approach to finding this length limit has been studied [11] [12] and is discussed in this dissertation.

Chapter 2

Solution Methods for Reflection on a Nonuniform Line

2.1 ABCD Parameters of a lossless 2-Port Matching Network

Analysis and design of two-port networks is easily done using ABCD Parameters. Figure 2.1 shows the transmission lines and impedances around a two-port device that will be matched. ABCD parameters can be used to mathematically represent any two-port network where discrete ports can be defined in an RF circuit. Voltages and currents on the source side of a transmission line are given the notations V_S and I_S, while V_L and I_L characterize the load side of the circuit. The ABCD parameters are defined in terms of these as follows:

$$V_S = AV_L + BI_L \tag{2.1}$$

$$I_S = CV_L + DI_L \tag{2.2}$$

For reciprocal networks, the determinant of the ABCD matrix will be equal to 1. This will give an additional equation:

$$1 = AD - BC \tag{2.3}$$

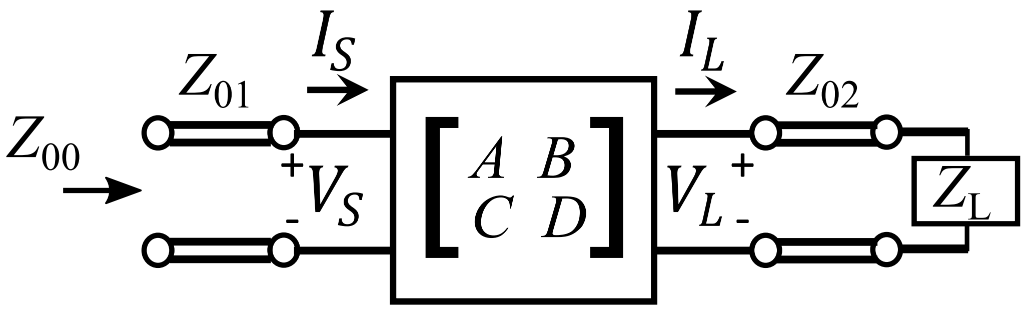

Figure 2.1: Matching network: the ABCD Matrix.

2.2 Modeling a Lossless Two-port Matching Network with ABCD Parameters

We will assume that the source and load impedances Z_{01} and Z_{02} are real. Then S_{11} for the circuit shown in Figure 2.1 is [13]:

$$S_{11} = \frac{AZ_{02} + B - CZ_{01}Z_{02} - DZ_{01}}{AZ_{02} + B + CZ_{01}Z_{02} + DZ_{01}} \tag{2.4}$$

This is true for any lossless two-port device or transmission line. The condition for no reflection at port 1 can be found by setting the numerator of (2.4) to zero:

$$0 = AZ_{02} + B - CZ_{01}Z_{02} - DZ_{01} \tag{2.5}$$

In the case of a lossless network, the parameters A and D will be real while B and C will be strictly imaginary. By separating the real and imaginary parts of (2.5), and setting each of them to 0, the following relationships are obtained:

$$0 = AZ_{02} - DZ_{01} \tag{2.6}$$

$$0 = B - CZ_{01}Z_{02} \tag{2.7}$$

For given values of Z_{01} and Z_{02}, (2.6) and (2.7) can be solved for the ABCD parameters needed to create the match. Now, (2.3) can be used to eliminate A, but three parameters, B, C, and D, remain to be determined, and only two equations are available to do so. By selecting a value for one of B, C, or D, a unique solution can be found for the other two variables. These universal relationships can then be used to determine ABCD parameter relationships for any lossless reciprocal matching network. These parameters will be used to solve for specific cases of nonuniform transmission line matching circuits.

2.3 Nonuniform Transmission Lines

The nonuniform transmission-line for the lossless line is expressed by the telegraphers' equations:

$$\frac{dV}{dx} = -j\omega L(x)I \tag{2.8}$$

$$\frac{dI}{dx} = -j\omega C(x)V \tag{2.9}$$

In equations (2.8) and (2.9), x is the spatial coordinate along the axis of the line, $L(x)$ is the inductance per unit length of the line, $C(x)$ is the capacitance per unit length and $\omega = 2\pi f$ is the angular frequency. The local characteristic impedance of the line is

$$Z_0(x) = \sqrt{\frac{L(x)}{C(x)}} \tag{2.10}$$

which we will assume to be positive and real. It can be difficult to measure, or know a priori the inductance or capacitance per unit length along a nonuniform transmission line. It is more convenient to describe these lines in terms of the local characteristic impedance Z_0. The telegraphers' equations are converted into a form defined only by Z_0, V and I by introducing a new variable τ:

$$\tau = \int_0^x \frac{dx'}{v(x')} = \int_0^x \sqrt{L(x')C(x')}dx' \tag{2.11}$$

where $v(x) = 1/\sqrt{L(x)C(x)}$ is the local wave velocity. As defined, τ has the meaning of delay time of a wave traveling between 0 and x along the line [12]. As long as $L > 0$ and $C > 0$, τ will be a monotonic increasing function of x. The telegraphers' equations (2.8) and (2.9) can now be expressed in terms of τ as

$$\frac{dV(\tau)}{d\tau} = -j\omega Z_0(\tau)I(\tau) \tag{2.12}$$

$$\frac{dI(\tau)}{d\tau} = -\frac{j\omega}{Z_0(\tau)}V(\tau) \tag{2.13}$$

This form of the telegraphers' equations can be solved without knowing the specific values of $C(x)$ and $L(x)$, but only the characteristic impedance Z_0 as a function of τ. When a transmission line is in a homogeneous medium, τ and x will vary proportionally, as in stripline construction. In microstrip lines, however, the fringing field is not contained entirely within in the dielectric. The effective dielectric constant at a point along a nonuniform microstrip transmission line is the combined impact of electromagnetic fields contained within the dielectric slab and fringing fields in the air near the trace. Wider lines have a higher percentage of their field contained within the dielectric, while thinner transmission lines will have a larger percentage of energy in fringing field outside of the dielectric. When designing and constructing circuits in a homogeneous medium like a stripline circuit, using the time delay, τ, to compute an impedance taper produces the same taper in the physical dimension x. When constructing the same circuit in a microstrip configuration, the variation in x will have to take into account the changing effective dielectric constant due to fringing fields. The circuits shown in Chapter 4 were fabricated using the homogeneous stripline configuration to simplify the computation of the tapers along the physical dimension of the nonuniform transmission line.

The current I can be eliminated from (2.12) and (2.13) by taking the derivative of (2.12) and using (2.12) and (2.13):

$$\frac{d^2V(\tau)}{d\tau^2} - 2N\frac{dV(\tau)}{d\tau} + \omega^2 V(\tau) = 0 \tag{2.14}$$

where we have defined:

$$N(\tau) = \frac{1}{2}\frac{Z_0'(\tau)}{Z_0(\tau)} \tag{2.15}$$

and $Z_0'(\tau)$ is the derivative of $Z_0(\tau)$ with respect to τ. Equation (2.14), is a second order differential equation for voltage. The quantities that vary as a function of the variable, τ, are the voltage, V, and N which is the relative rate of change of the characteristic impedance.

Often, it is the reflection coefficient that is of primary importance, so it is customary to define a local reflection coefficient [14]:

$$\Gamma(\tau) = \frac{V(\tau) - Z_0(\tau)I(\tau)}{V(\tau) + Z_0(\tau)I(\tau)} \tag{2.16}$$

This local reflection coefficient is the most commonly used reflection coefficient in the study of nonuniform transmission lines. It has been constructed in a form of the reflection coefficient that is often associated with the study of uniform transmission lines, and simplifies to that form when $Z_0(\tau) = \text{constant}$. This gives a way to analyze the varying reflection coefficient along a nonuniform line in a format that is similar to the uniform line. The local reflection coefficient makes use of voltage, $V(\tau)$, current $I(\tau)$, and characteristic impedance $Z_0(\tau)$ that all are τ dependent. The local reflection and a global reflection coefficient will be further discussed in Appendix B.

Equation (2.14) is a differential equation that describes the voltage along a nonuniform transmission lines. It is useful to study the voltages along a line for several reasons including when there is a concern of reaching a breakdown voltage. In general, however, circuit designers are interested in reflection coefficient regardless of the magnitude of the voltages that appear on the line. Having an equation for the reflection coefficient along the nonuniform line is advantageous since it will not depend on the magnitude of the voltages and currents along the line. It is therefore useful to seek a differential equation that is satisfied by $\Gamma(\tau)$. This is accomplished by differentiating (2.16) with respect to τ.

$$\frac{d\Gamma(\tau)}{d\tau} = \frac{[V(\tau) + Z_0(\tau)I(\tau)][V(\tau) - Z_0(\tau)I(\tau)]' - [V(\tau) - Z_0(\tau)I(\tau)][(V(\tau) + Z_0(\tau)I(\tau)]'}{[V(\tau) + Z_0(\tau)I(\tau)]^2} \tag{2.17}$$

This can be evaluated by using the product rule for differentiation. By breaking the equation into a minuend and subtrahend, and removing the notation for the τ dependency on all instances of V, I, and Z_0,

$$\begin{aligned}\frac{d\Gamma}{d\tau} =& \frac{VV' - VZ_0I' - VIZ_0' + Z_0IV' - Z_0IZ_0I' - Z_0IIZ_0'}{[V + Z_0I]^2} \\ & - \frac{VV' + VZ_0I' + VIZ_0' - Z_0IV' - Z_0IZ_0I' - Z_0IIZ_0'}{[V + Z_0I]^2}\end{aligned} \tag{2.18}$$

Combining all like terms and removing those that cancel:

$$\frac{d\Gamma}{d\tau} = \frac{2(-VZ_0I' - VIZ_0' + Z_0IV')}{[V + Z_0I]^2} \tag{2.19}$$

Now, using (2.12) and (2.13), to replace all of the derivatives of V and I:

$$\frac{d\Gamma}{d\tau} = \frac{2(-VZ_0(\frac{-j\omega}{Z_0})V) - VIZ_0' + Z_0I(-j\omega Z_0I)}{[V + Z_0I]^2} \tag{2.20}$$

When separating terms that contain Z_0', it is noted that only the terms not containing Z_0' contain $j\omega$:

$$\frac{d\Gamma}{d\tau} = \frac{2j\omega(V^2 - Z_0^2I^2)}{[V + Z_0I]^2} - \frac{2VIZ_0'}{[V + Z_0I]^2} \tag{2.21}$$

Considering the first term on the right hand side, we get

$$\frac{2j\omega[(V - Z_0I)(V + Z_0I)]}{[(V + Z_0I)(V + Z_0I)]} = \frac{2j\omega(V - Z_0I)}{(V + Z_0I)} = 2\omega\Gamma \tag{2.22}$$

Using the definition for $\Gamma(\tau)$ in (2.16). Thus,

$$\frac{d\Gamma}{d\tau} = 2j\omega\Gamma - \frac{2VIZ_0'}{[(V + Z_0I)(V + Z_0I)]} \tag{2.23}$$

Using the definition (2.16), the following equation is obtained for $1 - \Gamma(\tau)^2$,

$$1 - \Gamma(\tau)^2 = 1 - \frac{[V(\tau) - Z_0(\tau)I(\tau)]^2}{[V(\tau) + Z_0(\tau)I(\tau)]^2} = \frac{(V + Z_0I)^2}{(V + Z_0I)^2} - \frac{[V(\tau) - Z_0(\tau)I(\tau)]^2}{[V(\tau) + Z_0(\tau)I(\tau)]^2} = \frac{4V(\tau)Z_0(\tau)I(\tau)}{[V(\tau) + Z_0(\tau)I(\tau)]^2} \tag{2.24}$$

Additionally:

$$N(1 - \Gamma(\tau)^2) = \frac{1}{2}\frac{Z_0'}{Z_0}\frac{4V(\tau)Z_0(\tau)I(\tau)}{[V(\tau) + Z_0(\tau)I(\tau)]^2} = \frac{2Z_0'V(\tau)I(\tau)}{[V(\tau) + Z_0(\tau)I(\tau)]^2} \tag{2.25}$$

Substituting (2.25) into (2.23), the result is a differential equation in terms of $\Gamma(\tau)$ and only one other τ dependency in the impedance variable $N(\tau)$:

$$\frac{d\Gamma(\tau)}{d\tau} = 2j\omega\Gamma(\tau) - N(\tau)\left[1 - \Gamma^2(\tau)\right] \tag{2.26}$$

This differential equation for Γ is called a Riccati equation and it is satisfied by the local reflection coefficient, $\Gamma(\tau)$. The differential equations (2.14) and (2.26) are not analytically solvable for all cases.

Solutions for voltage, or reflection coefficient, along a nonuniform transmission line can be solved using a few possible techniques. These equations can be solved in a variety of ways which will be detailed in the following sections. Each of these methods can give useful results for circuit designers, but care must be taken to understand the limitations of each technique.

2.3.1 Analytical Solutions for the Exponential Line Case

In some cases a direct solution to equations 2.14 and 2.26, can be found [15]. One of the cases which is when N =constant. Recall $N(\tau) = \frac{1}{2}\frac{Z_0'(\tau)}{Z_0(\tau)}$, so the case when N =constant is the case when voltage or reflection coefficient along a nonuniform transmission line is exponential with respect to τ, time delay along the line. The exponential line will be discussed in detail. What is novel in this study of the exponential line is that since there is no limitation on the values of Z_0 at the start and end of the line for the Riccati equation to be solvable, none will be imposed. This means that the exponential lines studied herein will be allowed to have discontinuities at the source and load ends of the line.

It is desirable to solve for ABCD parameters for a transmission line to incorporate the characteristics into a network. The solution for these parameters for an exponentially tapered line will be shown. When N is a constant in equation (2.14), the solution for voltage will have the form:

$$V = V_1 e^{m_1 \tau} + V_2 e^{m_2 \tau} \tag{2.27}$$

This defines the voltage on an exponential transmission line. Finding the correct values for m_1 and m_2 will give the solution for (2.14). Substituting (2.27) into (2.14).

$$V_1 e^{m_1 \tau}(m_1^2 - 2Nm_1 + \omega)^2 + V_2 e^{m_2 \tau}(m_2^2 - 2Nm_1 + \omega)^2 = 0 \tag{2.28}$$

This must be true for any V_1, V_2, so setting $V_2 = 0$, we must have:

$$V_1 e^{m_1 \tau}(m_1^2 - 2Nm_1 + \omega)^2 = 0 \tag{2.29}$$

since:

$$\frac{dV}{d\tau} = V_1 m_1 e^{m_1 \tau}$$

and

$$\frac{d^2V}{d\tau^2} = V_1 {m_1}^2 e^{m_1 \tau}$$

Equation (2.29) can be solved using the quadratic equation

$$m = \frac{2N \pm \sqrt{4N^2 - 4\omega^2}}{2}$$

$$m = N \pm \sqrt{N^2 - \omega^2}$$

These two solutions will produce the correct values for m_1 and m_2 to be used in (2.28):

$$\begin{aligned} m_1 &= N + \sqrt{N^2 - \omega^2} \\ m_2 &= N - \sqrt{N^2 - \omega^2} \end{aligned} \tag{2.30}$$

Next, rearrange (2.12)

$$I(\tau) = \frac{\frac{dV(\tau)}{d\tau}}{-j\omega Z_0(\tau)} \tag{2.31}$$

and use the derivative of (2.27):

$$\frac{dV}{d\tau} = m_1 V_1 e^{m_1 \tau} + m_2 V_2 e^{m_2 \tau} \tag{2.32}$$

In an effort to solve for A, the open circuit condition will be applied at the load end $I(T) = 0$ when $\tau = T$. Equation (2.12) is then used to solve (2.31) when $\tau = T$.

$$I(T) = 0 = \frac{1}{j\omega Z_0(T)}(m_1 V_1 e^{m_1 T} + m_2 V_2 e^{m_2 T}) \tag{2.33}$$

In order to solve for the ratio of $V1$ to $V2$, all of the outer constant factors are eliminated, and the equation for $I(T)$ is simplified to

$$m_1 V_1 e^{m_1 T} = -m_2 V_2 e^{m_2 T} \tag{2.34}$$

Or, rearranging (2.34)

$$\frac{V_1}{V_2} = \frac{-m_2 e^{m_2 T}}{m_1 e^{m_1 T}} \tag{2.35}$$

When $I(T) = 0$, $I(L) = 0$ in (2.1), therefore

$$A = \frac{V_S}{V_L} = \frac{V_0}{V_T} = \frac{V_1 + V_2}{V_1 e^{m_1 T} + V_2 e^{m_2 T}} \tag{2.36}$$

or,

$$A = \frac{\frac{V_1}{V_2} + 1}{\frac{V_1}{V_2} e^{m_1 T} + e^{m_2 T}} = \frac{-m_2 e^{m_2 T} + m_1 e^{m_1 T}}{-m_2 e^{m_2 T} e^{m_1 T} + e^{m_2 T} m_1 e^{m_1 T}} \tag{2.37}$$

Inserting values for m_1 and m_2 from (2.30) and defining $S = \sqrt{N^2 - \omega^2}$,

$$A = \frac{-(N-S)e^{(N-S)T} + (N+S)e^{(N+S)T}}{-(N-S)e^{(N-S)T}(e^{(N+S)T}) + e^{(N-S)T}(N+S)e^{(N+S)T}}$$

$$= \frac{-Ne^{NT}e^{-ST} + Se^{NT}e^{-ST} + Ne^{NT}e^{ST} + Se^{NT}e^{ST}}{-Ne^{2NT} + Se^{2NT} + Ne^{2NT} + Se^{2NT}} \tag{2.38}$$

All terms have e^{NT}. This can be removed from all terms and numerator and denominator cancel.

$$A = \frac{-Ne^{-ST} + Se^{-ST} + Ne^{ST} + Se^{ST}}{-Ne^{NT} + Se^{NT} + Ne^{NT} + Se^{NT}} = \frac{N(e^{ST} - e^{-ST}) + S(e^{ST} + e^{-ST})}{2Se^{NT}} \tag{2.39}$$

The terms in parenthesis in 2.39 can be expressed in terms of sinh and cosh

$$A = \frac{N(2\sinh ST) + S(2\cosh ST)}{2Se^{NT}} \tag{2.40}$$

$$A = \frac{e^{-NT}}{S}(N\sinh ST + S\cosh ST) \tag{2.41}$$

This is the solution for A in the ABCD matrix for all exponential lines. B, C, and D have been found by a number of authors using similar techniques, e. g., [16, 17]. For parameter definitions as used in (3.1), these can be expressed as:

$$\begin{aligned} B &= j\omega \frac{Ke^{NT}}{S}(\sinh ST) \\ C &= j\omega \frac{e^{-NT}}{SK}(\sinh ST) \\ D &= \frac{e^{NT}}{S}(S\cosh ST - N\sinh ST) \end{aligned} \tag{2.42}$$

where

$$S = \sqrt{N^2 - \omega^2} \tag{2.43}$$

The characteristics of the ABCD matrix describe completely the parameters for an exponential line regardless of the impedances of the connecting lines or loads. This means that exponential lines with discontinuities at the source or load end can be investigated using the ABCD technique. The study of these designs is described in Chapter 3.

2.3.2 Numerical Solution: Runge-Kutta

In most cases, it is not possible to write down an analytical solution for 2.14. One option is to solve it using a numerical solution based, for example, on the Runge-Kutta method[18]. The accuracy of this solution will be limited by computational capabilities, and the any possible round-off error associated with the significant figures used. In general, this method can be used to obtain very accurate results. The Runge-Kutta method is an iterative stepping method to solve a first-order differential equation. In this case it will be used to solve the reflections along a transmission line as defined in (2.14). The principal of the Runge-Kutta method approximates $\Gamma'(\tau)$ by a finite difference $\frac{\Gamma(\tau+\Delta\tau)-\Gamma(\tau)}{\Delta\tau}$. Runge-Kutta improves on this by choosing weighting points to reduce error. The most commonly used Runge-Kutta Method uses information from four data points along an interval to iteratively solve for the function at the next point[18]. This is commonly abbreviated RK4.

The Runge-Kutta method can be used to solve for reflection coefficient in any two-port transmission line. For illustrative purposes, the method has been applied to an exponential line which has been solved analytically. Figure 2.2 shows the case of an exponential transmission line

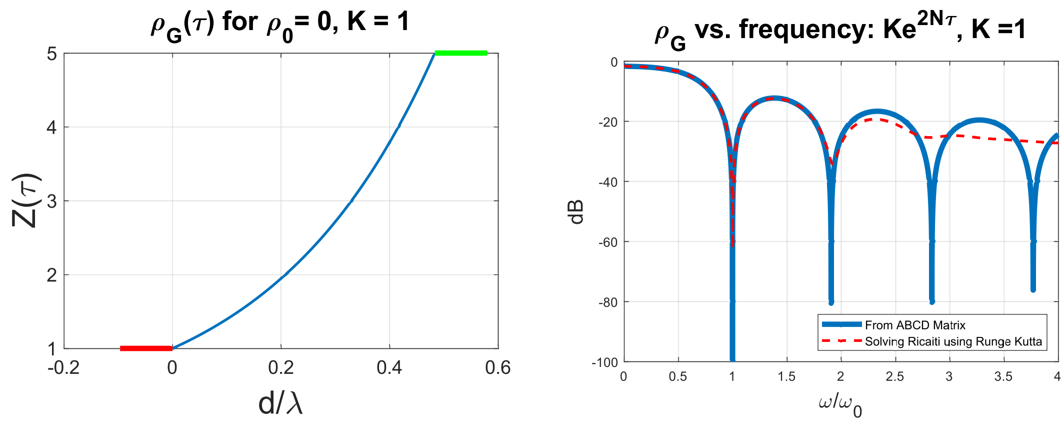

Figure 2.2: Exponential Taper Solution: Analytical vs Runge-Kutta (RK4) with 10 discrete steps.

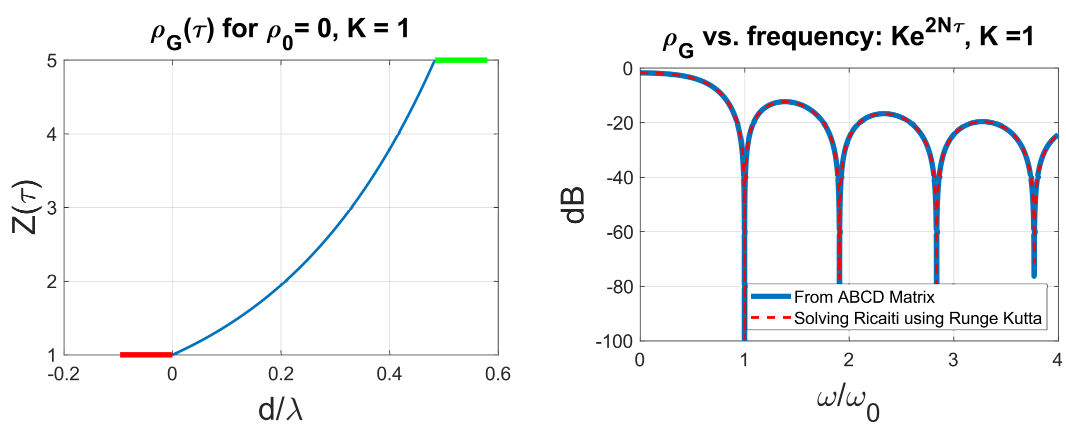

Figure 2.3: Exponential Taper Solution: Analytical vs Runge-Kutta (RK4) with 50 discrete steps.

with no discontinuities and a 10:1 impedance ratio solved using RK4 with only 10 discrete steps along the length of the line. The results are then converted into a frequency response which aligns well through the design frequency ($\omega = \omega_0$), but begins to show errors at higher frequencies. Figure 2.3 shows the same solution using RK4, but witn 50 steps used along the transmission line. This result has very little error in the frequency response at all frequencies up to four times the design frequency.

2.3.3 WKB Approximate Solution

An alternative method treating nonuniform lines analytically is what we will call the WKB approximation, though it is more properly attributed to Rayleigh, Bolinder, and Bremmer [19],[20], [21], [22], [23]. It has been used in the design of gradual-taper matching sections, e. g. in [24], [25], [26]. It consists in neglecting the term $\Gamma^2(\tau)$ compared to 1 on the right side of (2.26), so that we have approximately

$$\Gamma(\tau) \simeq \Gamma(\tau_0)e^{2j\omega(\tau-\tau_0)} - \int_{\tau_0}^{\tau} N(\tau')e^{2j\omega(\tau-\tau')}\, d\tau' \tag{2.44}$$

The WKB approximation gives the most accurate results when the taper rate $N(\tau)$ is small compared to ω—it can be viewed either as a high-frequency or gentle-taper approximation. The errors for the WKB solution will be at largest at lower frequencies or for nonuniform line segments that are relatively short compared to a wavelength.

In Figure 2.4, the exponential taper with no discontinuities at the source and load end is displayed and shows a comparison of the frequency response of the circuit computed using equation (2.26) and (2.44). Frequencies $\omega/\omega_0 > 2$ have good agreement with deviations of 0.2 dB in the areas of response near -20 dB. For frequencies $\omega/\omega_0 < 2$ there is a significant deviation when using WKB for a 10:1 impedance transformation. At the lowest frequencies near $\omega/\omega_0 = 0$, the WKB response even exceeds 0 dB which is a physically unrealizable condition for a passive circuit. The WKB approximation solutions for nonuniform lines exhibit several characteristics that can be seen in Figure 2.4. First, at the lowest frequencies, the reflection coefficient is computed to have a value $\Gamma > 1$, or , $\Gamma >$ 0dB. This violates passivity for passive nonuniform transmission lines.

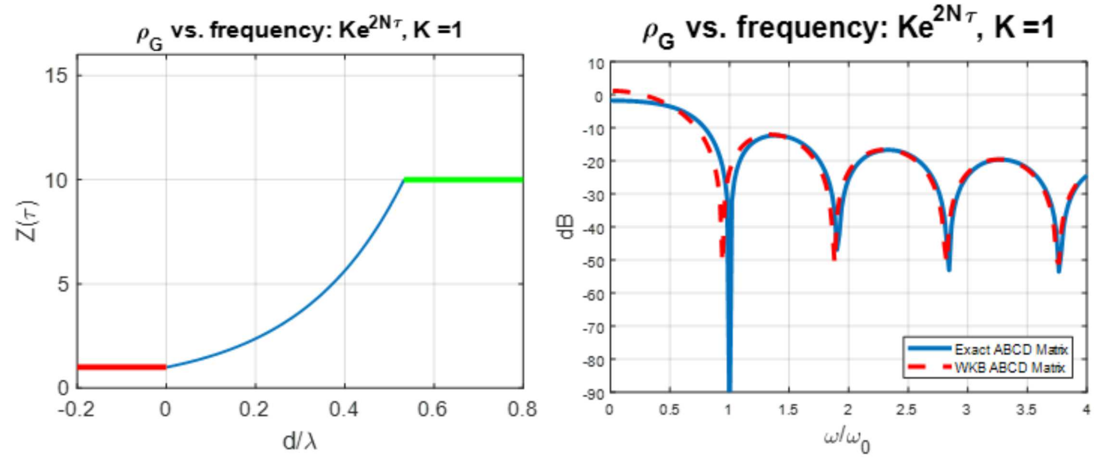

Figure 2.4: Exponential Taper Solution: Analytical vs WKB.

The frequency at which the reflection shows the deepest null, or lowest reflection, is lower than the design frequency for the match due to the approximation. In fact, all frequencies are shifted slightly lower with the most dramatic shifting at lower frequencies. At higher frequencies, the WKB results track closely to the analytical solution.

2.3.4 ABCD as a Power Series

An additional option for solving equation (2.14) is to use a power series expansion of the ABCD matrix. A section of lossless nonuniform transmission line between $\tau = 0$ and an arbitrary point τ can be described in terms of chain parameters through the equation

$$\begin{bmatrix} V(0) \\ I(0) \end{bmatrix} = \begin{bmatrix} A(\tau) & B(\tau) \\ C(\tau) & D(\tau) \end{bmatrix} \begin{bmatrix} V(\tau) \\ I(\tau) \end{bmatrix} \tag{2.45}$$

(see [12] and references therein).

By reciprocity ($AD - BC = 1$),this relationship can be rewritten as

$$\begin{bmatrix} V(\tau) \\ I(\tau) \end{bmatrix} = \begin{bmatrix} D(\tau) & -B(\tau) \\ -C(\tau) & A(\tau) \end{bmatrix} \begin{bmatrix} V(0) \\ I(0) \end{bmatrix} \tag{2.46}$$

and the initial conditions require that $A(0) = D(0) = 1$ and $B(0) = C(0) = 0$.

Inserting (2.46) into the telegrapher's equations (2.12) (2.13) and requiring the result to be true for any values of $V(0)$ and $I(0)$ gives two decoupled sets of differential equations

$$\frac{d}{d\tau}B(\tau) = j\omega Z_0(\tau)A(\tau); \qquad \frac{d}{d\tau}A(\tau) = \frac{j\omega}{Z_0(\tau)}B(\tau) \tag{2.47}$$

$$\frac{d}{d\tau}D(\tau) = j\omega Z_0(\tau)C(\tau); \qquad \frac{d}{d\tau}C(\tau) = \frac{j\omega}{Z_0(\tau)}D(\tau) \tag{2.48}$$

which are identical except for the fact that the initial conditions are different. Here,

$$Z_0 = \sqrt{\frac{L}{C}}$$

is the τ-dependent characteristic impedance of the nonuniform line. For lossless structures, Z_0 is real and positive; it may have step discontinuities, but practical considerations dictate that it must be bounded away from 0 and ∞. It is reasonable to assume that $Z_0(\tau)$ and $1/Z_0(\tau)$ are integrable functions.

The solutions to these equations can be expressed as power series in $j\omega$ [12]. These series are essentially those obtained by Peano's method of successive approximations [27, 28]. Writing

$$\begin{aligned}
A(\tau) &= A_0(\tau) + (j\omega)^2 A_1(\tau) + (j\omega)^4 A_2(\tau) + \dots \\
B(\tau) &= (j\omega) B_0(\tau) + (j\omega)^3 B_1(\tau) + (j\omega)^5 B_2(\tau) + \dots \\
C(\tau) &= (j\omega) C_0(\tau) + (j\omega)^3 C_1(\tau) + (j\omega)^5 C_2(\tau) + \dots \\
D(\tau) &= D_0(\tau) + (j\omega)^2 D_1(\tau) + (j\omega)^4 D_2(\tau) + \dots
\end{aligned} \tag{2.49}$$

we substitute these expansions into (2.47) and (2.48) and equate terms with identical powers of $j\omega$ to get

$$\frac{d}{d\tau} A_0(\tau) = \frac{d}{d\tau} D_0(\tau) = 0;$$
$$\frac{d}{d\tau} B_0(\tau) = Z_0(\tau) A_0(\tau); \qquad \frac{d}{d\tau} C_0(\tau) = \frac{1}{Z_0(\tau)} D_0(\tau);$$
$$\frac{d}{d\tau} A_1(\tau) = \frac{1}{Z_0(\tau)} B_0(\tau); \qquad \frac{d}{d\tau} D_1(\tau) = Z_0(\tau) C_0(\tau)$$

and in general:

$$\begin{aligned}
\frac{d}{d\tau} B_n(\tau) = Z_0(\tau) A_n(\tau); &\qquad \frac{d}{d\tau} C_n(\tau) = \frac{1}{Z_0(\tau)} D_n(\tau); \\
\frac{d}{d\tau} A_{n+1}(\tau) = \frac{1}{Z_0(\tau)} B_n(\tau); &\qquad \frac{d}{d\tau} D_{n+1}(\tau) = Z_0(\tau) C_n(\tau)
\end{aligned} \tag{2.50}$$

for $n \geq 0$. The initial conditions for these equations are

$$A_0(0) = D_0(0) = 1; \qquad A_n(0) = D_n(0) = 0 \quad (n > 0);$$

$$B_n(0) = C_n(0) = 0 \quad (n \geq 0)$$

so we can solve the differential equations recursively by quadratures:

$$A_0(\tau) = D_0(\tau) \equiv 1;$$

$$B_0(\tau) = \int_0^\tau Z_0(\tau_1)\, d\tau_1; \qquad C_0(\tau) = \int_0^\tau \frac{1}{Z_0(\tau_1)}\, d\tau_1$$

and in general:

$$\begin{aligned}
A_{n+1}(\tau) &= \int_0^{\tau} \frac{1}{Z_0(\tau_1)} B_n(\tau_1)\, d\tau_1 \\
B_{n+1}(\tau) &= \int_0^{\tau} Z_0(\tau_1) A_{n+1}(\tau_1)\, d\tau_1 \\
D_{n+1}(\tau) &= \int_0^{\tau} Z_0(\tau_1) C_n(\tau_1)\, d\tau_1 \\
C_{n+1}(\tau) &= \int_0^{\tau} \frac{1}{Z_0(\tau_1)} D_{n+1}(\tau_1)\, d\tau_1
\end{aligned} \tag{2.51}$$

for $n \geq 0$. When A_n, etc. are written without an argument, it will be assumed that $\tau = T$: $A_n(T) \equiv A_n$ and so on, where T is the total "length" (i. e., time delay) of the entire section of nonuniform line. With the exception of the constants A_0 and D_0, all of the coefficients $A_n(\tau)$, $B_n(\tau)$, $C_n(\tau)$ and $D_n(\tau)$ are positive monotonically increasing functions of τ.

It should be noted that this series solution is also applicable to the problem of plane-wave reflection and transmission from an inhomogeneous layer. In the electromagnetic case, if the permittivity of the layer is $\epsilon(x)$ and the permeability is $\mu(x)$, then a wave that varies as $e^{-jk_y y}$ obeys the transmission-line equations if we put [15, p. 20]

$$L(x) = \mu(x); \qquad C(x) = \epsilon(x) - \frac{k_y^2}{\omega^2 \mu(x)}$$

in the TE case (only E_z, H_x and H_y are nonzero), or

$$L(x) = \mu(x) - \frac{k_y^2}{\omega^2 \epsilon(x)}; \qquad C(x) = \epsilon(x)$$

in the TM case (only H_z, E_x and E_y are nonzero). If only terms up to first order (i. e., B_0 and C_0) are retained, we recover the approximate description of a thin inhomogeneous layer due to Drude [29, pp. 287-288] (see also [30, p. 301]).

The power series expansion above is another (in principal) exact solution for the ABCD matrix of any nonuniform transmission line. Since each of the parameters in the ABCD matrix is an infinite series, solving this set of equations for any specific transmission line requires either a numerical solution, or an approximation. The approximation can be computed by truncating the series after a certain number of terms has been solved. This can also be a useful way to evaluate impedance transformation using nonuniform transmission lines. Applications of this method will be explored in Chapter 5.

Chapter 3

General Analytical Design of Exponential Line Matching Circuits

In this chapter, the ABCD analysis from Chapter 2 is used to obtain a more general design of matching sections using the exponential line. The design will not be limited to exponential line circuits that have continuous impedance characteristics at the ends of the exponential taper. By allowing the freedom of discontinuities at either end of the exponential line segment, an broad range of matching characteristics with very few limitations.

For the designs created in this chapter, a software tool has been created to design an exponentially tapered nonuniform transmission line to match an input and load impedance. The circuit is created for a center frequency and impedance ratio by choosing an electrical length or maximum impedance discontinuity. With these inputs, the shape of the nonuniform is produced [31].

3.1 ABCD Parameters for Exponential Transmission Lines

In equation 2.15, the case where N = constant defines the exponential line as shown in Figure 3.1. From the diagram in Figure 2.1 we take $Z_{01} = Z_{00}$ and $Z_{02} = Z_L$ (both real) hereafter since our goal is to find circuits that provide a match. Consider a transmission line with total time delay T (normalized line length), a tapered impedance value defined by an initial impedance K and a constant taper rate N:

$$Z_0(\tau) = Ke^{2N\tau} \tag{3.1}$$

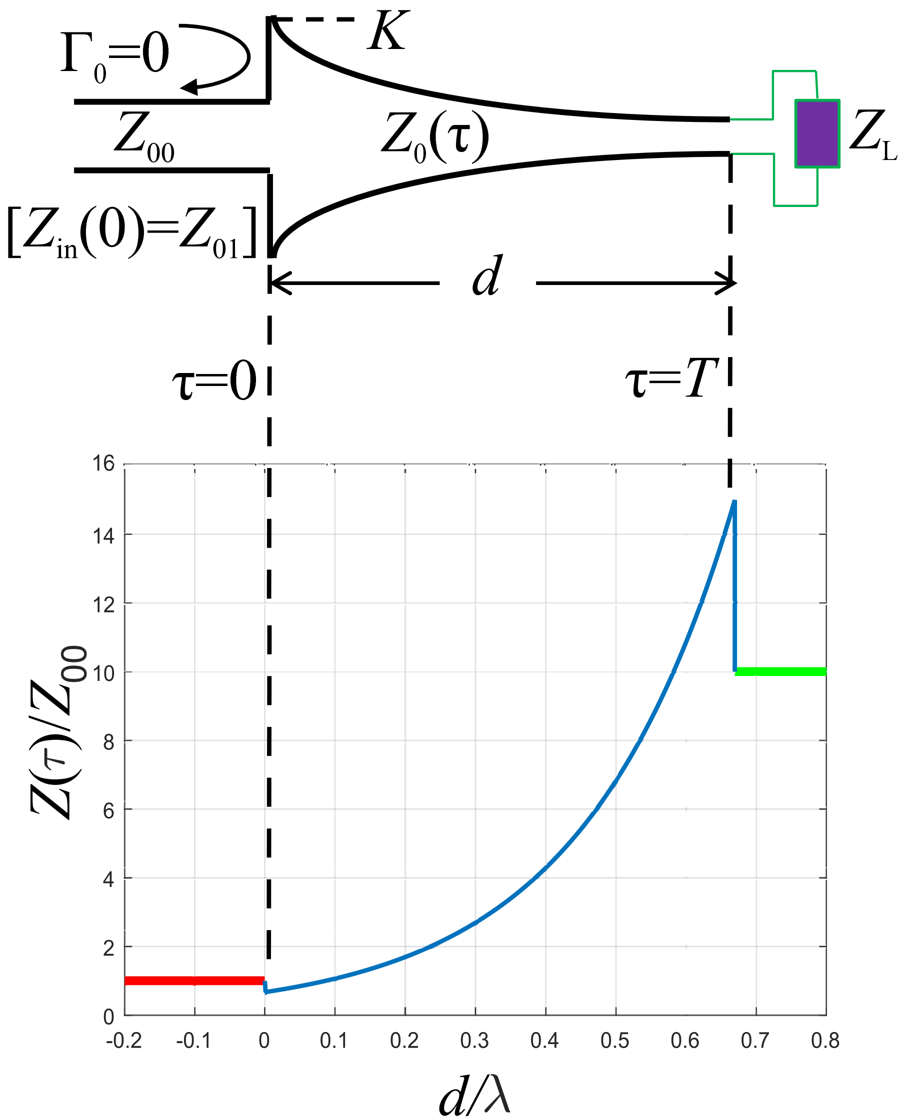

Figure 3.1: Exponential-line transformer with impedance discontinuities.

ABCD was derived in section 2.3.1. Recalling equations 2.51 and 5.7:

$$\begin{aligned} A &= \frac{e^{-NT}}{S}(S\cosh ST + N\sinh ST) \\ B &= j\omega\frac{Ke^{NT}}{S}(\sinh ST) \\ C &= j\omega\frac{e^{-NT}}{SK}(\sinh ST) \\ D &= \frac{e^{NT}}{S}(S\cosh ST - N\sinh ST) \end{aligned} \tag{3.2}$$

where

$$S = \sqrt{N^2 - \omega^2} \tag{3.3}$$

In order to find the exponential line characteristics which will give a perfect match, the A and D parameters from equation (3.2) are first inserted into (2.6), giving:

$$\begin{aligned} 0 = \frac{e^{-NT}}{S}\left(S\cosh ST + N\sinh ST\right) Z_L - \\ \frac{e^{NT}}{S}\left(S\cosh ST - N\sinh ST\right) Z_{00} \end{aligned} \tag{3.4}$$

Grouping all of the terms containing ST, this can be rewritten as:

$$\frac{1}{NT}\left(\frac{Z_{00}e^{2NT} - Z_L}{Z_{00}e^{2NT} + Z_L}\right) = \frac{\tanh(ST)}{ST} \equiv Q \tag{3.5}$$

Note that Q is a function of the three variables ω, N and T. Inserting the B and C parameters from equation (3.2) into (2.7) gives:

$$0 = Ke^{NT} - \frac{e^{-NT}}{K}Z_{00}Z_L \tag{3.6}$$

Solving for K:

$$K = \sqrt{\frac{Z_{00}Z_L}{e^{2NT}}} = \sqrt{Z_{00}Z_L}e^{-NT} \tag{3.7}$$

Given a frequency ω, the two conditions (3.6) and (3.7) for zero reflection ($S_{11} = 0$) relate the three variables K, N and T. By choosing a value for any one of these three variables, and using equations (3.6)(3.7), a unique solution can be found for the other two variables. In our procedure, a family of solutions will be obtained by choosing K (the initial impedance value of the exponential section of transmission line) and determining the product NT from (3.7). Substituting this result into (3.6) gives an equation that must be solved numerically using a root finding algorithm for the product ST. From equation (3.3), we can get ωT which now completely defines the parameters of the taper and electrical length.

As an example, an exponential line with no discontinuities is designed to match a source-load mismatch of 10:1 at a design frequency of ω_0. For no discontinuities, the source side impedance is selected to be $K/Z_{00} = 1$. With this one parameter chosen, N and T are solved using (3.6) and (3.7). The impedance taper, $Ke^{N\tau}$, is shown in Figure 3.2 along with the frequency response of the system.

For additional insight into how this type of nonuniform line creates a match, the Local Reflection Coefficient Γ is shown on a Smith Chart in Figure 3.2. On the Smith Chart, it can be noted that "locally" there is no discontinuity at the load or source end of the nonuniform line, and along all other points along the line a loop is traced representing local reflections which contribute to the overall match at the source end. A more in-depth description of types of reflection coefficients can be found in Appendix B.

Similarly, the design of a much shorter impedance transforming nonuniform transmission line can be produced by allowing for larger discontinuities at either end of the exponential line. For the 10:1 impedance ratio, an input impedance of $K/Z_{00} = 10$ was chosen. Repeating the procedure of solving (3.6) and (3.7), N and T were found. The resulting impedance taper, frequency response, and Smith Chart can be seen in Figure 3.3.

The exponential lines with large discontinuities create a match at ω_0 in a much shorter length of transmission line and a negative value of N. The discontinuities have a large contribution to the matching process which can be visualized in the renormalizations in Figure 3.3. The sacrifice for this shortened length is a narrowing of bandwidth in the frequency response. This analytic study does not yet take into account the parasitic effects of the impedance discontinuities. This will be studied in later chapters.

For exponential tapers created for impedance matching by (3.6) and (3.7), the midpoint

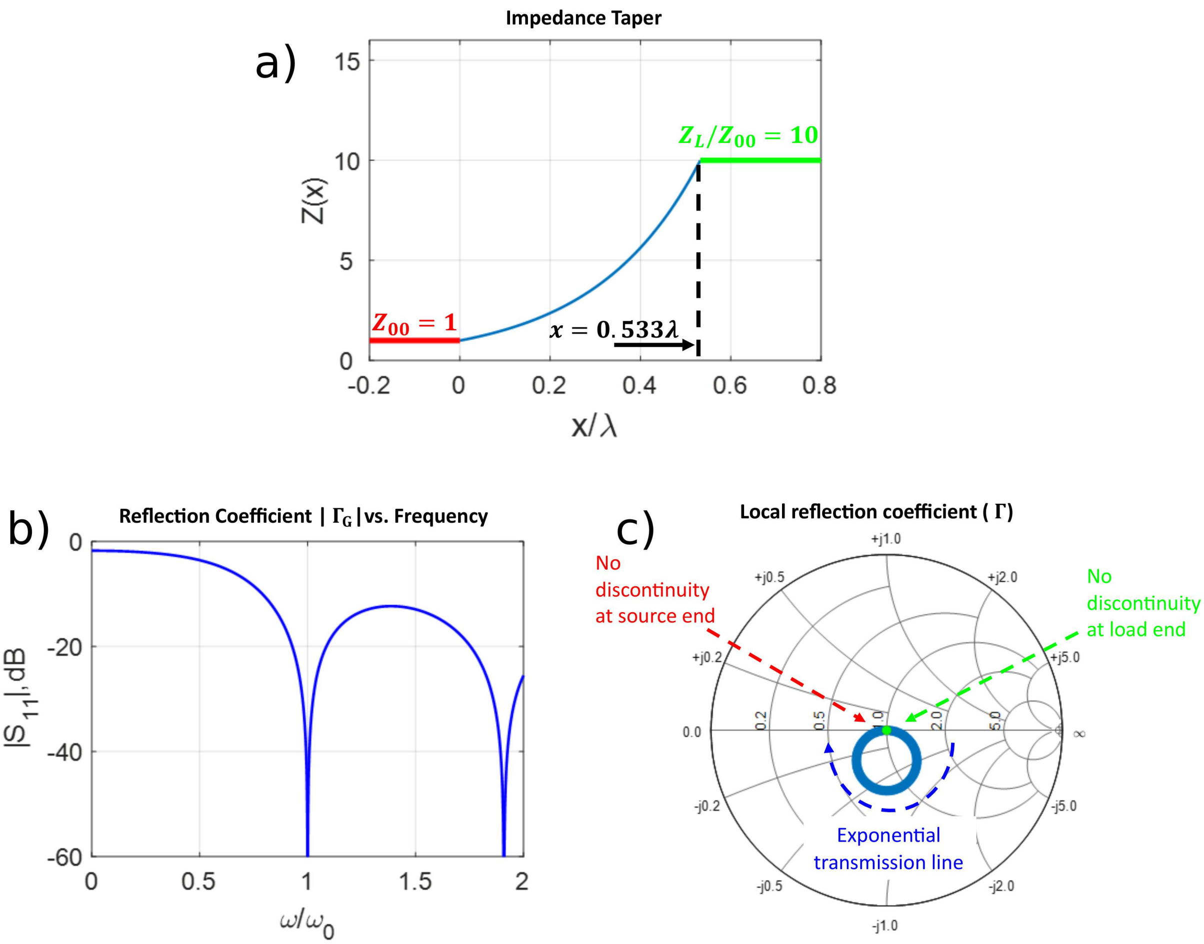

Figure 3.2: a) Exponential line with $K/Z_{00} = 1$ for matching 10:1 impedance mismatch. b) Input reflection coefficient ($\Gamma_G @ \tau = 0$) vs. frequency. c) Local Reflection Coefficient (Γ) vs. position along transmission line ($\tau @ \omega = \omega_0$).

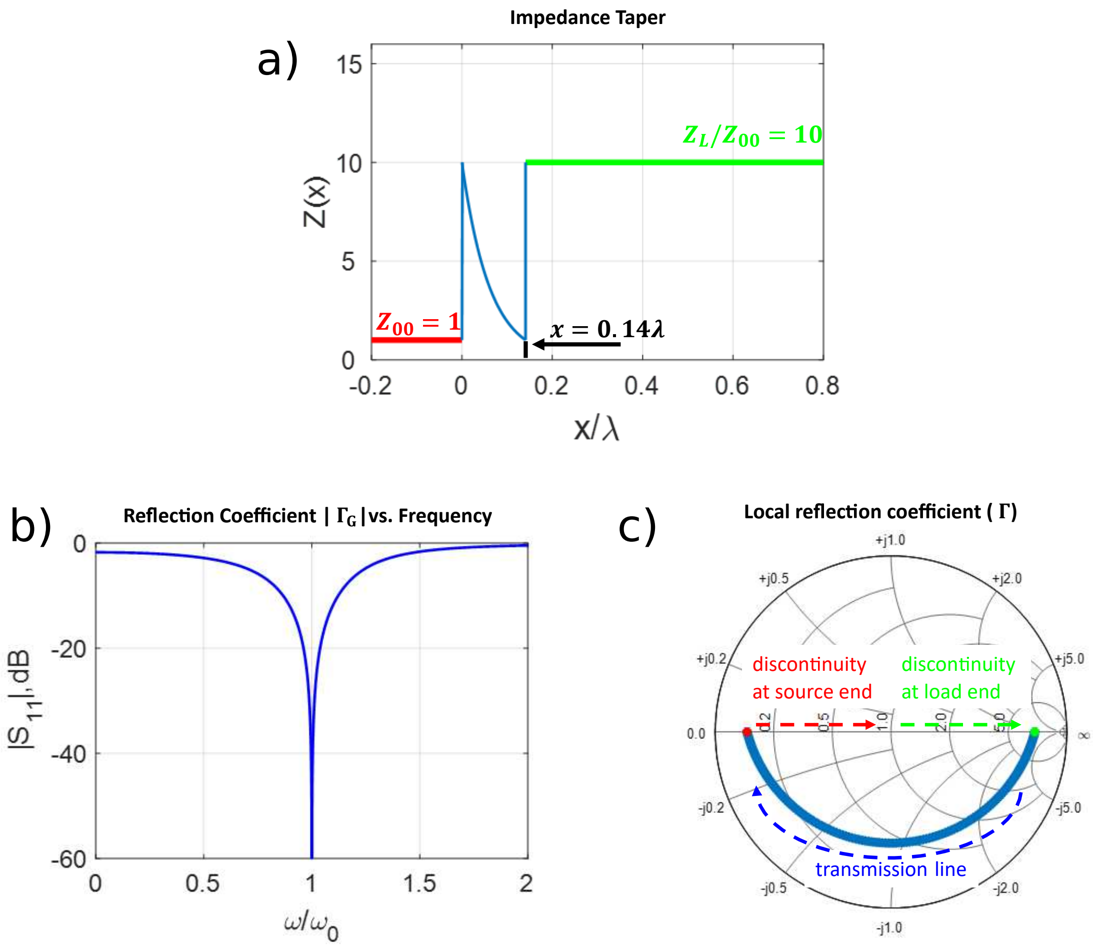

Figure 3.3: a) Exponential line with $K/Z_{00} = 10$ for matching 10:1 impedance mismatch. b) Input reflection coefficient ($\Gamma_G@\tau = 0$) vs. frequency. c) Local Reflection Coefficient (Γ) vs. position along transmission line ($\tau@\omega = \omega_0$).

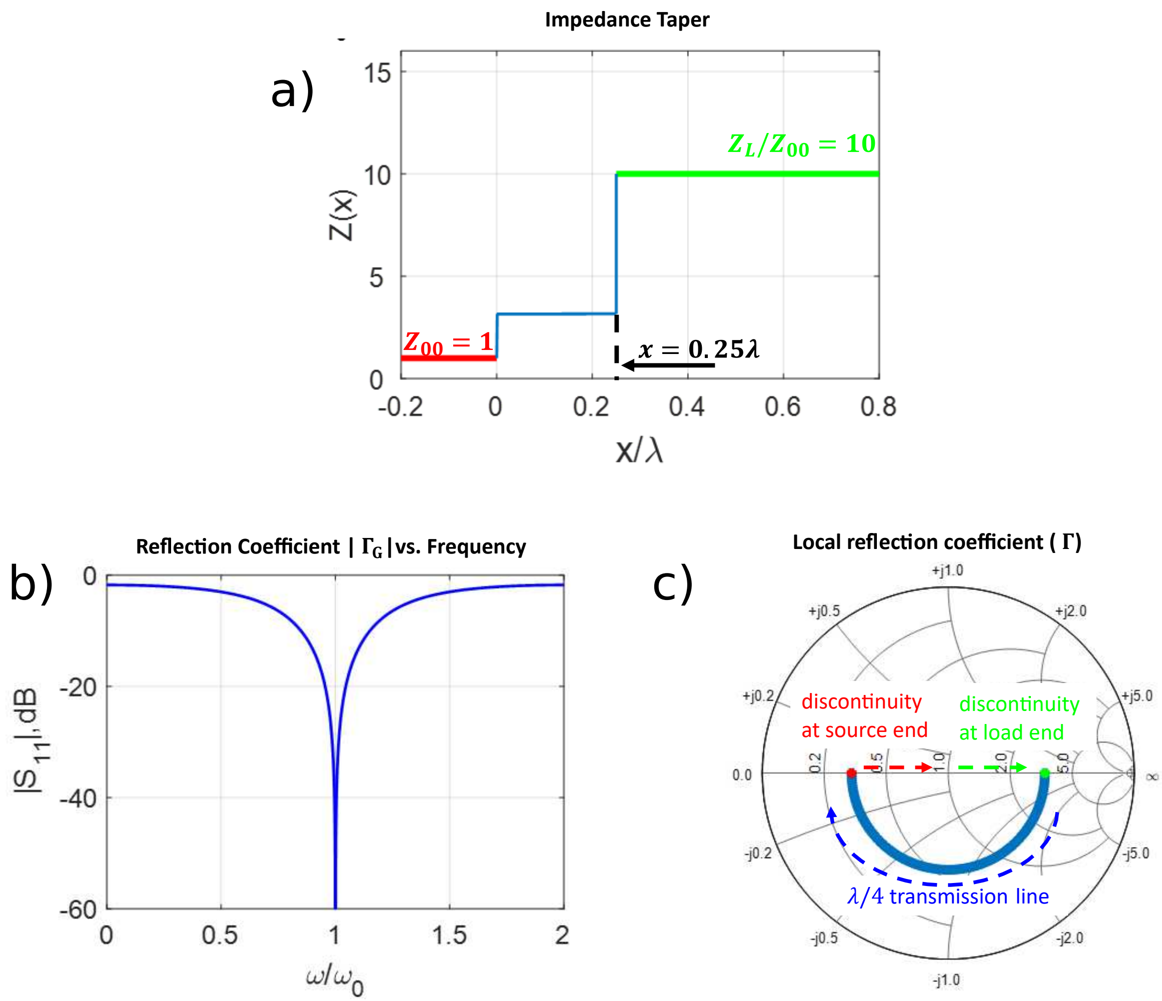

Figure 3.4: a) Exponential Line with $K/Z_{00} = 3.16$ ($\lambda/4$ transformer) for matching 10:1 impedance mismatch. b) Input reflection coefficient ($\Gamma_G @ \tau = 0$) vs. frequency. c) Local Reflection Coefficient (Γ) vs. position along transmission line ($\tau @ \omega = \omega_0$).

impedance is always the geometric mean of the source and load (for the case of these studies $\sqrt{10 * 1} \approx 3.16$). This value is also that of the uniform line associated with the quarter-wave transformer. Figure 3.4 shows the response for the quarter-wave transformer computed in the same way as the $K/Z_{00} = 1$ and $K/Z_{00} = 10$ exponentially tapered impedance transformers.

To aid in the visualization of the number and types of exponential matching circuits that can be realized, six discrete tapers are shown in Figure 3.5. The frequency response for each of these six tapers can be seen in Figure 3.8. While the six discrete cases give an idea of what types of exponential tapers can be designed to match 10:1 impedance discontinuities, the total number of solutions can be thought of as a continuum of relationships between the variables defined herein as K, N, and T. Using some factors to normalize these values to ω, Figures 3.6 and 3.7 show what solutions can be created by this design technique. The six discrete exponential tapers are also noted in Figures 3.6 and 3.7 using stars associating them with Figure 3.8. Figures 3.6 and 3.7 also include the characteristics for exponential lines designed to match impedance tapers of 2:1 and 5:1.

The magnitude of S_{11} as a function of frequency for the exponential transmission lines with different values of K shown in Figure 3.5 have been computed using equations (3.6) and (3.7), and results are shown in Figure 3.8. For all cases, a deep null is realized at the design frequency $\omega = \omega_0 = 2\pi f_0$. The bandwidth is broader for K values closer to $K = Z_{00}$. As K is increased, creating a larger discontinuity between K and Z_{00}, the transmission line is shortened, but bandwidth is also narrower. The commonly used quarter-wave transformer (Figure 3.5d) is seen to be a special case of our family of designs, in which $K = \sqrt{Z_{00} Z_L}$, $N = 0.$ and $d/\lambda = \frac{\omega T}{2\pi} = 1/4$.

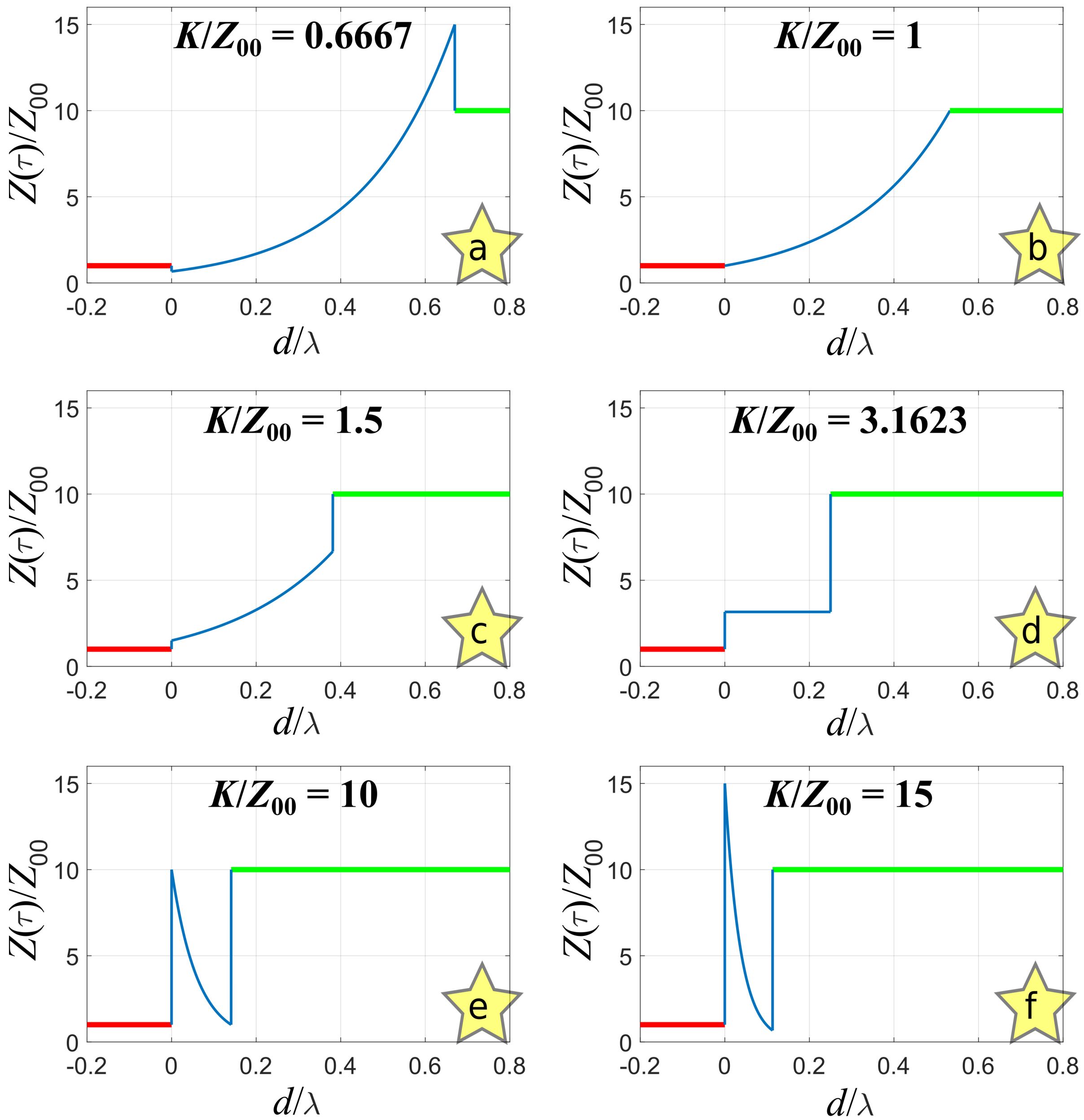

Figure 3.5: Exponential Taper Impedance Model for 6 Values of K with $Z_L/Z_{00} = 10$.

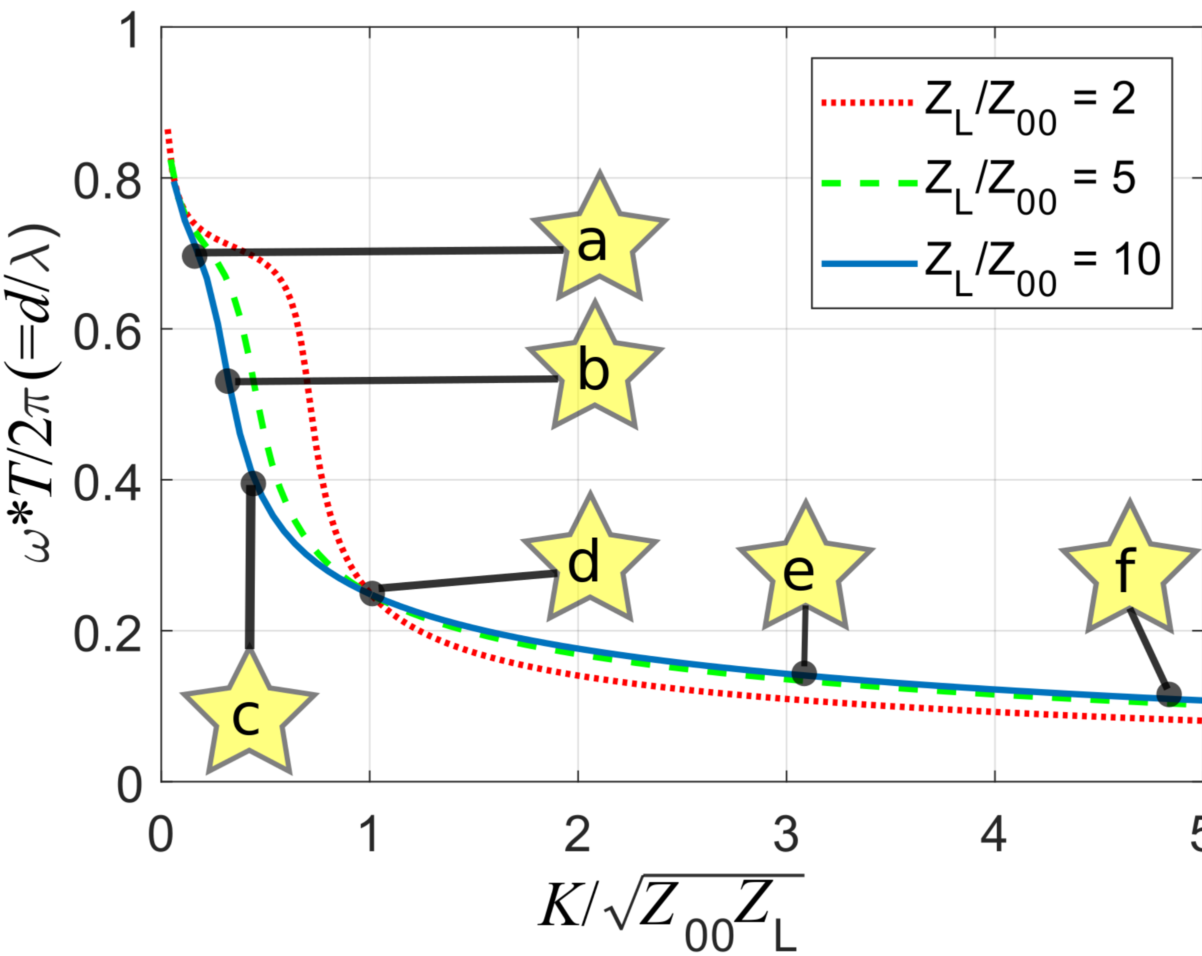

Figure 3.6: Normalized overall transmission line length vs. normalized impedance at the source end.

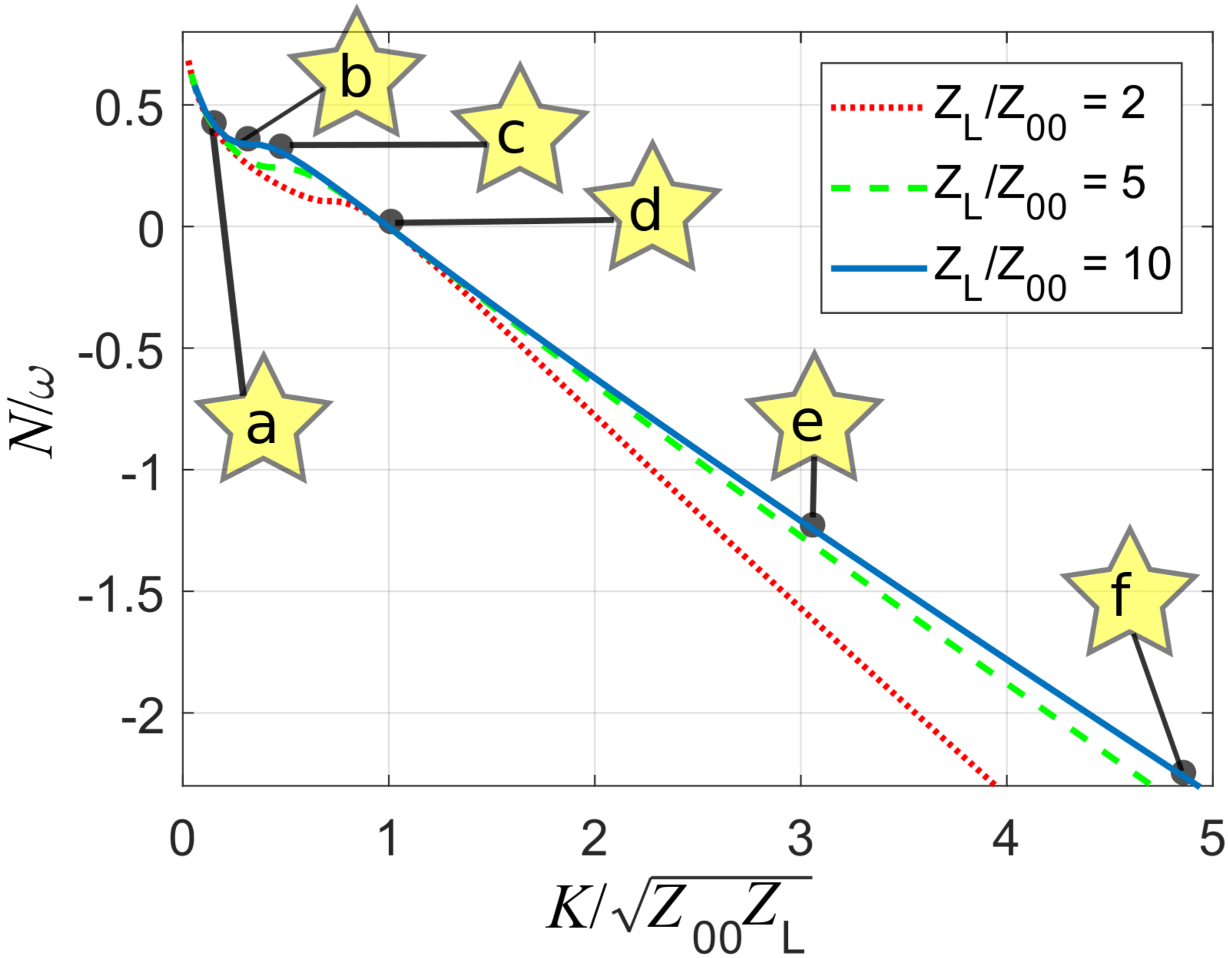

Figure 3.7: Normalized taper rate of exponential transmission line vs. normalized impedance at the source end.

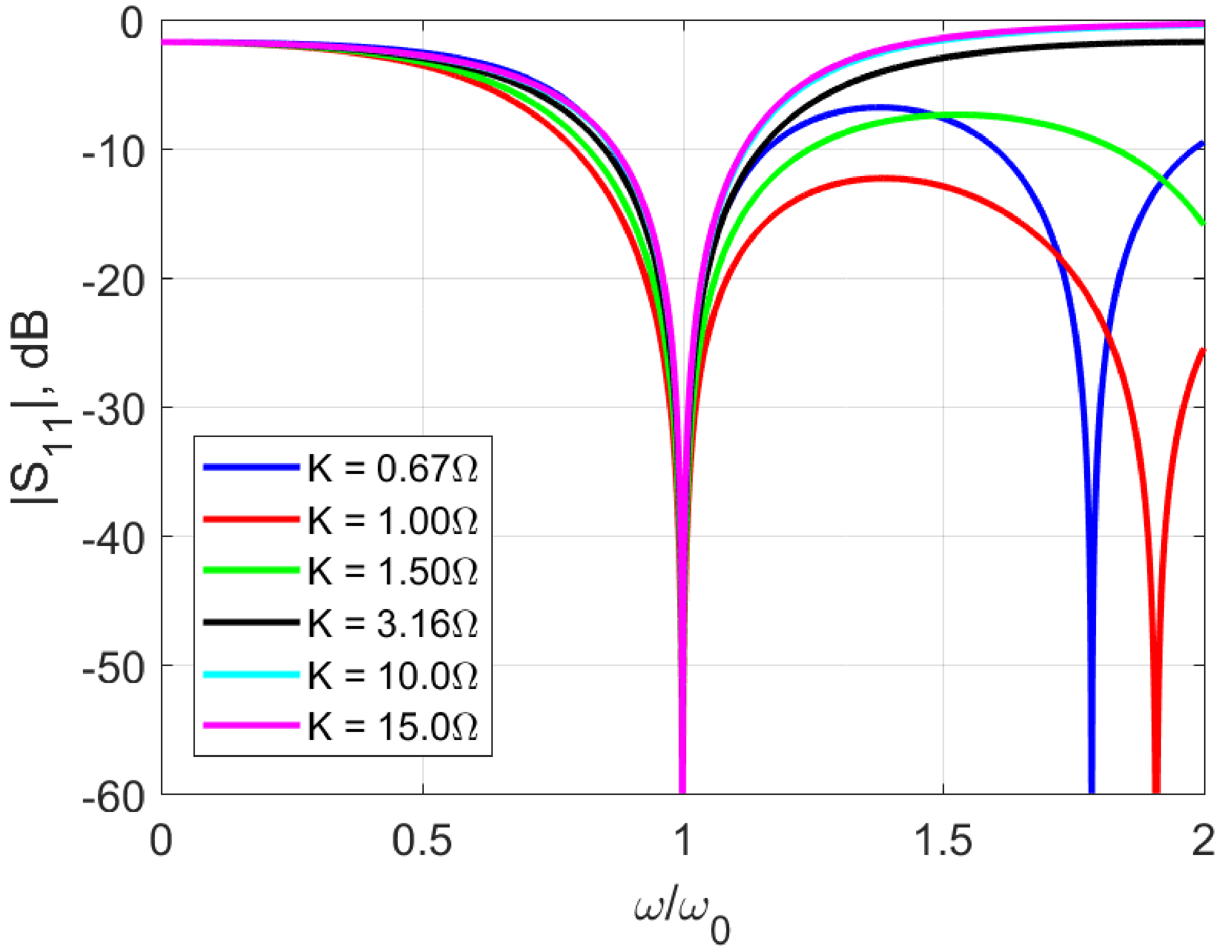

Figure 3.8: Input reflection coefficient $|S_{11}|$ computed from the ABCD Matrix for $Z_{00} = 1\,\Omega$ and $Z_L = 10\,\Omega$ (Note: The cases $K = 10\,\Omega$ and $K = 15\,\Omega$ are nearly identical).

3.1.1 Comparison of "short" ($L \lesssim \lambda/4$) impedance transformers

The Bramham [6], or two-step transformer (Figure 3.9) is another example of a transmission line that can be used for zero-reflection impedance transformation.

This transmission line has a shorter overall length than the quarter-wave transformer for a given frequency and a reduced bandwidth. This gives a viable design choice for applications where a shorter transmission line is desired due to space constraints, or material losses must be minimized.

Out of this family of narrow band responses, as is well known, the quarter-wave transformer has a ripple such that at frequencies above the design frequency, the reflection reaches the same level as at frequency = 0, before decreasing again to have a match at $3\omega_0$ and this is repeated periodically after that. For exponential transmission lines that are shorter than the quarter-wave transformer, not only does the bandwidth at ω_0 decrease, but the rebound at frequencies above the design frequency can actually be higher than at frequency = 0 (See Figure 3.8). For exponential lines that are longer than the quarter-wave transformer, we see that the rebound after ω_0 is not as high and the response has begun to take on a high-pass character that will be discussed in more detail in subsection 3.1.2.

While the quarter-wave and Bramham transformers give two possible design configurations for zero-reflection impedance transformation, the family of exponential curves that have been analytically treated in the previous section of this paper provide a great deal of flexibility for choosing an optimal circuit length. Results from equations (3.6) and (3.7) show that exponential line transformers that perfectly match Z_L to Z_{00} can also be significantly shorter than $\lambda/4$. Two examples of this are the tapers of Figure 3.5e, for which $K = Z_L$ and the same impedance discontinuities as the Bramham circuit, and that of Figure 3.5f, which has larger impedance discontinuities at $\tau = 0$ and $\tau = T$. In both cases, $K > \sqrt{Z_L Z_{00}}$ and the length of the transmission line section is reduced as K increases. To compare the bandwidth of these circuits, a level below which the reflection is considered to be within the passband must be selected. In practice, this choice will be application dependent, but the -20 dB level was chosen here as representative. A comparison of section length

Transmission line	Length	-20 dB Bandwidth
Exponential (K=1.0Ω)	.533λ	15.7%
Exponential (K=1.105Ω)	.487λ	15.1%
Exponential (K=1.5Ω)	.381λ	12.0%
Exponential (K=3.16Ω) ($\lambda/4$)	.250λ	9.0%
Exponential (K=Z_L=10Ω)	.141λ	7.7%
Bramham	.093λ	7.7%
Exponential (K=15Ω)	.113λ	7.5%
Exponential (K=21Ω)	.093λ	7.3%
Exponential (K=25Ω)	.084λ	7.3%
Exponential (K=30Ω)	.075λ	7.2%

Table 3.1: Bandwidth comparison for short lines: Quarter-wave, Bramham and exponential tapers.

and frequency bandwidth for these two exponential tapers along with the Bramham transformer can be found in Table 3.1. Note especially that exponentially tapered matching sections of shorter length than the Bramham circuit are possible with very little reduction in bandwidth compared with the quarter-wave transformer.

3.1.2 Comparison of "long" ($L \gtrsim \lambda/4$) impedance transformers

Most published work for the exponentially tapered impedance transformer has been done with no impedance discontinuities at the ends of the taper. When implemented with relatively small or no impedance discontinuities, the exponential line can produce a good impedance match for a large, high-pass frequency range. The length of such a tapered line will exceed a half wavelength. In this case, the exponential taper compares to other smooth tapered transmission line matching sections such as the Klopfenstein taper [25]. The figure of merit for the frequency response of a high-pass matching circuit with ripple amplitude below a certain threshold must be described in a different way than in terms of a percent bandwidth. The well-known equal-ripple Klopfenstein taper is designed to have a given maximum ripple height above a given design frequency. Other high-pass tapers are probably best characterized in terms of the limiting ripple level as $\omega \to \infty$, as well as the worst (highest) ripple level above the design frequency. The ripple level has no direct connection with the level that was chosen in the previous subsection to define the bandwidth of

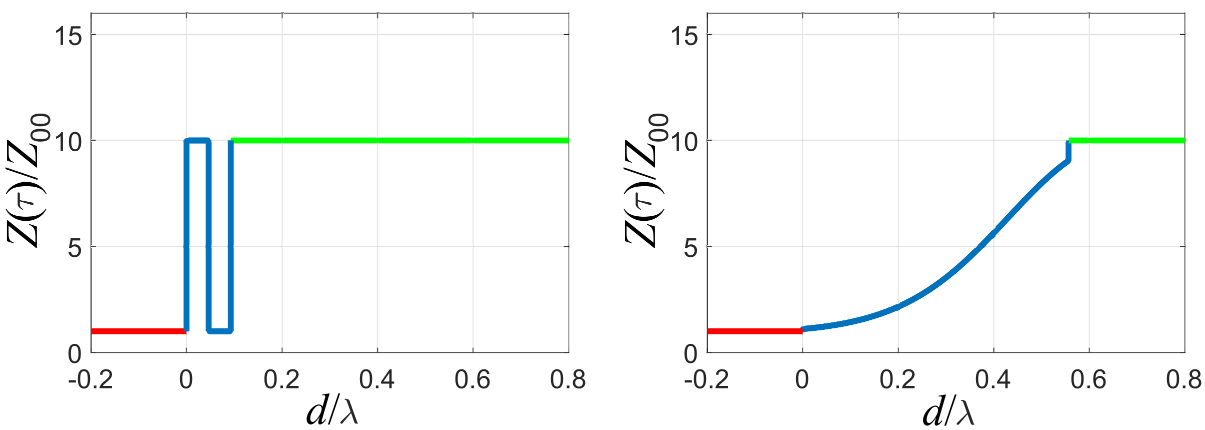

Figure 3.9: Bramham (left) and Klopfenstein (right) transformers for $Z_L/Z_{00} = 10$.

short-length matching sections.

Klopfenstein tapered transmission line matching sections are realized by using a formula that defines the taper and the two impedance discontinuities at the ends. This solution is optimized to provide a known maximum ripple in the high frequency pass band at frequencies above the band-edge frequency. This maximum ripple, however, is traditionally computed using the assumptions of the WKB approximation, which requires that the impedance taper rate N is not too large, or the frequency is not too small. A numerically "exact" solution for the Klopfenstein taper can be implemented, for example, using the Runge-Kutta method.

A Klopfenstein impedance taper with -20 dB ripple along with an exponential taper with $K = 1.105\ \Omega$ for comparison are shown in Figure 3.10. The exponential taper was chosen with identical impedance discontinuities at the ends so as to create a high-pass circuit whose ripple stabilizes to -20 dB at high frequencies. Both circuits were designed to have a perfect match at ω_0. The results shown in Figure 3.10 were calculated using the Runge-Kutta method for the Klopfenstein taper, and from the analytical formulas for the exponential taper. The ripple levels are not all exactly -20 dB for either taper. In the case of the Klopfenstein taper, this is because the WKB approximation is used for the design, and at sufficiently low frequencies does not quite agree with the exact solution, particularly at the first ripple. When the Klopfenstein design technique is used for a smaller impedance mismatch such as 2:1, the approximate result more closely resembles the exact solution than for the impedance mismatch of 10:1 that has been considered here. The exponential line has a shorter overall length, but gives a poorer match at frequencies in the range $1 < \omega/\omega_0 < 5$. Both tapers have $|S_{11}|$ remaining < 0 dB as $\omega \to 0$, as should be expected.

The exponential taper with $K = 1.105\ \Omega$ shown in Figure 3.10 has a ripple that approaches -20 dB at the highest frequencies. The first ripple, however, is measured at -11.8 dB. Figure 3.11 compares that same exponential taper compared to a Klopfenstein taper that has a ripple height at the -11.8 dB S_{11} level. This Klopfenstein is slightly shorter with larger impedance discontinuities that the $K = 1.105\ \Omega$ exponential taper.

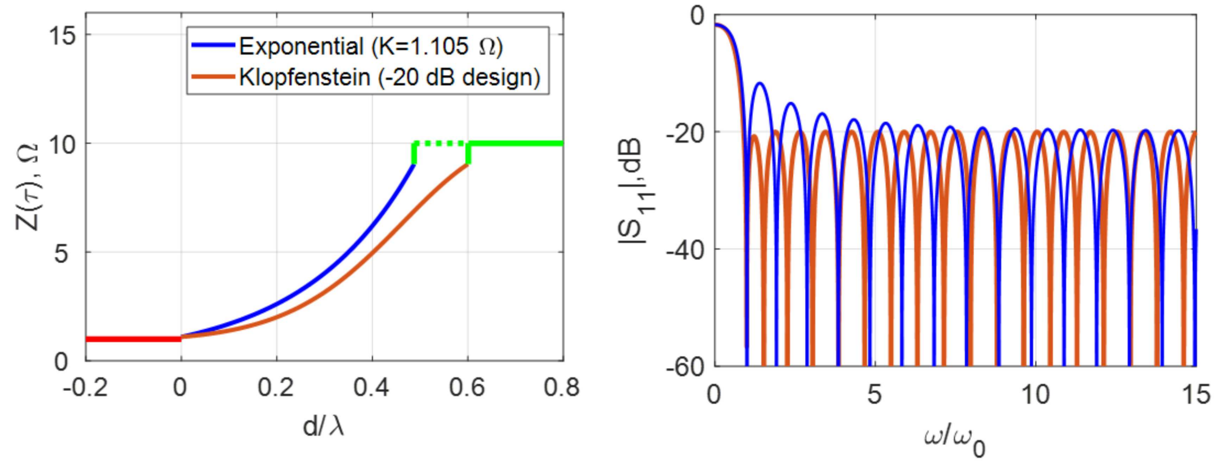

Figure 3.10: Taper and $|S_{11}|$ of Klopfenstein and exponential taper with same discontinuities.

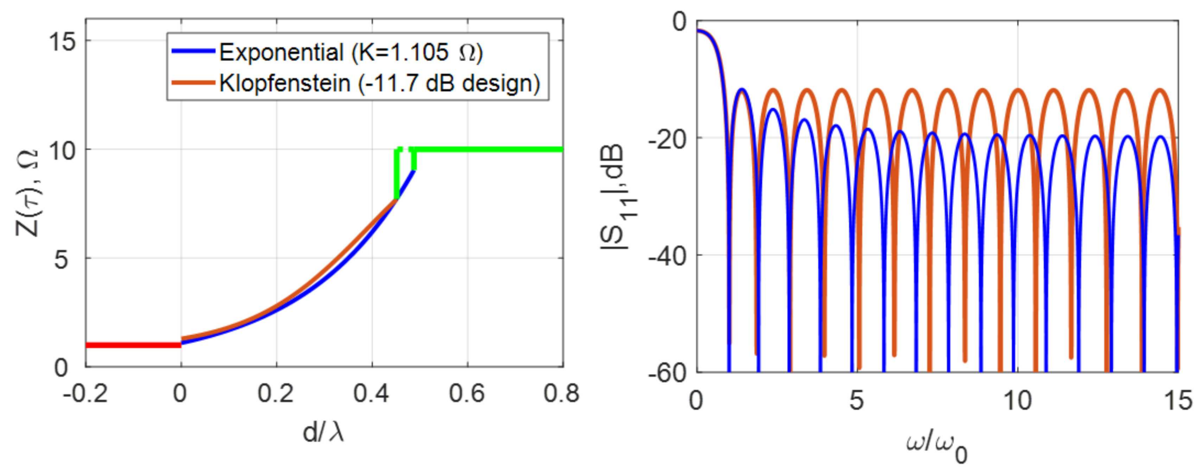

Figure 3.11: Taper and $|S_{11}|$ of Klopfenstein and exponential taper with same first $|S_{11}|$ ripple height.

Chapter 4

Numerical and Experimental Verification of Analytical Results

Equations (3.6) and (3.7) give exact matching solutions for all cases of the exponential line impedance transformer. However, parasitic capacitance and inductance are not accounted for in these models. Several exponential circuits have been fabricated and tested to verify the design procedures in Chapter 3 and are presented in this chapter. HFSS full-wave models have been created to study the parasitic effects and material losses, but not fabrication imperfections.

Balanced stripline construction was selected in order to excite TEM modes where all of the fields could be contained within the dielectric material regardless of stripline width. 20 mil Rogers TC350 ($\epsilon_r = 3.5$) was selected as a favorable substrate for widths of the highest and lowest impedances required as shown in Figure 4.1.

In Chapter 3, several impedance ratios were investigated, but most emphasis has been placed on impedance ratios where $R_L/Z_{00} = 10$. This ratio was chosen as large enough to have significant need for impedance transformation, yet not so large that there would be too few practical applications that could make use of the design. All of the designs investigated in Chapter 4 have $Z_{00}/R_L = 10$. This normalized impedance ratio was realized for HFSS and the fabricated units by setting $Z_{00} = 5\Omega$ and $R_L = 50\Omega$.

4.1 Verification Using Full-Wave Simulation

A simulation model was created using Ansys HFSS to compare with the analytically computed results from Chapter 3. The HFSS model takes into account parasitic inductance and capacitance.

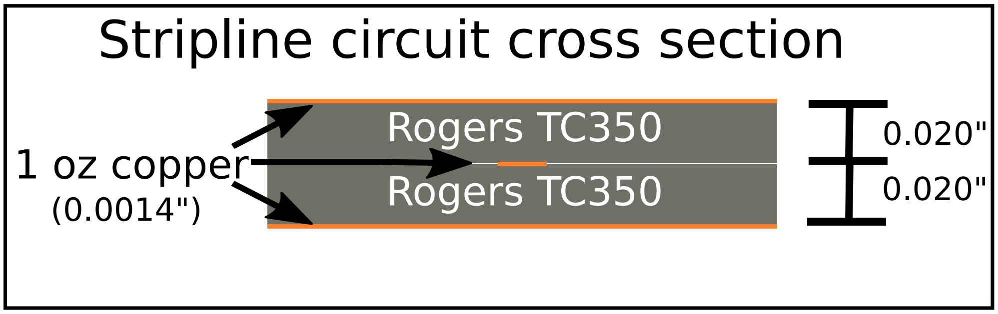

Figure 4.1: Material stack-up for stripline circuits.

The ABCD model has been created assuming lossless material, so an additional HFSS study has been made to examine the impact of dielectric material and copper loss. These circuits were designed to create a match at different frequencies on the same material stack-up in order to understand these impacts at different frequencies.

The structure used for comparison is a balanced stripline using Rogers TC350 ($\epsilon_r = 3.5$), creating a $0.040''$ spacing between the ground planes as shown in Figure 4.1. Stripline widths were chosen using the formulas in [32], but these formulas tended to have inaccuracies for the narrowest and widest strips; therefore, Ansys Electronics 2D Extractor was used to find more precise widths for the tapers which have the necessary impedances. Parameters were chosen so that $Z_{00} = 5\,\Omega$ (width $= 0.3713''$) and $Z_L = 50\,\Omega$ (width $= 0.0197''$). In Chapter 3, only normalized frequencies (ω_0/ω) were discussed. In the HFSS simulation, lengths of the exponential tapers were chosen for a design frequency of 1 GHz. The selection of the design frequency will be further discussed in section 4.1.1 after a few examples of the HFSS results have been shown.

Figure 4.2 shows the results for an exponentially tapered impedance transformer with no impedance discontinuities. In this case, $Z_{00} = K = 5\,\Omega$ corresponding to $K/Z_{00} = 1$ in Figures 3.5. The HFSS model matches closely to the analytical ABCD prediction. The null depth for the matched region is nearly -60 dB, and the bandwidth of the matched region is nearly identical. Interestingly, the HFSS results show a 1% frequency shift toward higher frequencies for the match. Frequency shifts for the $K/Z_{00} = 1$ case are attributed to the distributed parasitic capacitance and inductance along the taper. Since there are no abrupt changes in the characteristic impedance along the taper, it is expected that the impacts of capacitive and inductive parasitics will be small.

When the initial impedance of the tapered selection of the transmission line design is selected to be the geometric mean of the input and load impedances ($\sqrt{Z_{00}R_L}$), the quarter-wave transformer is created. In Figure 4.3, $K = \sqrt{Z_{00}R_L} = 15.81\Omega$. The resultant HFSS reflection coefficient vs. frequency shows another good match to the analytical ABCD design. The null is less deep than for the $K = 5\,\Omega$ case, but at -35.5 dB, it is still very good for most applications. The frequency shift in this case has moved the resonance 1.5% lower than the design frequency. The only nonuniformities in this model are the abrupt discontinuities at either end of the quarter-wave transformer. This type of parasitic capacitances and inductances from abrupt changes in characteristic impedance drives the response to lower frequencies. In practice, this can be compensated for by shortening the length of the central section slightly.

Figures 4.4 and 4.5 show examples of exponential tapers that have an impedance taper with decreasing slope ($N < 0$). In both cases, there is a larger frequency shift toward lower frequencies produced by the larger parasitic capacitance and inductance. Based on inference from the $K = 5\,\Omega$ and $K = 15.81\,\Omega$ cases, the dominant parasitic impact is produced by the large impedance discontinuities present at $\tau = 0$ ($x = 0$) and $\tau = T$ ($x/\lambda = d$). For the $K = 50\,\Omega$ and $K = 75\,\Omega$ cases, the frequency response is shifted 4% and 5.5% respectively. The null depth achieved for the models of these impedance transformers is still very good (< -30 dB). Recalling that both of these exponential lines are shorter than $\lambda/4$, Figures 4.4 and 4.5 show very usable impedance transformers for any application where a small reduction in frequency bandwidth can be accepted. Again, the frequency of the match can be corrected to match the design frequency by shortening the matching circuit even more.

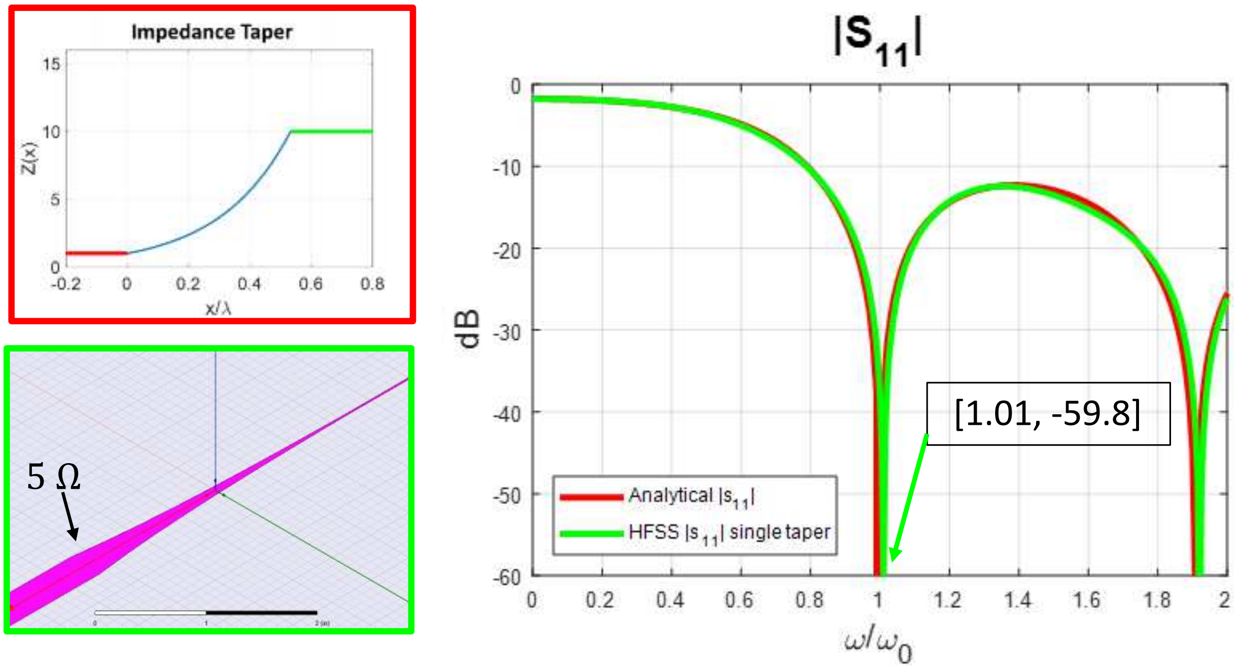

Figure 4.2: ABCD and HFSS solutions for $K = 5\ \Omega$ with $Z_{00} = 5\ \Omega$ and $Z_L = 50\ \Omega$. All other physical parameters as specified in the text.

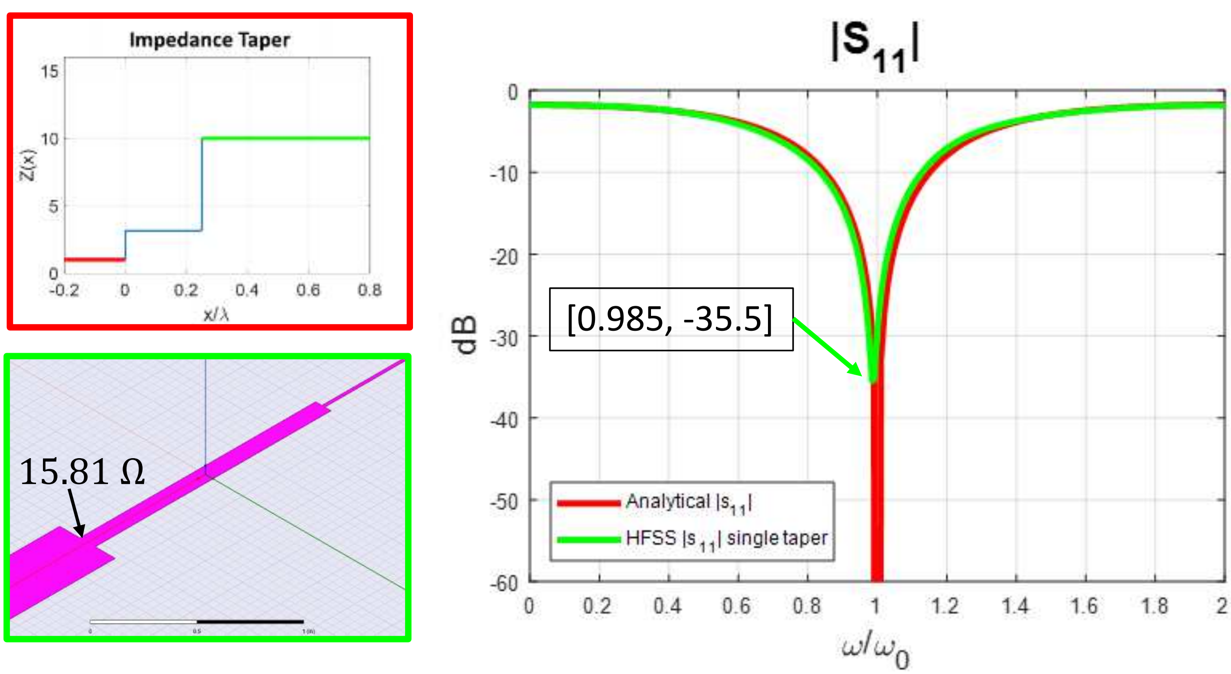

Figure 4.3: ABCD and HFSS solutions for the quarter wave-transformer ($K = 15.81\ \Omega$) with $Z_{00} = 5\ \Omega$ and $Z_L = 50\ \Omega$. All other physical parameters as specified in the text.

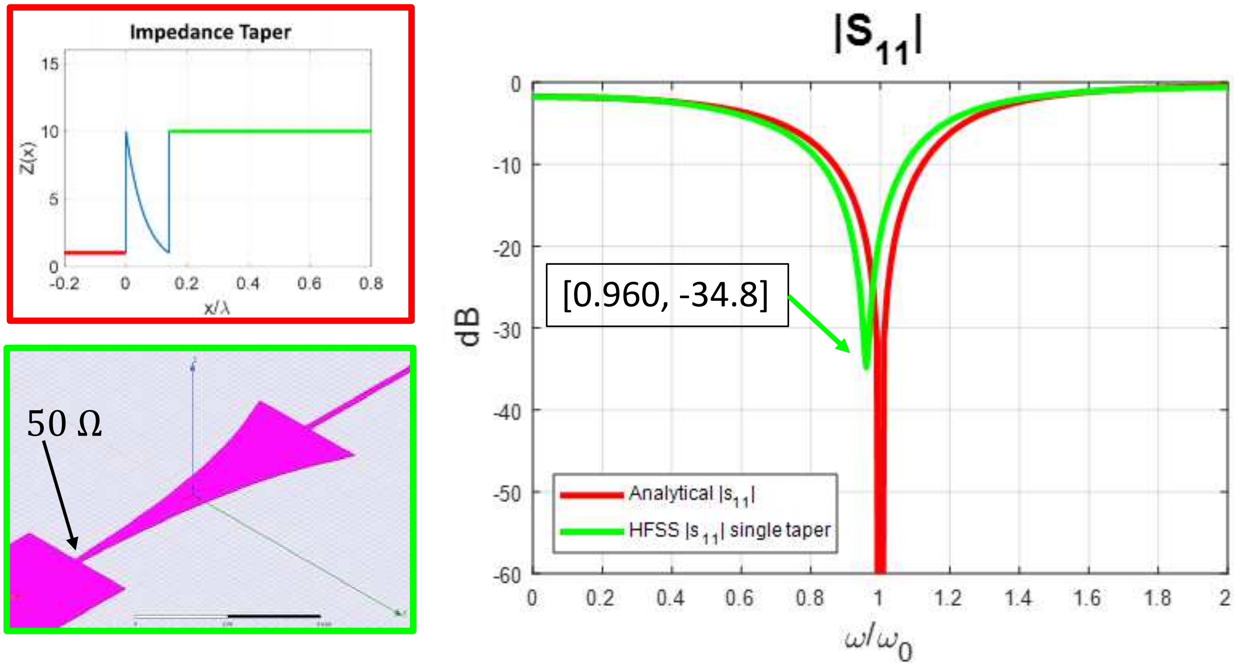

Figure 4.4: ABCD and HFSS solutions for $K = 50\ \Omega$ with $Z_{00} = 5\ \Omega$ and $Z_L = 50\ \Omega$. All other physical parameters as specified in the text.

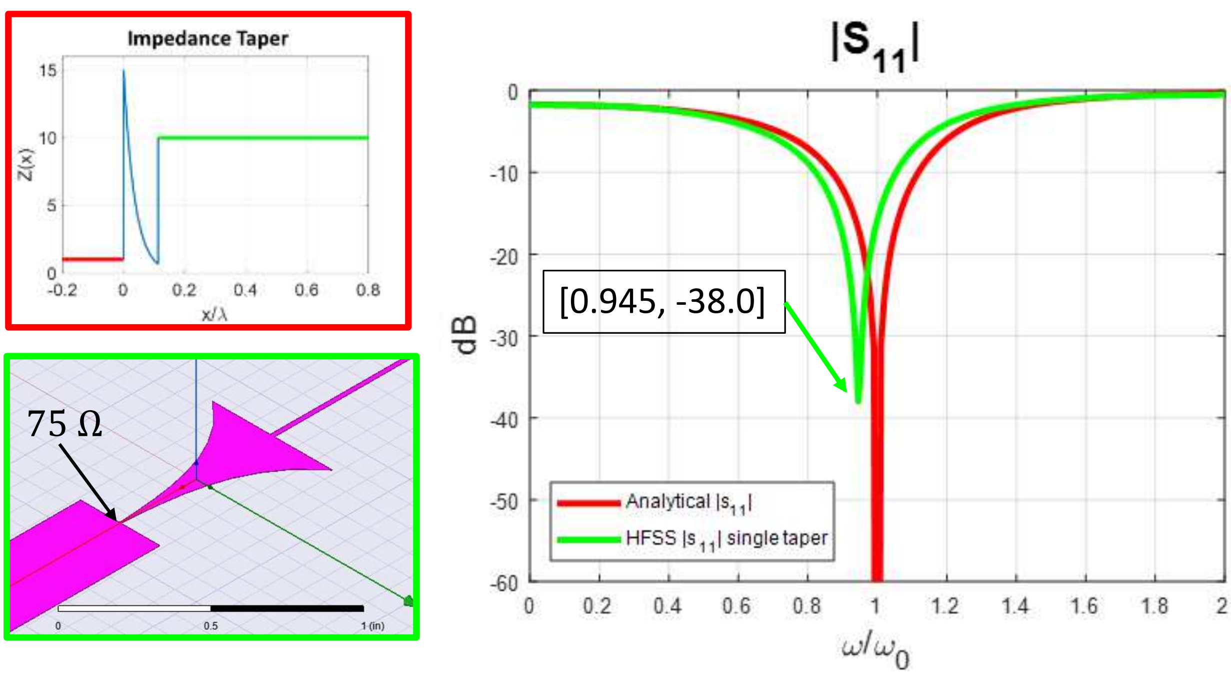

Figure 4.5: ABCD and HFSS solutions for $K = 75\ \Omega$ with $Z_{00} = 5\ \Omega$ and $Z_L = 50\ \Omega$. All other physical parameters as specified in the text.

4.1.1 Frequency and Loss Considerations Using Full-Wave Simulation

Figure 4.6 shows full-wave models for the $K/Z_{00} = 10$ case for three different design frequencies. The $K/Z_{00} = 10$ case was chosen as a good case to test for frequency shift compared to design frequency since the lossless model exhibits a 4% frequency shift in Figure 4.4, and uses no characteristic impedance values higher or lower than the impedance values of Z_{00} and R_L. Simulated results can be seen compared to the ABCD solution in Figure 4.6. When $f_0 = 250$ MHz, the parasitic effects are relatively small and the simulation agrees with the results given by the ABCD solution. As higher f_0 are selected, the null depth and bandwidth characteristics remain similar to the analytical solution, but the parasitic effects add electrical length to the line and decrease the center frequency of the response ($f/f_0 = 0.825$ for the 4 GHz case). When loss characteristics for TC350 ($tan\delta = 0.002$) and copper conductivity ($58\,MS/m$) are considered, the center frequency is shifted slightly lower. This change in frequency response is never more than 1% compared to the lossless HFSS case. The nulls at matched frequencies are also changed, but are always around -30 dB or lower.

For this reason, the design frequency (f_0) of 1 GHz was selected for both HFSS and fabrication studies. This frequency is high enough to show the sensitivity of the circuit performance to the effect of parasitics at the impedance transitions in the circuit, but low enough to reduce measurement errors due to small scale fabrication features when the circuits are built.

The advantage of stripline circuits over microstrip is that all fields are contained in the same dielectric material. With microstrip circuits, there is a fringing field which exists in the air. As the width of the microstrip trace changes, the percentage of the total field contained in the dielectric or air will vary. This variation creates a non-proportional relation between the delay time along the transmission line, τ, and distance along the same line x, as defined in equation (2.11). By choosing stripline, tapers dependence on the physical dimension, x, is easily related to the dependence on τ. Additionally, there is a dispersive effect on microstrip lines. As frequency increases, there is a tendency for more of the field energy to concentrate in the dielectric. This creates an additional

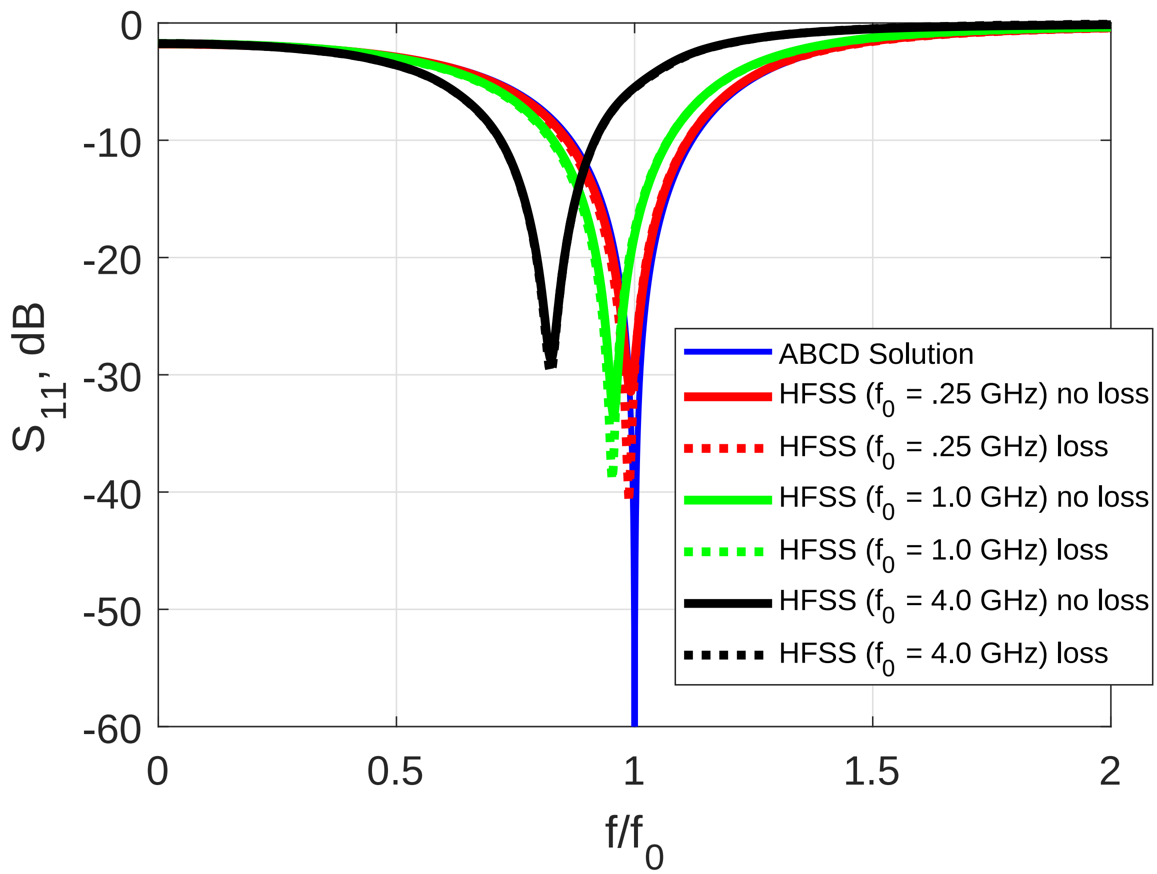

Figure 4.6: ABCD and HFSS solutions comparing theoretical and full-wave simulation results with and without lossy material for $K = 5\ \Omega$ with $Z_{00} = 5\ \Omega$ and $Z_L = 50\ \Omega$. All other physical parameters as specified in the text.

effect that the microstrip propagation constant will not simply be proportional to frequency. This dispersive effect can also be avoided by building stripline circuits.

4.2 Experimental Verification Using Stripline Circuits

Physical stripline models were also built to verify the practicality of the designs. Circuits corresponding to Figure 3.5 “b”, “d”, “e”, and “f” were fabricated for comparison to the analytically produced results. A picture of the cross section of the fabricated stripline is shown in Figure 4.1.

4.2.1 Circuit Fabrication

Stripline circuits are often fabricated by combining two dielectric boards with an adhesive laminate between them. Copper features for the middle trace can be milled using controlled-depth milling, or chemical etching the features of the central trace. In this case, fabrication was completed using a chemical etch solution in order to have accurate dimensions of the trace, and in order to not remove any of the dielectric material near the edge of the trace which would create a small air gap when the top dielectric comes in contact with the copper trace. The second side of the dielectric material was stripped of all copper. The two halves were held together during testing with clamps to minimize the air gap associated with the thickness of the 1 oz copper strip (see Figure 4.1). The etch process was performed in the fabrication laboratory at the University of Colorado, Boulder and pictures of the process can be seen in Figures 4.7-4.10.

The circuit designs were exported as .dxf files from HFSS and transferred onto a standard paper as dark images from a laser printer (see Figure 4.7). Those dark images were adhered to the copper cladding on one side of the 0.020” Rogers TC350 dielectric board by heat transfer using a laminator (see Figure 4.8). In Figure 4.9 the paper is being removed from the top side of the dielectric board by soaking in water. When the board with the black artwork was removed from the water and the paper removed, some gaps were noticed in the traces. Those gaps were filled with a black marker to keep copper within the boundary of where the stripline traces are intended to stay. The dielectric board with the image of the transmission lines was then placed in a cupric chloride

($CuCl_2$) solution to etch away the unnecessary copper from the dielectric board. In Figure 4.10 shows the small etching tank with circulating pump used to remove copper everywhere on the side of the board with the stripline transmission line segments. Another set of boards was etched completely on one side using the same process described above to create the opposing side of the stripline circuit.

These stripline circuits were designed with $50\,\Omega$ traces at both ends leading into exponentially tapered sections that then connect with a much wider $5\,\Omega$ trace in the center of the board, in a so-called "back-to-back" configuration. This type of construction allows for $50\,\Omega$ connectors to be placed on both ends for measurements with a network analyzer. The method for retrieving single-ended reflection coefficients from the measurements of this type of back-to-back circuit will be presented in section 4.2.4. HFSS simulations were also created in the back-to-back configuration to verify the raw measurements and processing technique that computes the single-ended reflection coefficients.

Eight stripline matching circuits were fabricated, four on each of two boards. Additional metallic traces of 0.0197″ wide were placed on either side of each matching circuit in order to create a standard boundary for any evanescent fields that may decay laterally from the exponential traces, as shown in Figure 4.11. The 0.0197″ trace width was selected to be the correct width for a $50\,\Omega$ trace so that can be used for baseline measurements to check equipment calibration and troubleshoot any erroneous measurements. An image of the two circuit boards with traces already etched can be seen in Figure 4.11.

4.2.2 Measuring the Stripline Circuits

The two boards shown in Figure 4.11 were placed on 0.25" aluminum block with tapped screw holes in the edges. SMA edge launch connectors were fixed to the edge (see Figure 4.12. The trace protruding from the SMA connectors is spaced 0.020" from the surface of the aluminum block to allow the dielectric board to be inserted between the block and the SMA trace. The SMA trace is 0.020" wide which overlaps the $50\,\Omega$ trace on the dielectric board almost perfectly. The

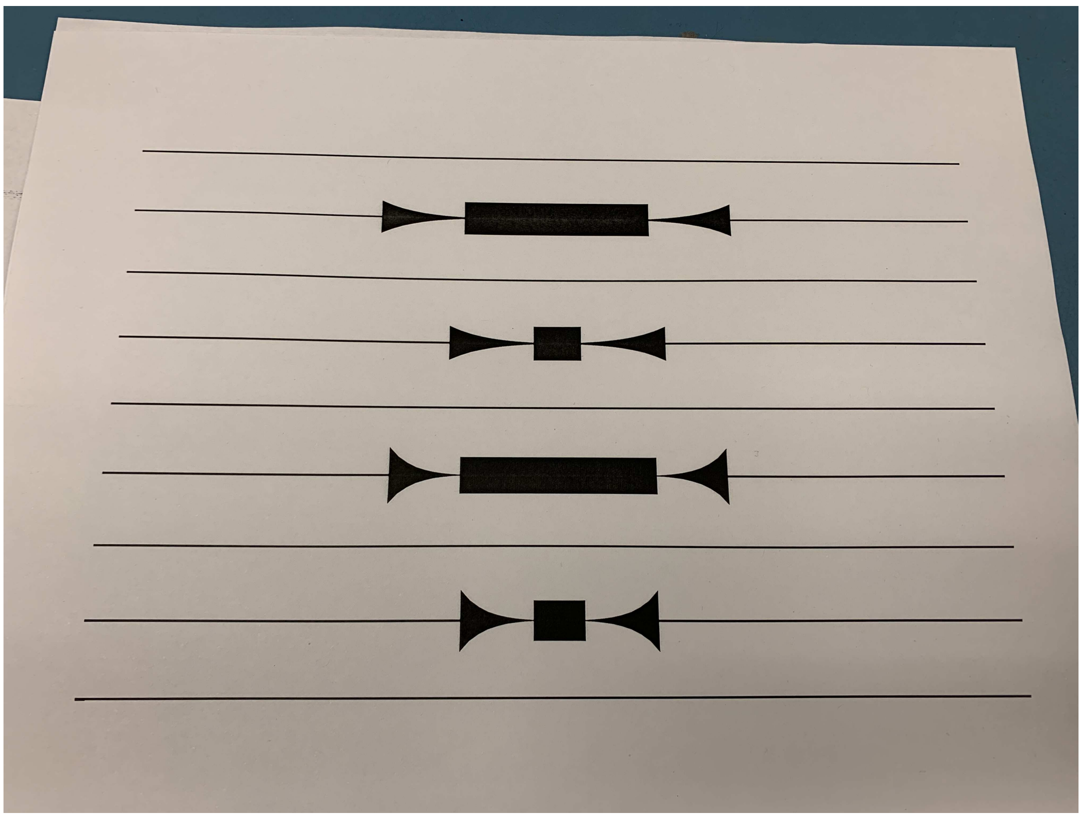

Figure 4.7: Mask used for stripline circuit.

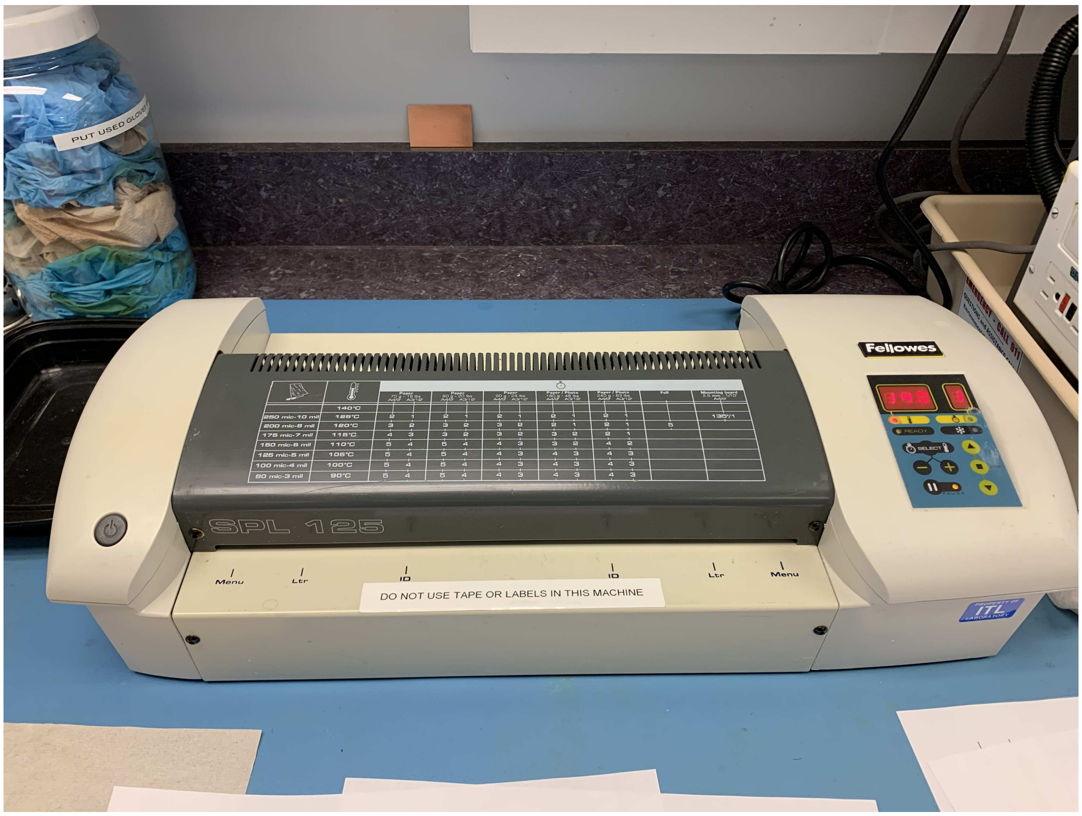

Figure 4.8: Lamination device for transferring artwork to the copper clad dielectric substrate.

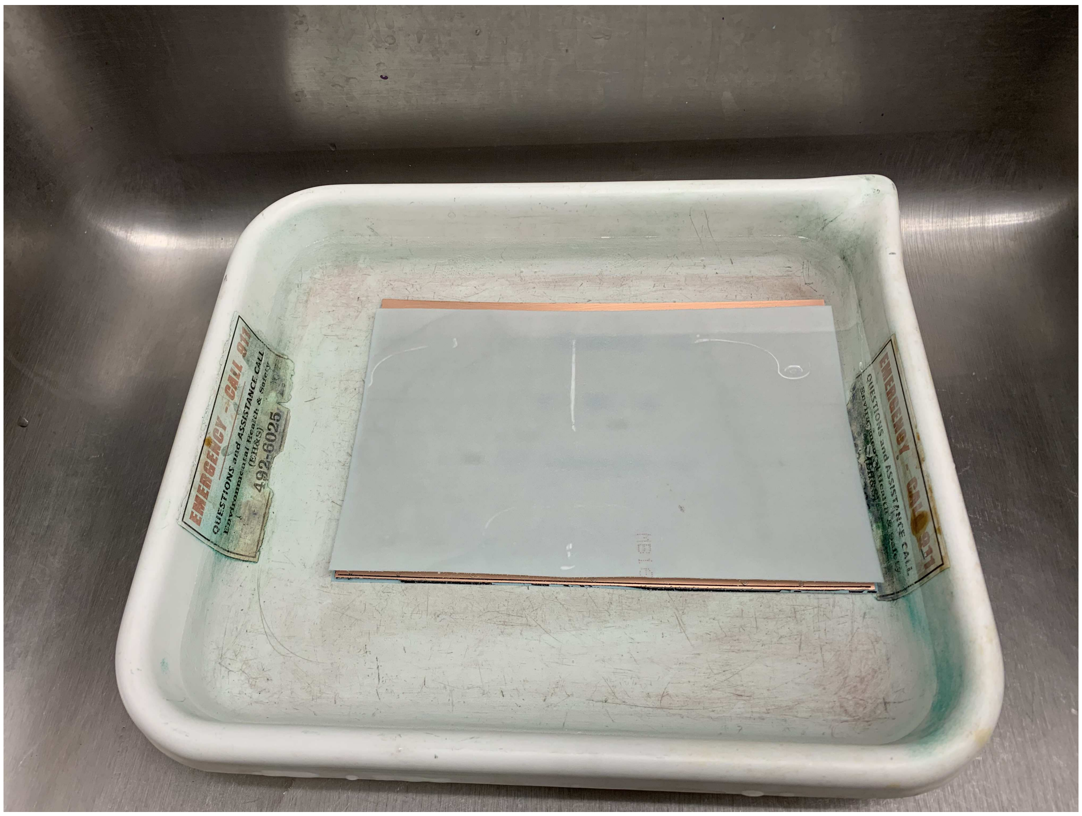

Figure 4.9: Water bath to remove the paper from the dielectric board.

Figure 4.10: Etching bath with circulating pump.

$50\,\Omega$ stripline trace for the circuit to be measured was aligned with the SMA trace of the connector and the blank top dielectric board was carefully placed over the trace to form the full stripline circuit, as seen in Figure 4.12. The top board of the stripline has a full groundplane on one side, and no copper at all on the other side. In Figure 4.12, a small “mouse hole” can be seen next to the connector. This was found to be necessary to allow a visual inspection of the trace alignment before measurements were taken. The small hole also kept the excessive pressure from being applied to the SMA trace. The SMA trace has a thickness of approximately 0.005”, and applying higher levels of pressure directly to the trace either caused the trace to break, or a larger air bubble to be present along the trace creating reflections which obscured the measurement. After the top of the stripline circuit was placed on the trace to be measured, a small cylinder of Teflon ($\epsilon_r = 2.02$) that had been cut from a piece of coaxial cable was placed into the ”mouse hole” to create a more homogeneous dielectric near the transition from SMA coax to SMA trace (see Figure 4.13). This was not a perfect, homogeneous ($\epsilon_r = 3.5$) transition but, through a process of trial and error, was shown to minimize reflections at the coax-stripline interface while reducing strain and eventual breakage of the coax connectors. Subsequently, another 0.25” aluminum block was placed on top of the stripline stack-up and clamped in place. As seen in Figure 4.12, two different methods of clamping the stripline boards were employed to create even pressure across the entire circuit area. The best configuration was found to be when the clamps were placed farther from the SMA connectors and the pressure transferred to the rest of the board through the 0.25” flat aluminum blocks. Additional screws were inserted into the top aluminum block to secure the SMA connector, and provide a ground path near the coax to stripline transition. Copper tape was also applied along the edges of the stripline stackup to ensure continuity between the two groundplanes.

4.2.3 Measurement of Back-to-Back Stripline Circuits

Calibrated network analyzer leads were connected to the two SMA ports. S-parameter data was recorded for the eight circuits. Each of the four exponentially tapered transmission lines designed to be tested was manufactured both with a 0.5” and with a 2” uniform $5\,\Omega$ section in the

Figure 4.11: 2 Boards with etched circuits for stripline Construction

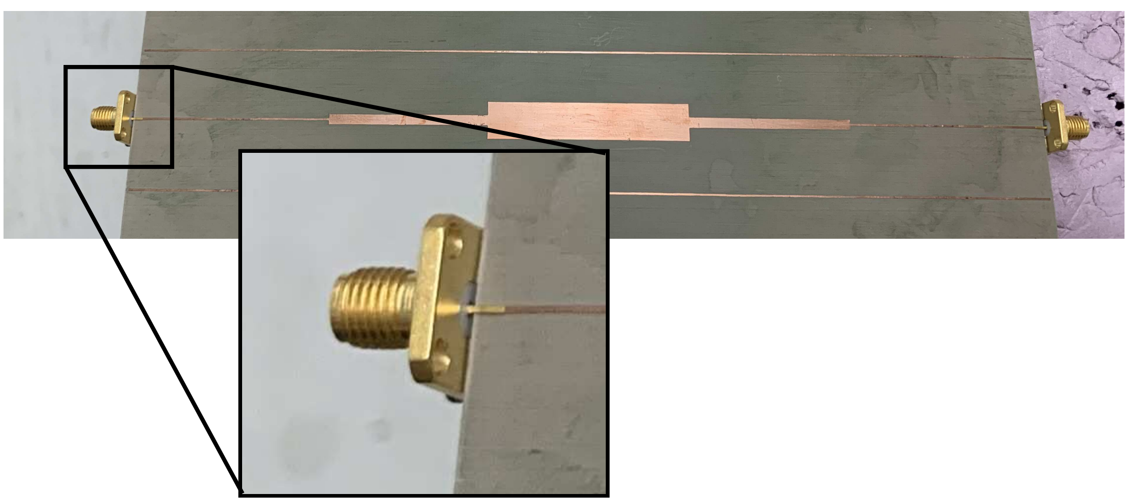

Figure 4.12: SMA connector attachment and trace alignment

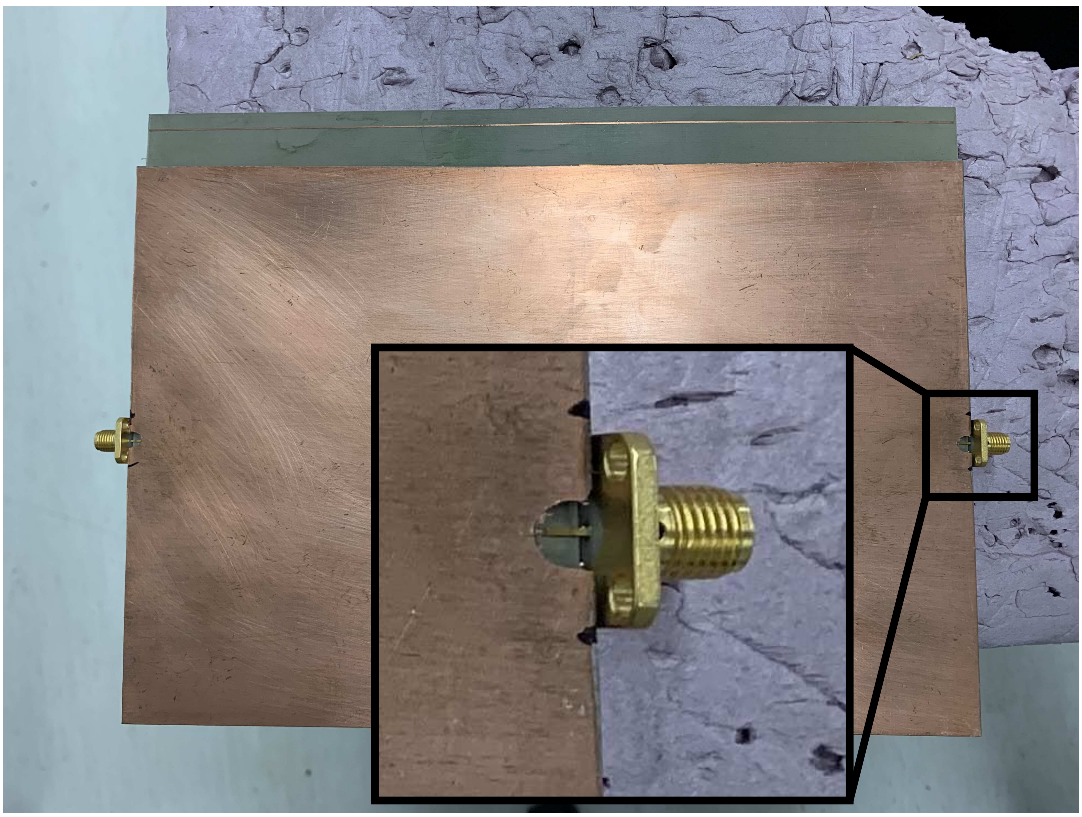

Figure 4.13: Detail of "mouse hole" at SMA connector point

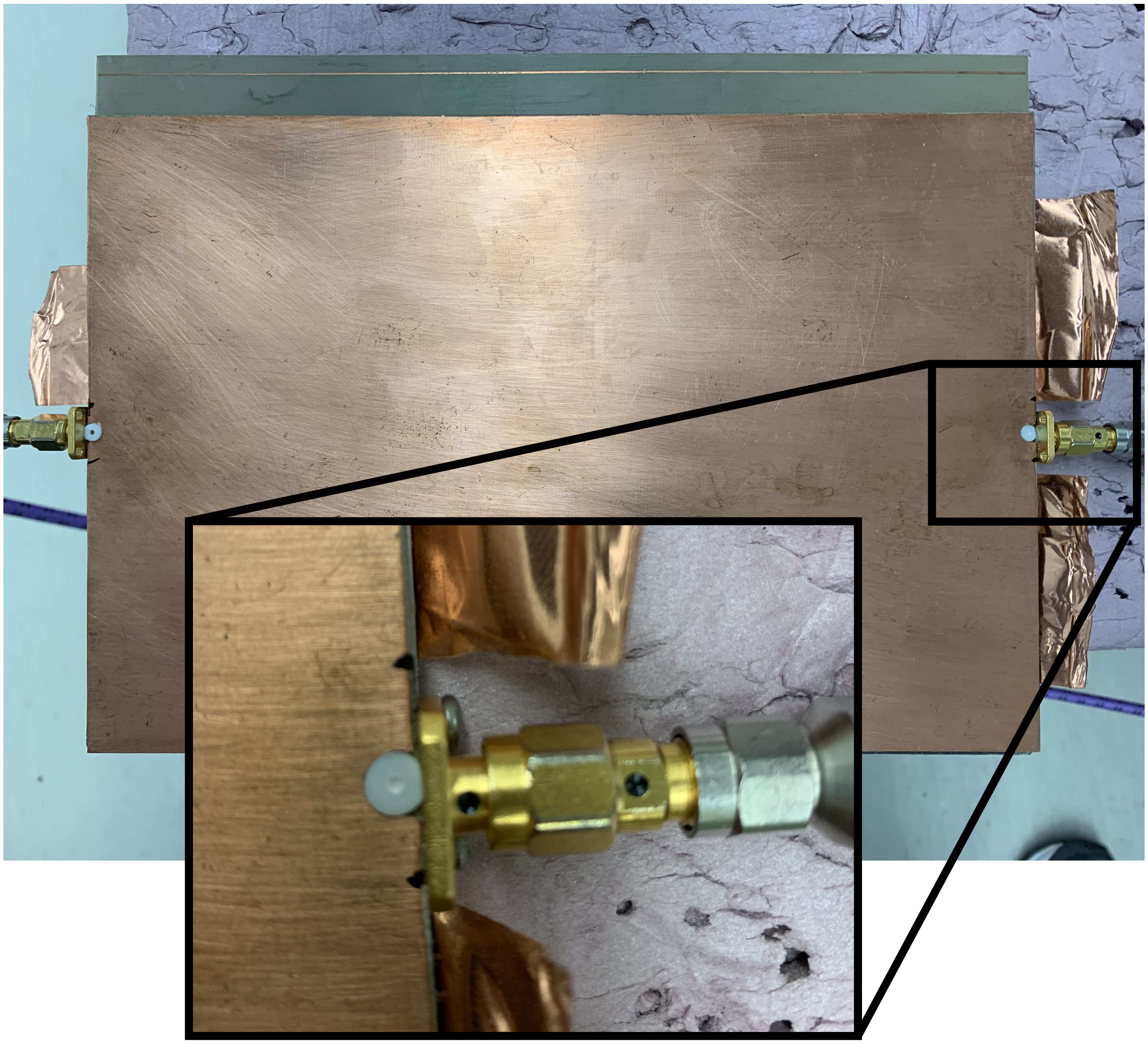

Figure 4.14: "Mouse hole" filled with Teflon dielectric

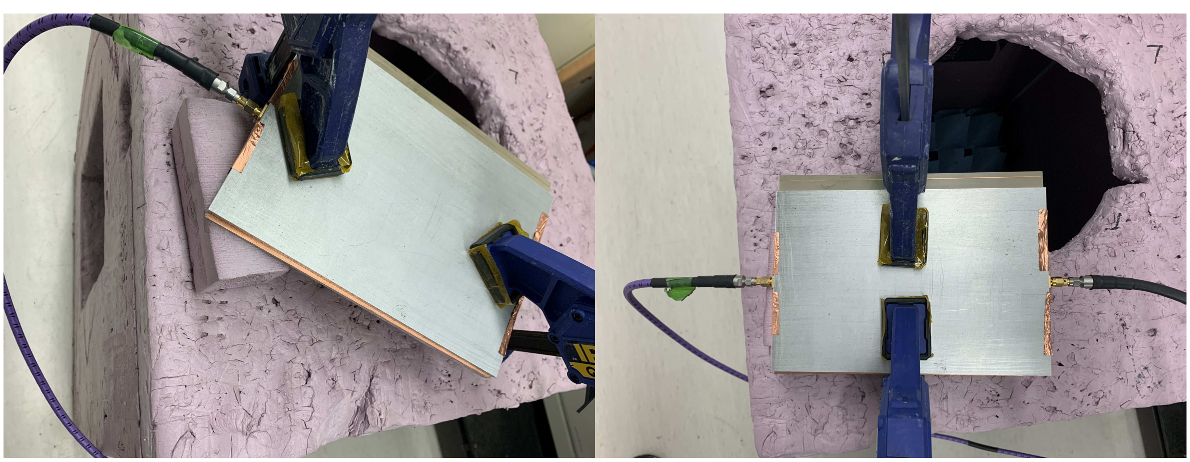

Figure 4.15: Final clamped stripline circuit

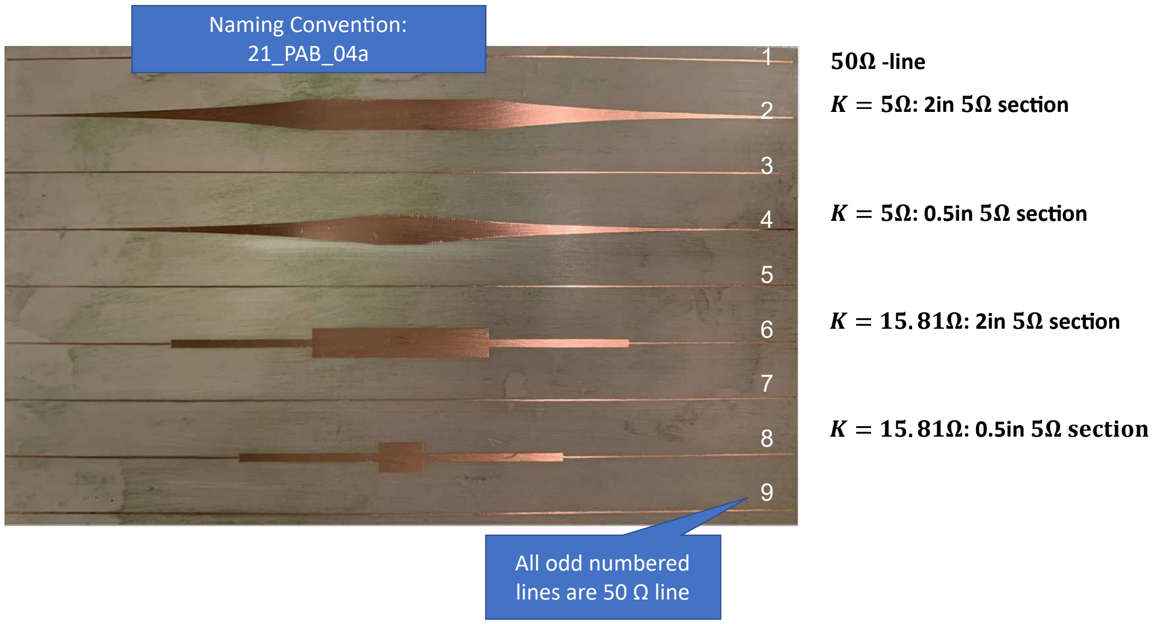

Figure 4.16: Circuit Board 21 PAB 04a

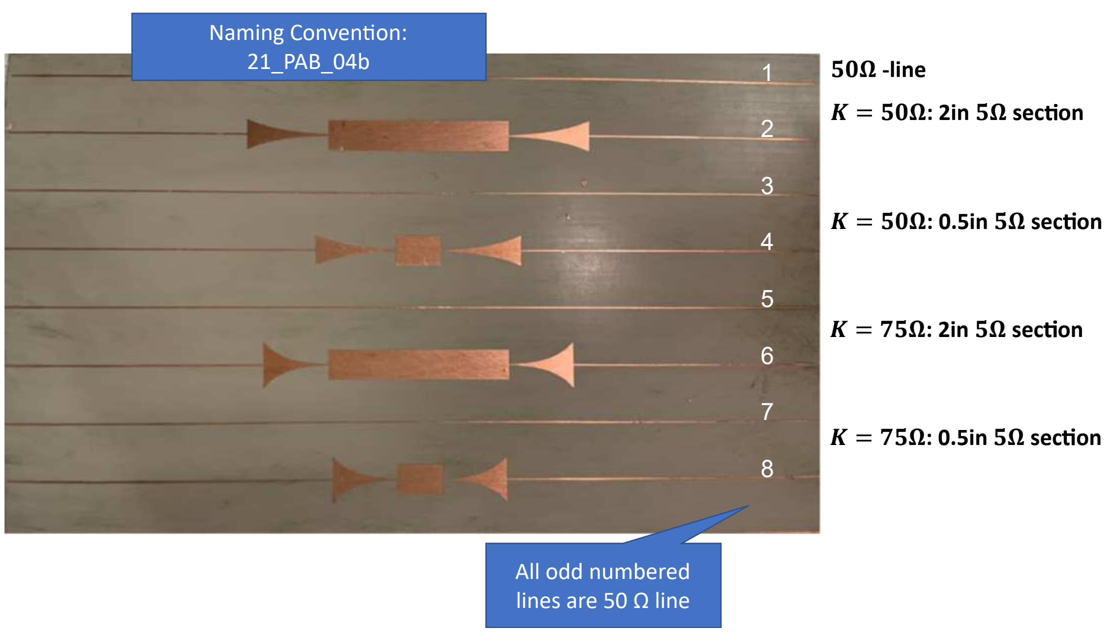

Figure 4.17: Circuit Board 21 PAB 04b

middle. This section of 5 Ω transmission line acts as a Z_{00} section that needs to be matched to the $R_L = 50$ Ω section at either end of the line. The 50 Ω sections provide a convenient location to connect to a 50 Ω network analyzer with minimal reflections at the coax-stripline transition. HFSS models of the eight back-to-back circuits were also created as a control to allow the fabrication and testing anomalies to be examined. These boards are shown in detail in Figures 4.16 and 4.17.

As an example of measurement data from back-to-back circuits, Figure 4.18 shows the measured values for $|S_{11}|$ for the first trace at the top of Figure 4.16. This measurement is labeled "21_PAB_04a #2". The first stripline circuit in the top of Figure 4.16 is a 50 Ω trace constructed as a boundary between trace #2 and the edge of the board. Therefore, trace "21_PAB_04a #2" is an exponential impedance tranforming circuit with $Z_{00} = K = 5$ Ω and a 2" central $R_L = 50$ Ω, section. Figure 4.18 shows both the fabricated circuit measurement $|S_{11}|$ and its corresponding HFSS model. At first glance, the frequency response seems rather complicated compared to typical reflection coefficient plots for impedance transformers. Looking specifically at the reflection coefficient of the HFSS circuit in Figure 4.18, it is clear that there is a passband around the design frequency $\omega/\omega_0 = 1$ or 1 GHz. There is a general agreement in the shape of the reflection coefficient over frequency, but the measured response is clearly shifted higher in frequency. Of the eight measured circuits, this one has the worst correlation to the HFSS model.

There are a few reasons why the reflection coefficient measurement for "21_PAB_04a #2" has the worst correlation of all the measured stripline circuits. This exponential taper is the longest of the eight circuits with a relatively long, 2-inch $R_L = 5$ Ω section. This means there are relatively short leading $Z_L = 50$ Ω sections, and the coax stripline section is close to the beginning of the tapered section, where the small air gaps and Teflon section in the "mouse hole" are located. This was also the first trace that was measured after fabrication, and one end of the trace delaminated from the board and broke off. It was replaced with a piece of copper tape soldered in place. The small bump from the solder, surely increased the small air gap on the trace near the tapered section of the exponential line. It makes sense, that the frequency response would be shifted higher in frequency when the design was created expecting homogeneous $\epsilon_r = 3.5$ stripline, but the

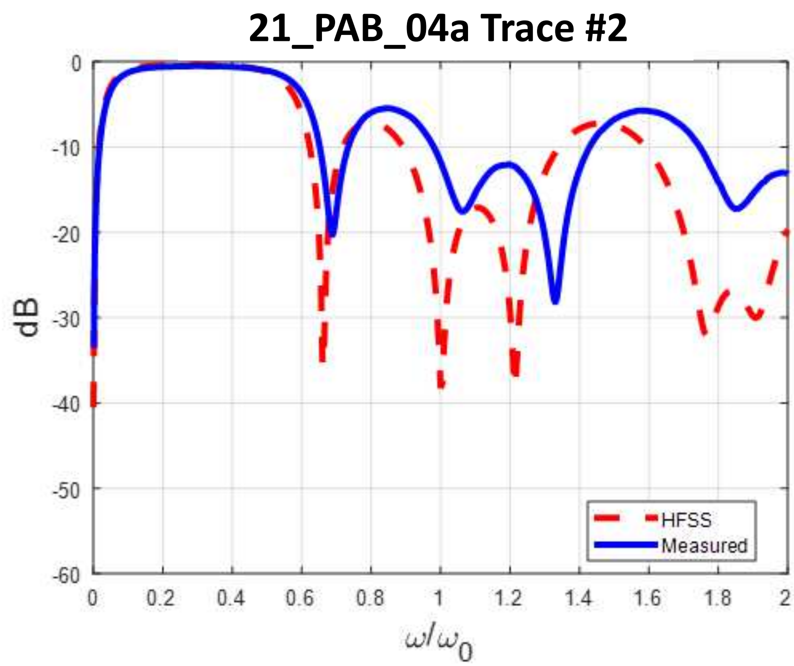

Figure 4.18: Trace 2 Results Measured Compared to HFSS

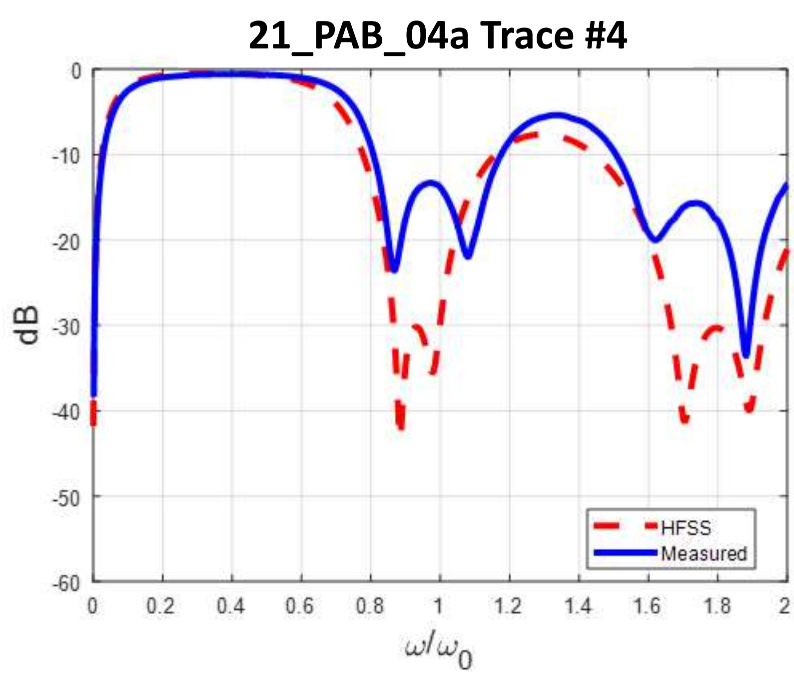

Figure 4.19: 21 PAB 04a Trace 4 Results Measured Compared to HFSS

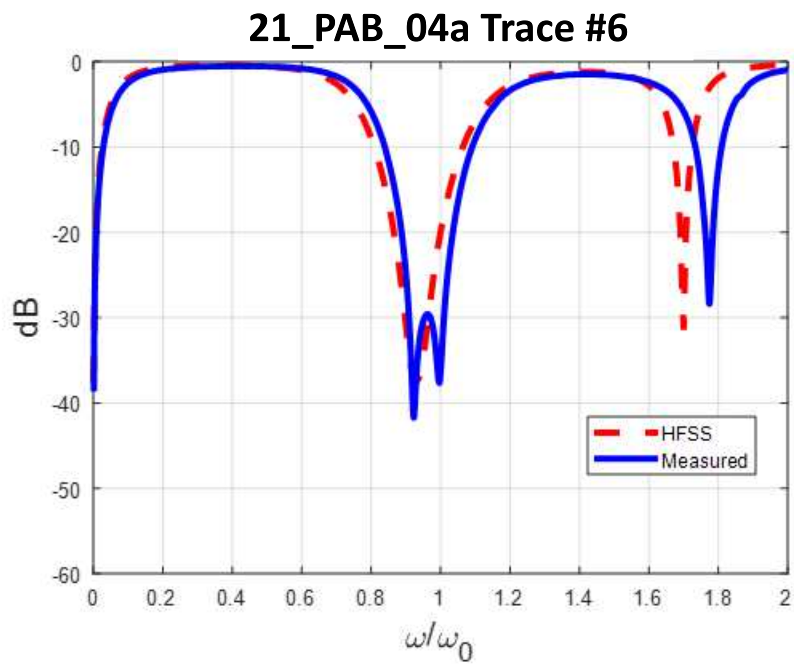

Figure 4.20: 21 PAB 04a Trace 6 Results Measured Compared to HFSS

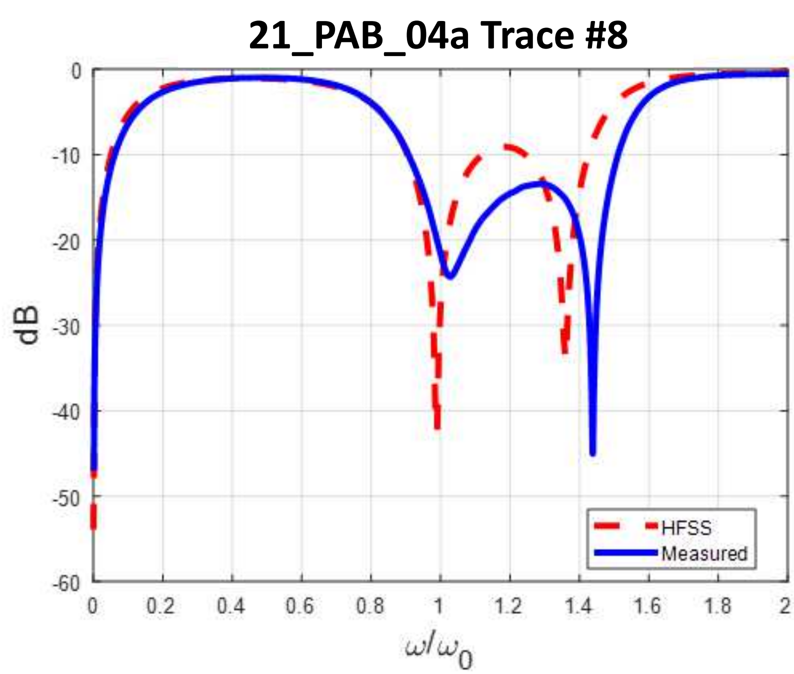

Figure 4.21: 21 PAB 04a Trace 8 Results Measured Compared to HFSS

measured circuit has the $\epsilon_r = 3.5$ with a significant pocket of error on one side of the trace.

Reflection coefficient measurements for “21_PAB_04a #4” are shown in Figure 4.19. This is the second longest circuit fabricated, but does not have the mechanically repaired characteristics of “21_PAB_04a #2”. The comparison of HFSS to fabricated $|S_{11}|$ result is better, and in general correlates rather well. There is a significant upward frequency shift of the measured data around the design frequency, $\omega/\omega_0 = 1$.

Figures 4.20 and 4.21 show the reflection coefficients for the two quarter-wave transformer circuits associated with “21_PAB_04a #6” and “21_PAB_04a #8” in Figure 4.16. The quarter-wave transformer circuits do show some upward shift in frequency that may be associated with very small separations between the two halves of the stripline board, but in general show good agreement, and the deviations between measured and HFSS data are a good representation of what sensitivities impedance transformers have to fabrication anomalies of prototype circuits built in a university laboratory.

The $|S_{11}|$ measurements for the circuits shorter than the quarter-wave transformers that have a negative sloped exponential taper ($N < 0$), are shown in Figures 4.22 through 4.25. These circuits are all shown on board “21_PAB_04b” in Figure 4.17. While these circuits are known to have narrow bandwidth regions of small reflection coefficient, and would be expected to be sensitive to fabrication abnormalities, the agreement between fabrication and HFSS is very good. It is still difficult to see the expected frequency response of the single ended impedance transformer by looking at the back-to-back measurements in Figures 4.22 through 4.25. It is necessary to somehow reduce the circuit in half of to eliminate the complicated multi-resonance response seen in the back-to-back measurements. This technique for the back-to-back to single-ended circuit reduction will be shown in the next section.

4.2.4 Retrieving Single-Ended S-Parameters for the Impedance Transformer

For each type of taper, a circuit was fabricated with two different lengths of $5\,\Omega$ central section, 0.5” and 2” were selected. This type of back-to-back circuit allows for measurements to be

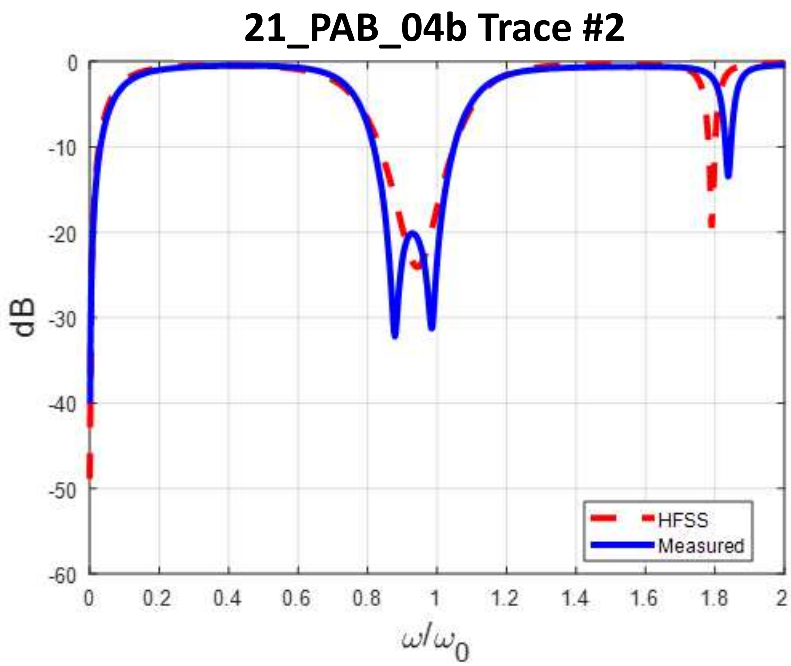

Figure 4.22: 21 PAB 04b Trace 2 Results Measured Compared to HFSS

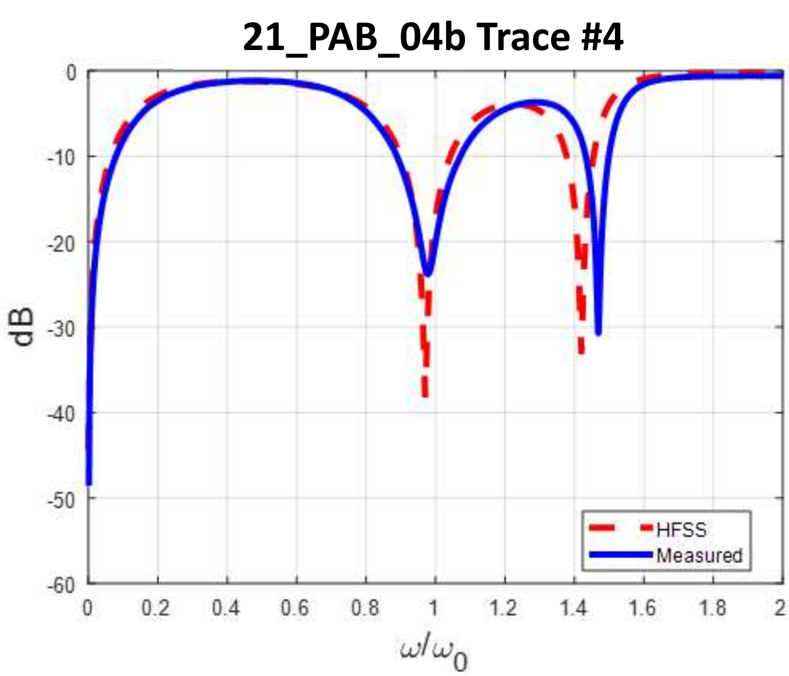

Figure 4.23: 21 PAB 04b Trace 4 Results Measured Compared to HFSS

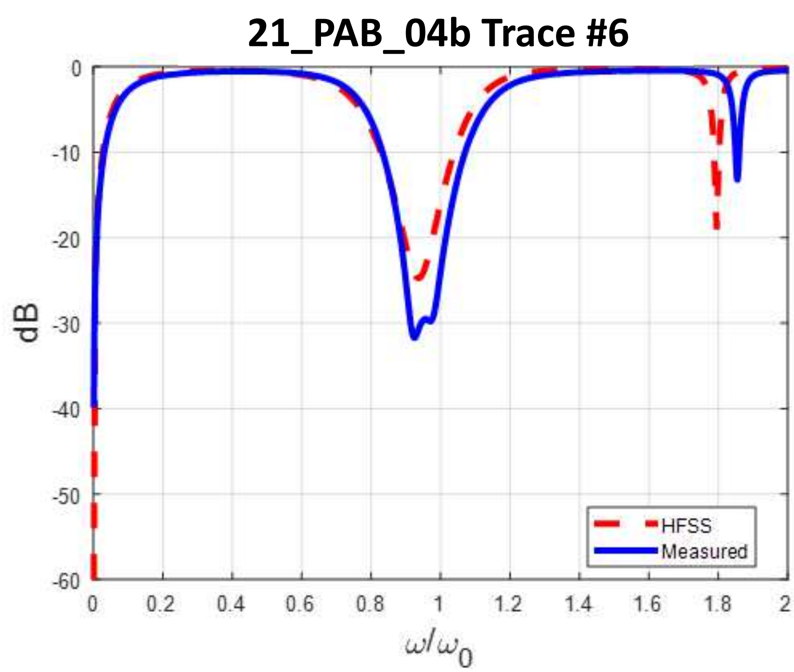

Figure 4.24: 21_PAB_04b Trace 6 Results Measured Compared to HFSS

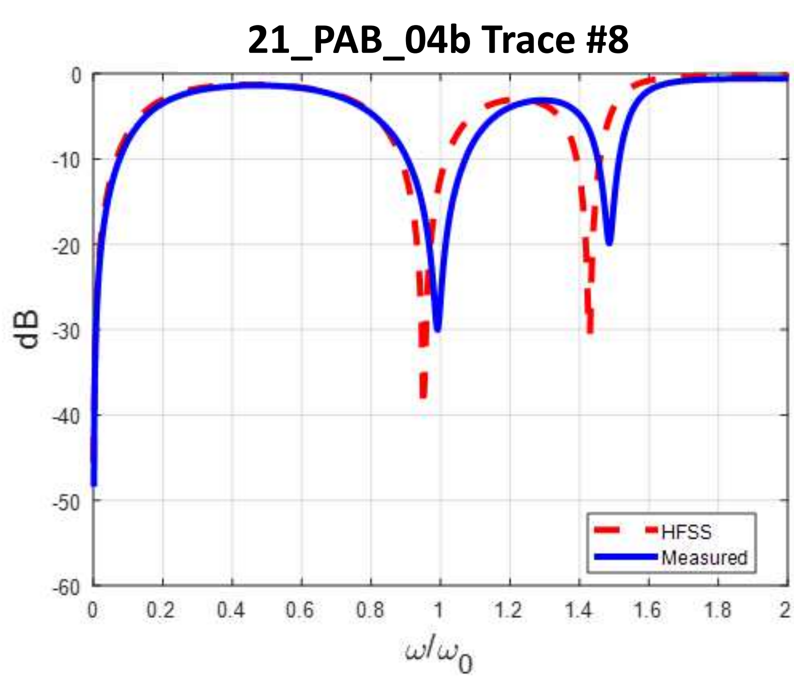

Figure 4.25: 21_PAB_04b Trace 8 Results Measured Compared to HFSS

carried out using $50\,\Omega$ connectors and network analyzer calibration. Typical results for two sets of 2-port S-parameters measured for back-to-back circuits have already been shown in Figures 4.18 - 4.25. Figure 4.26 shows $|S_{11}|$ measurements for two back-to-back circuits of the quarter-wave transformer with different $5\,\Omega$ central sections. It is interesting to note, that neither of these measurements give a very good indication of what a single-ended circuit performance might look like which will be shown in Figure 4.27.

Measured S-parameters for the back-to-back circuits can be used to extract the single-ended S-parameters for one half of the fabricated circuits [33] as follows:

$$S_{11} = \frac{S_{11}^{I} S_{21}^{II} e^{-\gamma l_2} - S_{11}^{II} S_{21}^{I} e^{-\gamma l_1}}{S_{21}^{II} e^{-\gamma l_2} - S_{21}^{I} e^{-\gamma l_1}} \tag{4.1}$$

$$S_{22} = \frac{S_{11}^{II} - S_{11}^{I}}{S_{21}^{II} e^{-\gamma l_2} - S_{21}^{I} e^{-\gamma l_1}} \tag{4.2}$$

$$S_{21}^{2} = \frac{2 S_{21}^{II} S_{21}^{I} \sinh[\gamma(l_1 - l_2)]}{S_{21}^{II} e^{-\gamma l_2} - S_{21}^{I} e^{-\gamma l_1}} \tag{4.3}$$

where S_{ik}^{I} are the measured S-parameters for a central section of length l_1, S_{ik}^{II} are the measured S-parameters for a central section of length l_2 and γ is the complex propagation constant of the central section.

The result for a quarter-wave transformer as shown in Figure 3.5 “d” has been computed. Measured back-to-back S-parameter data from Figure 4.26 have been used to extract single-ended $|S_{11}|$ shown in Figure 4.27. Likewise, for the additional circuits shown in Figures 3.5 “e”, “f”, and “b” extracted results are shown in Figures 4.28, 4.29, and 4.30 respectively. In all of these cases, the design frequency was 1 GHz.

Similar to Figure 4.6, the full-wave results shown in Figures 4.27, 4.28,and 4.29 show lowered match frequencies. Fabricated stripline results show the resonant frequency shifted slightly higher in frequency than HFSS, most likely due to the introduction of small air gaps around the stripline circuit where the two halves of the stripline circuit were pressed together. Higher frequency measurements, $\omega/\omega_0 > 1.2$, show some irregularities in the measurement that are indicative

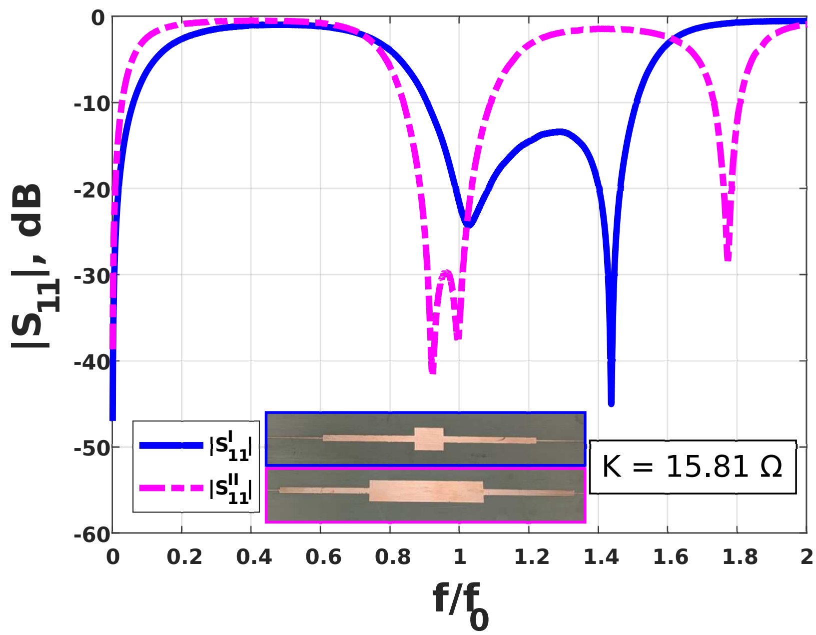

Figure 4.26: Measured $|S_{11}^{I,II}|$ for two back-to-back quarter-wave transformer circuits.

of fabrication issues rather than design inconsistencies. In general, measured results compare well to theoretical and full-wave simulated results.

Recall that the measurement for the exponential line impedance transformer with no impedance discontinuities, $K = 5\,\Omega$ had the back-to-back measurements with the most inconsistencies due to the impedance taper starting so close to the connector location, and the need to repair damaged traces (see Figures 4.18 and 4.19). The resultant single ended measurement shown in Figure 4.30 is likewise correlates poorly to analytical or HFSS results. Considering the difficulties in collecting usable data for these longer traces, the resulting single ended $|S_{11}|$ for single-ended data is not as bad as might have been expected. The main resonance occurs 15-20% higher than the design frequency, but $|S_{11}| < -20dB$ is still realized. The second resonance around 1.9 GHz is present, and overall the general shape of the $|S_{11}|$ is qualitatively correct.

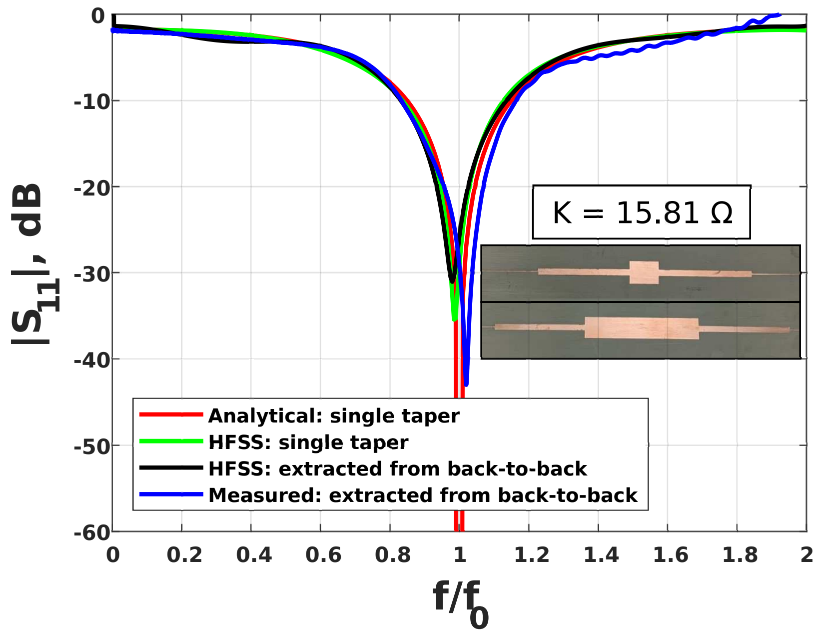

Figure 4.27: Quarter-wave transformer: Comparison of single ended $|S_{11}|$ computed analytically, modeled in HFSS, extracted from HFSS back-to-back stripline circuits, and extracted from measurements of physical stripline circuits.

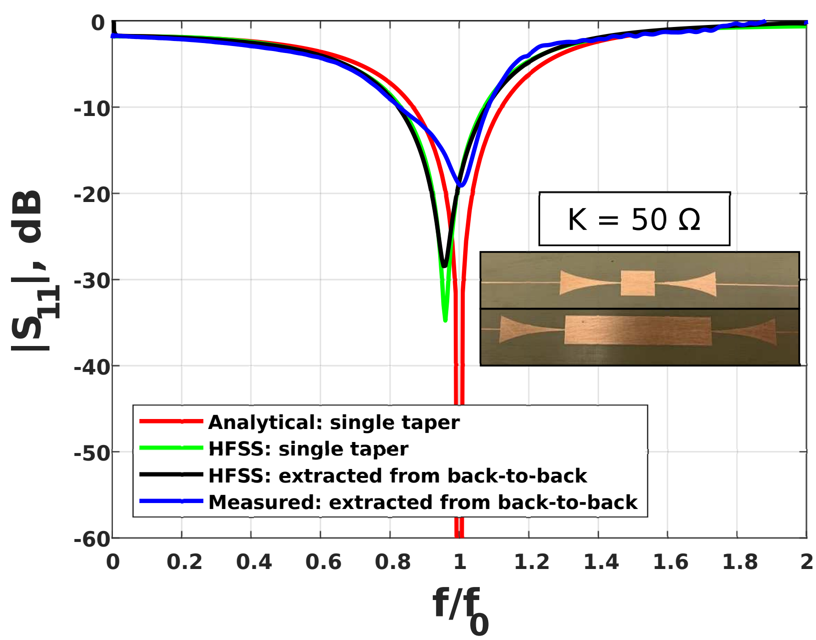

Figure 4.28: Exponential with $K = 50\ \Omega$: Comparison of single ended $|S_{11}|$ computed analytically, modeled in HFSS, extracted from HFSS back-to-back stripline circuits, and extracted from measurements of physical stripline circuits.

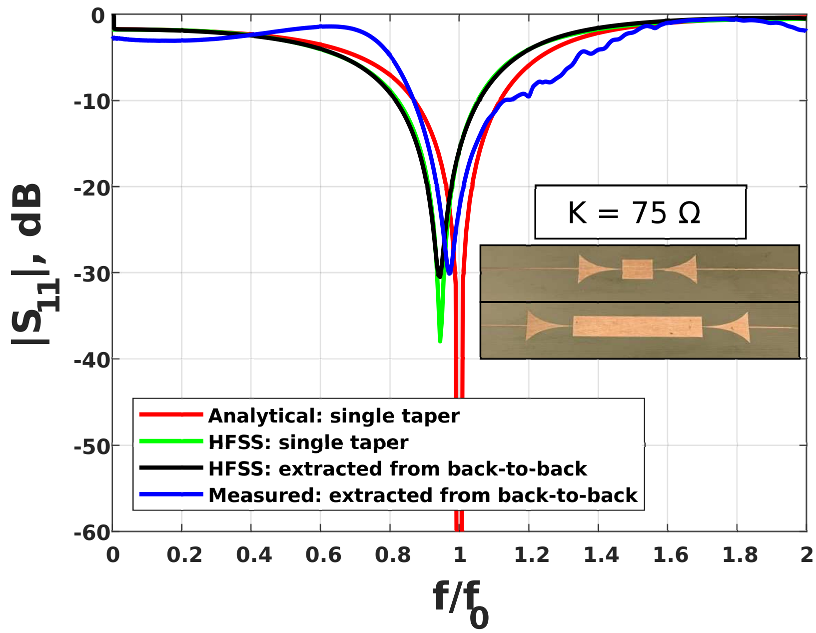

Figure 4.29: Exponential with $K = 75\ \Omega$: Comparison of single ended $|S_{11}|$ computed analytically, modeled in HFSS, extracted from HFSS back-to-back stripline circuits, and extracted from measurements of physical stripline circuits.

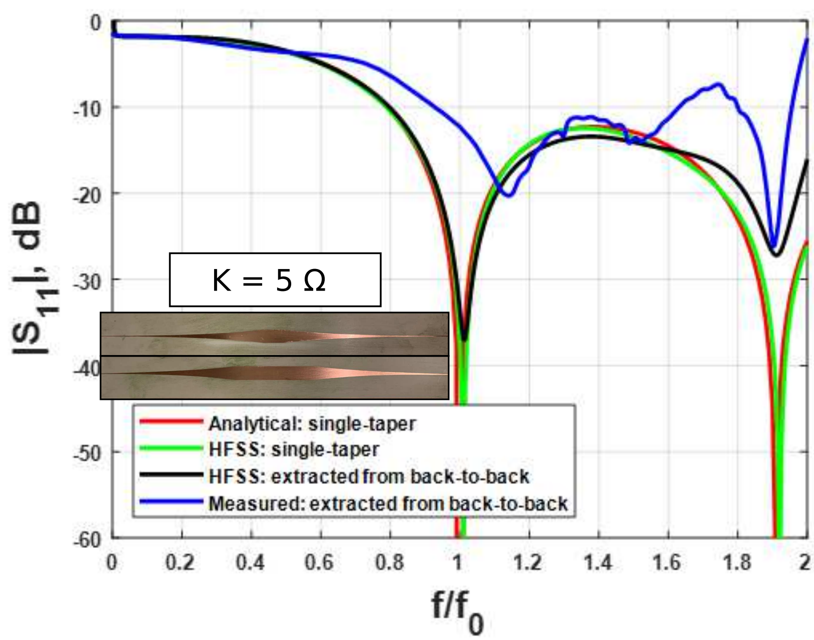

Figure 4.30: Exponential with $K = 5.0\ \Omega$: Comparison of single ended $|S_{11}|$ computed analytically, modeled in HFSS, extracted from HFSS back-to-back stripline circuits, and extracted from measurements of physical stripline circuits.

Chapter 5

Length Limits for Perfectly Matched Transmission Line Impedance Transformation

As stated in Chapter 2, an exact solution for the reflection coefficient can be found for any device with known ABCD parameters. When a very electrically short impedance transformer is required, a designer may want to know the shortest possible length before attempting a project with limited space. The ABCD matrix can be represented as a power series in terms of frequency, ω. This is a universal solution that will be accurate for any nonuniform transmission line. However, since the resulting power series is infinite and cannot be simplified universally, the number of coefficients available in the solution set will restrict the accuracy of the solution.

Although a full, infinite solution for all possible nonuniform transmission lines cannot be found by the power series expansion of the ABCD matrix, it is possible to determine a fundamental limit describing the shortest transmission line which will create a match between a given source and load impedance. This limit can also be thought of as giving the lowest frequency for which a perfect impedance match can be performed given a specific length of transmission line. One such limit has been presented using this idea [12], and an improvement to the quality of this limit is presented in this chapter.

It has been found that transmission line matching sections can be arbitrarily short if large characteristic impedance changes are allowed within the matching circuit [8]. In practical designs, parasitic effects and fabrication restrictions will limit the practical impedance between some maximum and minimum values. In the example of a stripline circuit, very high impedance lines will necessitate narrow transmission line traces. If the etch tolerance is 0.001", then a trace of 0.010" will be subject to 10% error in thickness and a corresponding error in characteristic impedance value. A trace of further increased impedance may have a width of 0.003", and would be subject to 33% error. Additionally, a trace that is designed to be only 0.001" in width, could become an open circuit due to physical gaps in the line and not function at all as an impedance transformer. For low impedance values, the traces can become so wide that higher order modes could be present on the circuit in some sections and will disturb the overall operation of the impedance transformer. For any type of transmission line, the physical characteristics of the materials and the design parameters will create an upper and lower limit for the impedance values that can be used for the matching circuit such that,

$$0 < Z_{0min} \leq Z_0 \leq Z_{0max} < \infty \tag{5.1}$$

This limitation in Z_{0max} and Z_{0min} will create a limit on the possible length for a nonuniform line impedance transformer at a specific frequency, or the lower frequency limit for an impedance transformer of known length.

5.1 Expressions for the Chain Parameters

In Chapter 2, chain parameters for a lossless nonuniform transmission line between $\tau = 0$ and an arbitrary point τ were shown to be:

$$\begin{aligned}
A(\tau) &= \sum_{n=0}^{+\infty}(j\omega)^{2n}A_n = A_0(\tau) + (j\omega)^2 A_1(\tau) + (j\omega)^4 A_2(\tau) + \ldots \\
B(\tau) &= \sum_{n=0}^{+\infty}(j\omega)^{2n+1}B_n = j\omega B_0(\tau) + (j\omega)^3 B_1(\tau) + (j\omega)^5 B_2(\tau) + \ldots \\
C(\tau) &= \sum_{n=0}^{+\infty}(j\omega)^{2n+1}C_n = j\omega C_0(\tau) + (j\omega)^3 C_1(\tau) + (j\omega)^5 C_2(\tau) + \ldots \\
D(\tau) &= \sum_{n=0}^{+\infty}(j\omega)^{2n}D_n = D_0(\tau) + (j\omega)^2 D_1(\tau) + (j\omega)^4 D_2(\tau) + \ldots
\end{aligned} \tag{5.2}$$

We substitute these expansions into (2.47) and (2.48) and equate terms with identical powers of ω. The ω^0 terms are only present in the coefficient related to A_0 and D_0

$$\frac{d}{d\tau}A_0(\tau) = \frac{d}{d\tau}D_0(\tau) = 0;$$

$$A_0(\tau) - A_0(0) = 0, \quad D_0(\tau) - D_0(0) = 0 \tag{5.3}$$

$$A_0(0) = D_0(0) = 1;$$

Therefore:

$$A_0(\tau) = D_0(\tau) \equiv 1;$$

The coefficients that are associated with ω^1 are B_0 and C_0, which are related to A_0 and D_0 as

$$\frac{d}{d\tau}B_0(\tau) = Z_0(\tau)A_0(\tau); \qquad \frac{d}{d\tau}C_0(\tau) = \frac{1}{Z_0(\tau)}D_0(\tau);$$
$$\frac{d}{d\tau}B_0(\tau) = Z_0(\tau)1; \qquad \frac{d}{d\tau}C_0(\tau) = \frac{1}{Z_0(\tau)}1;$$

$$B_0(\tau) = \int_0^\tau Z_0(\tau_1)d\tau_1; \qquad C_0(\tau) = \int_0^\tau \frac{1}{Z_0(\tau_1)}d\tau_1; \tag{5.4}$$

The ω^2 terms are then:

$$\frac{d}{d\tau}A_1(\tau) = \frac{1}{Z_0(\tau)}B_0(\tau); \qquad \frac{d}{d\tau}D_1(\tau) = Z_0(\tau)C_0(\tau)$$

Substituting what has been found for B_0 and C_0 from (5.4):

$$A_1(\tau) = \int_0^\tau \frac{1}{Z_0(\tau_1)} \int_0^{\tau_1} Z_0(\tau_2)d\tau_2\, d\tau_1; \qquad D_1(\tau) = \int_0^\tau Z_0(\tau_1) \int_0^{\tau_1} \frac{1}{Z_0(\tau_2)}d\tau_2\, d\tau_1 \tag{5.5}$$

and in general we have:

$$\begin{aligned} \frac{d}{d\tau}A_{n+1}(\tau) &= \frac{1}{Z_0(\tau)}B_n(\tau); & \frac{d}{d\tau}D_{n+1}(\tau) &= Z_0(\tau)C_n(\tau) \\ \frac{d}{d\tau}B_{n+1}(\tau) &= Z_0(\tau)A_{n+1}(\tau); & \frac{d}{d\tau}C_{n+1}(\tau) &= \frac{1}{Z_0(\tau)}D_{n+1}(\tau); \end{aligned} \tag{5.6}$$

for $n \geq 0$. The initial conditions for these equations are

$$A_n(0) = D_n(0) = 0 \quad (n > 0);$$

$$B_n(0) = C_n(0) = 0 \quad (n \geq 0)$$

and in general:

$$\begin{aligned}
A_{n+1}(\tau) &= \int_0^\tau \frac{1}{Z_0(\tau_1)} B_n(\tau_1)\, d\tau_1 \\
B_{n+1}(\tau) &= \int_0^\tau Z_0(\tau_1) A_{n+1}(\tau_1)\, d\tau_1 \\
D_{n+1}(\tau) &= \int_0^\tau Z_0(\tau_1) C_n(\tau_1)\, d\tau_1 \\
C_{n+1}(\tau) &= \int_0^\tau \frac{1}{Z_0(\tau_1)} D_{n+1}(\tau_1)\, d\tau_1
\end{aligned} \tag{5.7}$$

so we can solve the differential equations recursively by quadratures. With the exception of the constants A_0 and D_0, all of the coefficients $A_n(\tau)$, $B_n(\tau)$, $C_n(\tau)$ and $D_n(\tau)$ are positive monotonically increasing functions of τ.

We start with:

$$A_0(\tau) = D_0(\tau) \equiv 1;$$

From (5.4), recall:

$$B_0(\tau) = \int_0^\tau Z_0(\tau_1)\, d\tau_1; \qquad C_0(\tau) = \int_0^\tau \frac{1}{Z_0(\tau_1)}\, d\tau_1$$

Limits for the $Z_0(\tau)$ function of the nonuniform line use the observation about maximum and minimum values for $Z(\tau)$ in a given configuration from (5.1). We can then obtain bounds for the coefficients $A_n(\tau)$, $B_n(\tau)$, $C_n(\tau)$ and $D_n(\tau)$. For B_0 and C_0 this gives,

$$B_0(\tau) \leq \int_0^\tau Z_{0max}\, d\tau_1 = Z_{0max}(\tau); \qquad C_0(\tau) \leq \int_0^\tau \frac{1}{Z_{0min}} = \frac{\tau}{Z_{0min}}\, d\tau_1$$

Recalling (5.5),

$$A_1(\tau) = \int_0^\tau \frac{1}{Z_0(\tau_1)} \left[\int_0^{\tau_1} Z_0(\tau_2) d\tau_2 \right] d\tau_1; \qquad D_1(\tau) = \int_0^\tau Z_0(\tau_1) \left[\int_0^{\tau_1} \frac{1}{Z_0(\tau_2)} d\tau_2 \right] d\tau_1$$

The upper limits on the coefficients for A_1 and D_1 are then:

$$A_1(\tau) \leq \int_0^\tau \frac{1}{Z_{0min}} \left[\int_0^{\tau_1} Z_{0max} d\tau_2 \right] d\tau_1; \qquad D_1(\tau) \leq \int_0^\tau Z_{0max} \left[\int_0^{\tau_1} \frac{1}{Z_{0min}} \tau_1 d\tau_2 \right] d\tau_1 \tag{5.8}$$

Z_{0min} and Z_{0max} in (5.8) are no longer functions of τ, but constants that can be brought outside the integral:

$$A_1(\tau) \leq \frac{Z_{0max}}{Z_{0min}} \int_0^{\tau} \left[\int_0^{\tau_1} 1 \, d\tau_2 \right] d\tau_1; \qquad D_1(\tau) \leq \frac{Z_{0max}}{Z_{0min}} \int_0^{\tau} \left[\int_0^{\tau_1} 1 \, d\tau_2 \right] d\tau_1$$

Then evaluating the inner integrals, we have:

$$A_1(\tau) \leq \frac{Z_{0max}}{Z_{0min}} \int_0^{\tau} \tau_1 d\tau_1; \qquad D_1(\tau) \leq \frac{Z_{0max}}{Z_{0min}} \int_0^{\tau} \tau_1 d\tau_1$$

and upon integrating,

$$A_1(\tau) \leq \frac{Z_{0max}}{Z_{0min}} \left(\frac{\tau^2}{2} - \frac{0}{2} \right); \qquad D_1(\tau) \leq \frac{Z_{0max}}{Z_{0min}} \left(\frac{\tau^2}{2} - \frac{0}{2} \right)$$

$$A_1(\tau) \leq \frac{Z_{0max}}{Z_{0min}} \left(\frac{\tau^2}{2} \right); \qquad D_1(\tau) \leq \frac{Z_{0max}}{Z_{0min}} \left(\frac{\tau^2}{2} \right) \tag{5.9}$$

Using (5.7) and the solutions for A_1 and B_1 from (5.9), solutions for the upper limits of B_1 and C_1 are found:

$$B_1(\tau) \leq \int_0^{\tau} Z_{0max} A_1(\tau_1) \, d\tau_1; \qquad C_1(\tau) \leq \int_0^{\tau} \frac{1}{Z_{0min}} D_1(\tau_1) \, d\tau_1$$

$$B_1(\tau) \leq \int_0^{\tau} Z_{0max} \frac{Z_{0max}}{Z_{0min}} \left(\frac{\tau_1^2}{2} \right) d\tau_1; \qquad C_1(\tau) \leq \int_0^{\tau} \frac{1}{Z_{0min}} \frac{Z_{0max}}{Z_{0min}} \left(\frac{\tau_1^2}{2} \right) d\tau_1$$

$$B_1(\tau) \leq Z_{0max} \frac{Z_{0max}}{Z_{0min}} \int_0^{\tau} \left(\frac{\tau_1^2}{2} \right) d\tau_1 \, ; \qquad C_1(\tau) \leq \frac{1}{Z_{0min}} \frac{Z_{0max}}{Z_{0min}} \int_0^{\tau} \left(\frac{\tau_1^2}{2} \right) d\tau_1$$

$$B_1(\tau) \leq Z_{0max} \frac{Z_{0max}}{Z_{0min}} \left(\frac{\tau^3}{6} \right); \qquad C_1(\tau) \leq \frac{1}{Z_{0min}} \frac{Z_{0max}}{Z_{0min}} \left(\frac{\tau^3}{6} \right) \tag{5.10}$$

When A_n, etc. are written without an argument, it will be assumed that $\tau = T$: $A_n(T) \equiv A_n$ and so on, where T is the total "length" (i. e., time delay) of the entire section of nonuniform line. The bounds for the coefficients in the series (5.2) are found by mathematical induction:

$$\left(\frac{Z_{0min}}{Z_{0max}} \right)^n \frac{T^{2n}}{(2n)!} \leq A_n \leq \left(\frac{Z_{0max}}{Z_{0min}} \right)^n \frac{T^{2n}}{(2n)!}$$

$$\left(\frac{Z_{0min}}{Z_{0max}} \right)^n Z_{0min} \frac{T^{2n} + 1}{(2n+1)!} \leq B_n \leq \left(\frac{Z_{0max}}{Z_{0min}} \right)^n Z_{0max} \frac{T^{2n+1}}{(2n+1)!}$$

$$\left(\frac{Z_{0min}}{Z_{0max}}\right)^n \frac{1}{Z_{0max}} \frac{T^{2n}+1}{(2n+1)!} \leq C_n \leq \left(\frac{Z_{0max}}{Z_{0min}}\right)^n \frac{1}{Z_{0min}} \frac{T^{2n+1}}{(2n+1)!}$$

$$\left(\frac{Z_{0min}}{Z_{0max}}\right)^n \frac{T^{2n}}{(2n)!} \leq D_n \leq \left(\frac{Z_{0max}}{Z_{0min}}\right)^n \frac{T^{2n}}{(2n)!} \tag{5.11}$$

5.2 Matching Using the Chain Matrix

Recall from Chapter 2 the matched condition (2.5) from the ABCD solution of a matching circuit. The two necessary conditions required for a match are given by (2.6) and (2.7) and are rewritten below for clarity:

$$M = AZ_{02} - DZ_{01} = 0 \tag{5.12}$$

$$P = B - CZ_{01}Z_{02} = 0 \tag{5.13}$$

For a lossless circuit, the ABCD condition for the real portion of the reflection coefficient (5.12) has been named as the variable M, and the imaginary portion (5.13) is denoted with the variable P. Both have been set to 0 to enforce a matched condition with $S_{11} = \Gamma_0 = 0$. Figure 5.1 shows how $M = 0$ and $P = 0$ are satisfied by a quarter-wave transformer. The length, $\lambda/4$, creates a condition where $A = D = 0$ at the design frequency thereby creating the $M = 0$ condition regardless of the values of $Z_{01} = Z_{00}$ and $Z_{02} = R_L$. $P = 0$ for the quarter-wave transformer is accomplished at the design frequency and its odd multiples when the impedance of the uniform line has a value of $\sqrt{Z_{01}Z_{02}}$.

The conditions are also shown for an exponential line with no discontinuities and the impedance matching conditions $M = 0$ and $P = 0$ in Figure 5.2. In this case, $M = 0$ is achieved by a correct scaling of A and D to correspond to the 10:1 impedance discontinuity. The length of the exponential line then satisfies (5.13) since that length creates a point where B and C cross at zero and therefore satisfy $P = 0$.

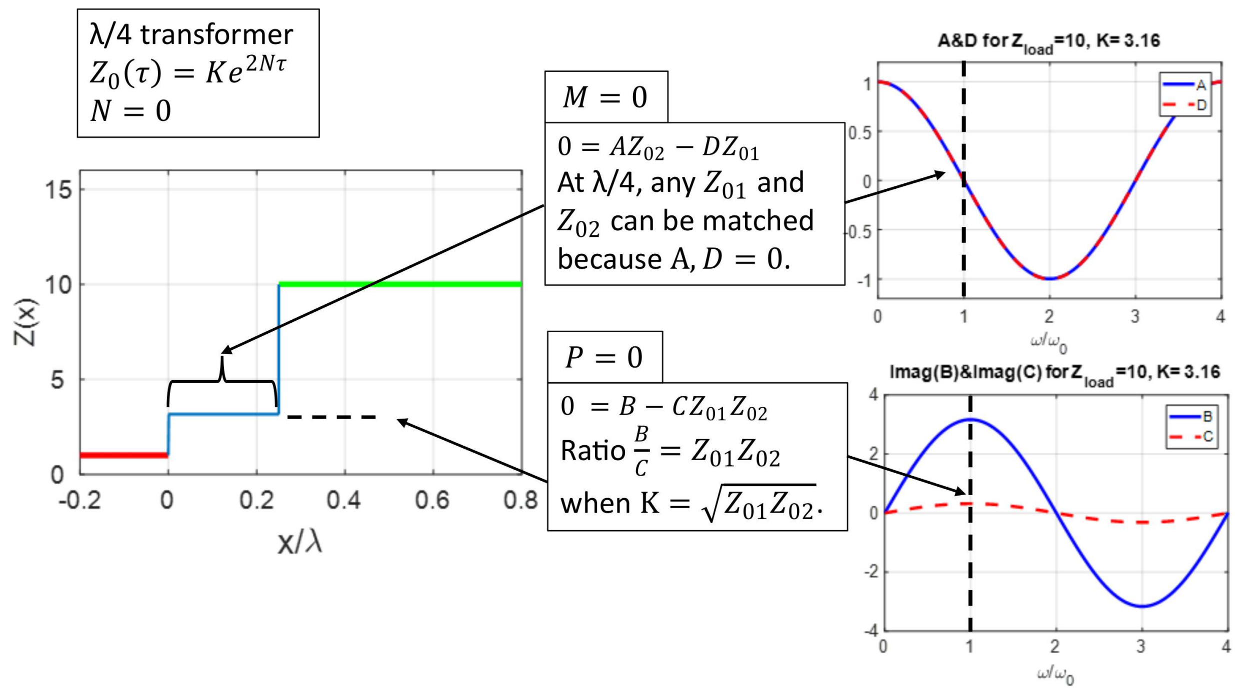

Figure 5.1: Quarter-wave transformer relationship between A, B, C, and D for matched condition.

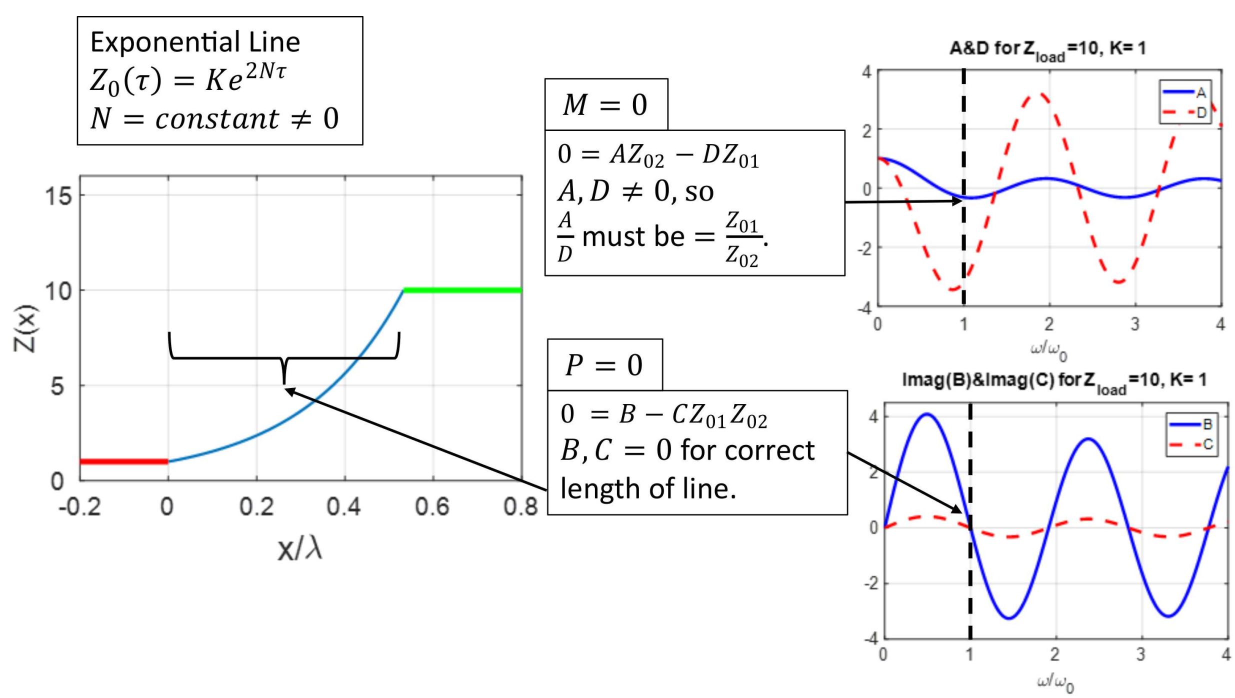

Figure 5.2: Exponential line relationship between A, B, C, and D for matched condition.

All transmission line impedance transformers create a combination of $M = 0$ and $P = 0$ conditions through line length and taper characteristics. While the two examples in Figures 5.1 and 5.2 have readily solvable ABCD parameters, by the use of the nested integrals of (5.7), all transmission line ABCD parameters can in principle be solved. The accuracy of the solution will depend on the number of coefficients that are computed.

5.3 Using the Coefficient Limits to Define a Length Limit

An initial but rather crude transmission line length limit for a particular impedance maximum and minimum on the nonuniform line was found in [12] and is shown in Figure 5.12 below. The bounds found there are not restricted to real ω , and can be quite poor. Here we will derive an improved bound for real-life circuits by using positive, real frequencies, ω from the start.

5.3.1 Satisfying $M = 0$

Applying (5.2) to (5.12) gives,

$$M = \sum_{n=0}^{+\infty}(j\omega)^{2n}A_nZ_{02} - \sum_{n=0}^{+\infty}(j\omega)^{2n}D_nZ_{01} = 0 \tag{5.14}$$

or, since $j^2 = -1$:

$$M = \sum_{n=0}^{+\infty}(-1)^n(\omega)^{2n}A_nZ_{02} - \sum_{n=0}^{+\infty}(-1)^n(\omega)^{2n}D_nZ_{01} = 0 \tag{5.15}$$

Since A_n and D_n are all positive and real, it is clear in (5.15) which coefficients will be positive or negative, so we regroup the terms as

$$M(\omega) = (A_p - A_m)Z_{02} - (D_p - D_m)Z_{01} = 0 \tag{5.16}$$

where A_p and D_p are the terms of (5.15) that will be positive and A_m and D_m are the terms that will be negative.

Forcing $M(\omega) = 0$ and re-arranging so both sides are positive,

$$A_pZ_{02} + D_MZ_{01} = A_mZ_{02} + D_pZ_{01} \tag{5.17}$$

Each half of this equation can be given a name for the purpose of finding where the two are equal:

$$\begin{aligned} F(\omega) &= A_p Z_{02} + D_m Z_{01} \\ G(\omega) &= A_m Z_{02} + D_p Z_{01} \end{aligned} \tag{5.18}$$

Expressions for F and G above (5.18) can be set to be equal to each other for a match of the circuit when all of the parameters are known. This is shown in Figure 5.3. Bounds on F and G are also useful for defining the length limits below which a match will not be possible for a particular Z_{0max} and Z_{0min}.

A few more quantities are defined to relate (5.18) to the chain parameter limits (5.11). Let $A_{lp}(\omega)$ be defined using the lower limits of the coefficients for A from (5.11) using only the even values of n in (5.15). Likewise, D_{lm} is defined from the **negative** coefficients of D_l from (5.15).

$$\begin{aligned} A_{lp}(\omega) = 1 + (W_l^2)^2 \frac{T^4}{4!}(\omega^4) + (W_l^2)^4 \frac{T^8}{8!}(\omega^8) + ... \\ D_{lm}(\omega) = 1 + (W_l^2) \frac{T^2}{2!}(\omega^2) + (W_l^2)^3 \frac{T^6}{6!}(\omega^6) + ... \end{aligned} \tag{5.19}$$

where

$$W_u^2 = \frac{Z_{0max}}{Z_{0min}}$$

and

$$W_l^2 = \frac{Z_{0min}}{Z_{0max}}$$

A lower limit for F is then:

$$F_l(\omega) = A_{lp}(\omega) Z_{02} + D_{lm}(\omega) Z_{01} \tag{5.20}$$

Similarly, defining A_{um} using the negative coefficients of the lower limit of the coefficients of A, and D_{up} as the lower bounds of the positive coefficients of D, an upper limit for G is obtained as:

$$G_u(\omega) = A_{um}(\omega) Z_{02} + D_{up}(\omega) Z_{01} \tag{5.21}$$

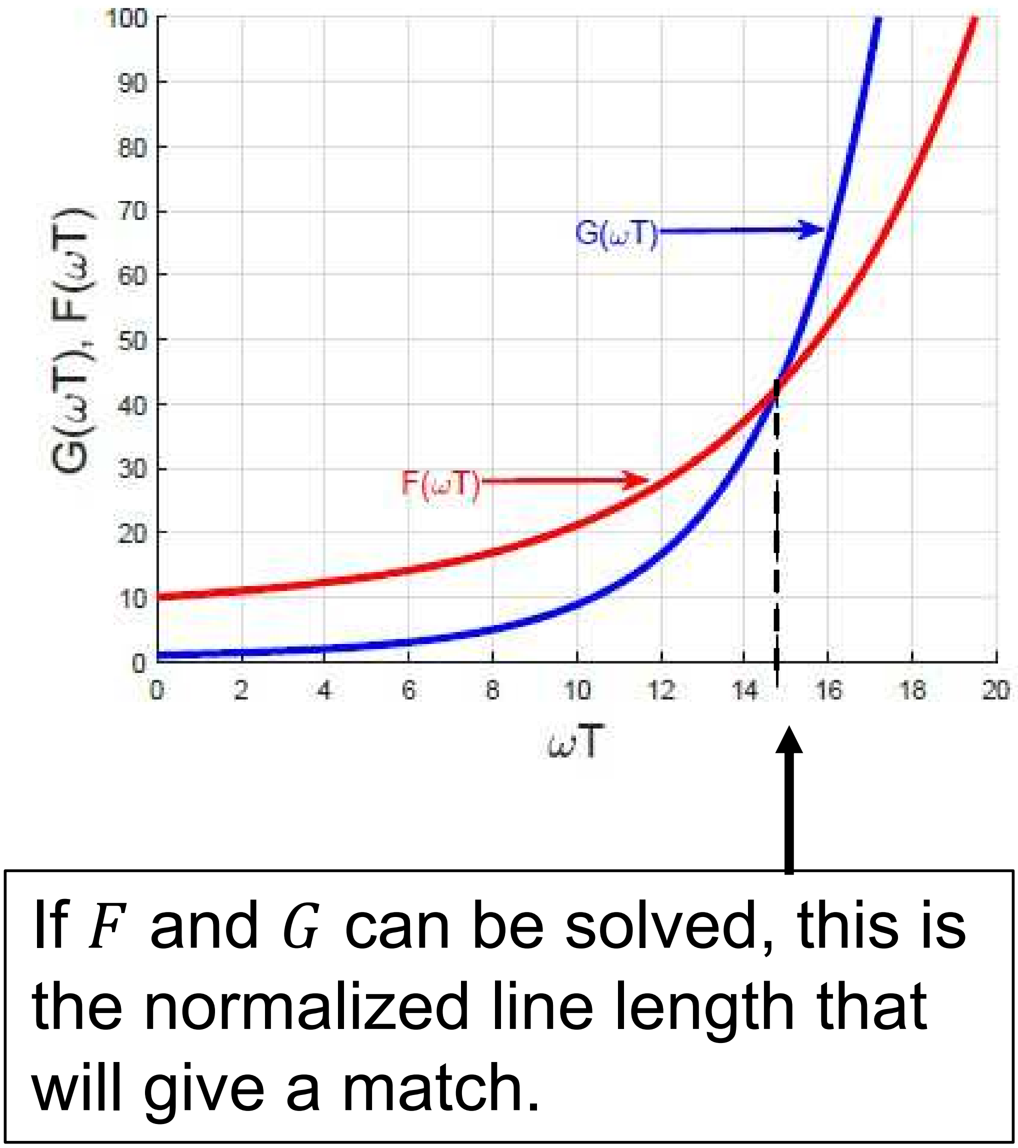

Figure 5.3: Location of typical exact impedance match

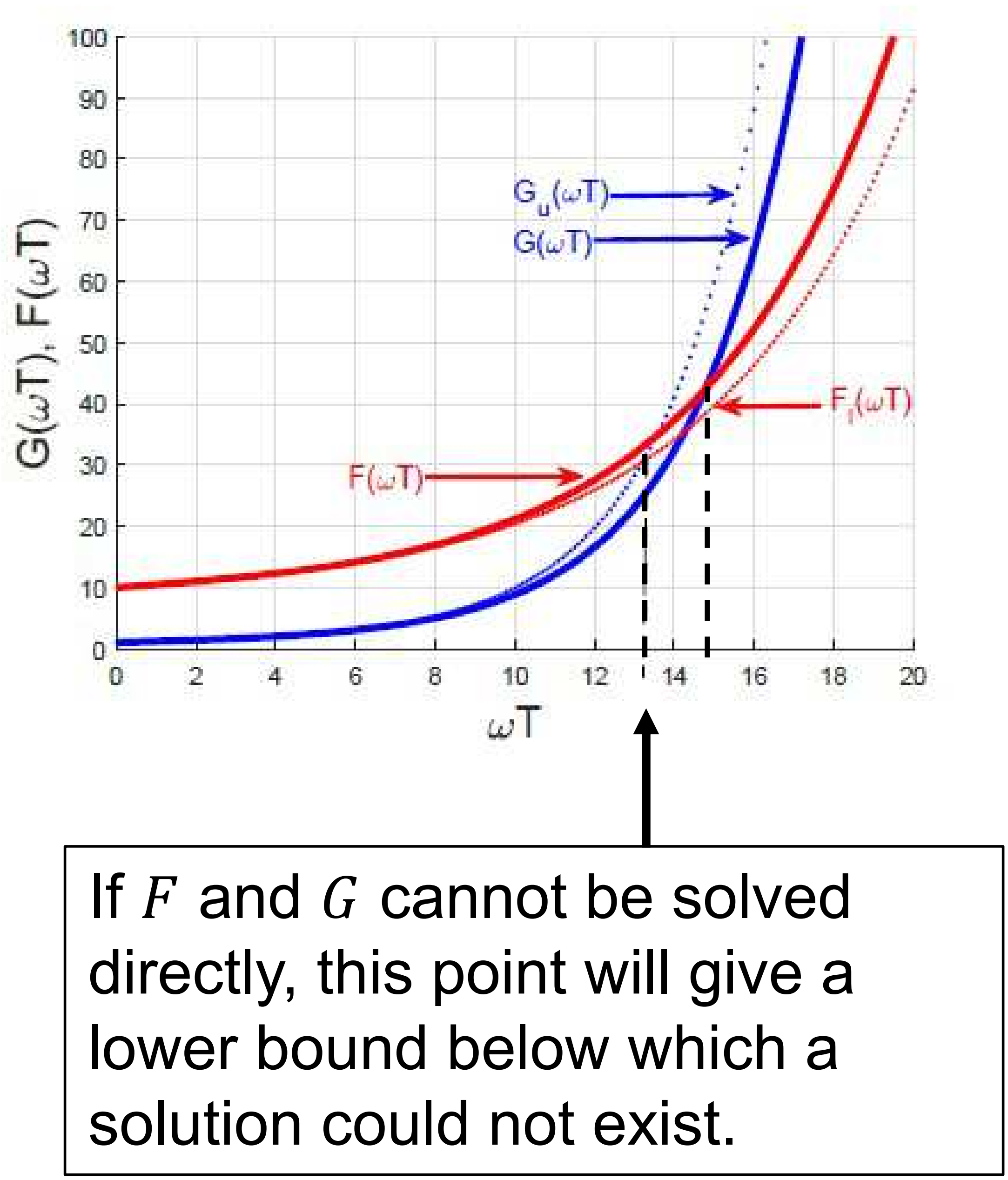

Figure 5.4: Lower limit of length for typical exact impedance match

Equations (5.20) and (5.21), will have a crossing point that will occur at a normalized length (relative to frequency: ωT) less than or equal to the length at which an exact match of the impedances R_L and Z_{00} is possible. A graphical representation of this F_l-G_u crossing can be seen in Figure 5.4, relative to the location of the exact match.

Equations (5.19) can be simplified using some trigonometric and hyperbolic power series:

$$\cos x = 1 - \frac{x^2}{2!} + \frac{x^4}{4!} - ...$$
$$\cosh x = 1 + \frac{x^2}{2!} + \frac{x^4}{4!} + ...$$

$$\frac{1}{2}(\cosh x + \cos x) = 1 + \frac{x^4}{4!} + \frac{x^8}{8!} + ... \tag{5.22}$$

$$\frac{1}{2}(\cosh x - \cos x) = 1 + \frac{x^2}{2!} + \frac{x^6}{6!} + ... \tag{5.23}$$

Substituting these identities into (5.19):

$$\begin{aligned} A_{lp}(\omega) &= \frac{1}{2}\big(\cosh(\omega T W_l) + \cos(\omega T W_l)\big) \\ D_{lm}(\omega) &= \frac{1}{2}\big(\cosh(\omega T W_l) - \cos(\omega T W_l)\big) \end{aligned} \tag{5.24}$$

so that,

$$F_l(\omega) = \frac{1}{2}\big(\cosh(\omega T W_l) + \cos(\omega T W_l)\big) Z_{02} + \frac{1}{2}\big(\cosh(\omega T W_l) - \cos(\omega T W_l)\big) Z_{01} \tag{5.25}$$

In a similar way G_u is given as:

$$G_u(\omega) = \frac{1}{2}\big(\cosh(\omega T W_u) - \cos(\omega T W_u)\big) Z_{02} + \frac{1}{2}\big(\cosh(\omega T W_u) + \cos(\omega T W_u)\big) Z_{01} \tag{5.26}$$

5.3.2 Satisfying $P = 0$

In a similar way, B and C parameters must satisfy the conditions in (5.13) in order for a nonuniform transmission line to perform a match.

Applying (5.2) to (5.13) gives,

$$P = \sum_{n=0}^{+\infty} (j\omega)^{2n+1} B_n - \sum_{n=0}^{+\infty} (j\omega)^{2n+1} C_n Z_{02} Z_{01} = 0 \tag{5.27}$$

or, since $j^2 = -1$:

$$P = j \sum_{n=0}^{+\infty} (-1)^n (\omega)^{2n+1} B_n - \sum_{n=0}^{+\infty} (-1)^n (\omega)^{2n+1} C_n Z_{01} Z_{02} = 0 \tag{5.28}$$

Since B_n and C_n are all positive and real, it is clear in (5.28) which coefficients will be positive or negative, so we regroup the terms as

$$P(\omega) = (B_p - B_m) - (C_p - C_m) Z_{01} Z_{02} = 0 \tag{5.29}$$

where B_p and C_p are the terms of (5.28) that will be positive and B_m and C_m are the terms that will be negative.

Forcing $P(\omega) = 0$ and re-arranging so both sides are positive,

$$B_p + C_m Z_{01} Z_{02} = B_m + C_p Z_{01} Z_{02} \tag{5.30}$$

Each half of this equation can be given a name for the purpose of finding where the two are equal:

$$\begin{aligned} jH(\omega) &= B_p + C_m Z_{01} Z_{02} \\ jJ(\omega) &= B_m + C_p Z_{01} Z_{02} \end{aligned} \tag{5.31}$$

We have included the factor j on the left side of (5.31) to make H and J real. Solutions for H and J above (5.31) are set to be equal to each other for a match of the circuit when all of the parameters are known. H and J can also be used for obtaining length limits below which a match will not be possible for a particular Z_{0max} and Z_{0min}. Here,

$$\begin{aligned} B_p(\omega) &= \omega B_0 + \omega^5 B_2 + \omega^9 B_4 + ... \\ B_m(\omega) &= \omega^3 B_1 + \omega^7 B_3 + \omega^1 1 B_5 + ... \\ C_p(\omega) &= \omega C_0 + \omega^5 C_2 + \omega^9 C_4 + ... \\ C_m(\omega) &= \omega^3 C_1 + \omega^7 C_3 + \omega^1 1 C_5 + ... \end{aligned} \tag{5.32}$$

Additional quantities are defined to relate (5.31) to the chain parameter limits (5.11). Let $B_{lp}(\omega)$ be defined using the lower limits of the coefficients for B from (5.11) using only the even values of n in (5.28). Likewise, C_{lm} is defined from the **negative** coefficients of C_l from (5.28).

$$\begin{aligned} B_{lp}(\omega) &= \omega Z_{0min} T + \omega^5 (W_l^2)^2 Z_{0min} \frac{T^5}{5!} + \omega^9 (W_l^2)^4 Z_{0min} \frac{T^9}{9!} + ... \\ C_{lm}(\omega) &= \omega^3 (W_l^2)^1 \frac{1}{Z_{0max}} \frac{T^3}{3!} + \omega^7 (W_l^2)^3 \frac{1}{Z_{0max}} \frac{T^7}{7!} + \omega^{11} (W_l^2)^5 \frac{1}{Z_{0max}} \frac{T^{11}}{11!} + ... \end{aligned} \tag{5.33}$$

where

$$W_u^2 = \frac{Z_{0max}}{Z_{0min}}$$

and

$$W_l^2 = \frac{Z_0 min}{Z_0 max}$$

$$\begin{aligned} B_{lp}(\omega) &= \frac{Z_{0min}}{W_l} \left(\omega W_l T + \omega^5 W_l^5 \frac{T^5}{5!} + \omega^9 W_l^9 \frac{T^9}{9!} + ... \right) \\ C_{lm}(\omega) &= \frac{1}{W_l Z_{0max}} \left(\omega^3 W_l^3 \frac{T^3}{3!} + \omega^7 W_l^7 \frac{T^7}{7!} + \omega^{11} W_l^{11} \frac{T^{11}}{11!} + ... \right) \end{aligned} \tag{5.34}$$

The lower limit for H is defined as:

$$H_l(\omega) = B_{lp}(\omega) + C_{lm}(\omega) Z_{01} Z_{02} \tag{5.35}$$

Similarly, defining B_{um} using the negative coefficients of the lower bounds of the coefficients of B and C_{up} using the lower bound of the positive coefficients of C, an upper limit for J is obtained:

$$J_u(\omega) = B_{um}(\omega) + C_{up}(\omega) Z_{01} Z_{02} \tag{5.36}$$

Equations (5.35) and (5.36) will have a crossing point that will occur at a length (relative to frequency: ωT) less than or equal to the length at which an exact match of the impedances R_L and Z_{00} is possible.

Equation (5.33) can be simplified using some trigonometric and hyperbolic power series.

$$\sin x = x - \frac{x^3}{3!} + \frac{x^5}{5!} - ...$$

$$\sinh x = x + \frac{x^3}{3!} + \frac{x^5}{5!} + ...$$

$$\frac{1}{2}(\sinh x + \sin x) = x + \frac{x^5}{5!} + \frac{x^9}{9!} + ... \tag{5.37}$$

$$\frac{1}{2}(\sinh x - \sin x) = \frac{x^3}{3!} + \frac{x^7}{7!} + ... \tag{5.38}$$

Substituting these identities into (5.33):

$$\begin{aligned} B_{lp}(\omega) &= \frac{Z_{0min}}{W_l}\frac{1}{2}\big(\sinh(\omega TW_l) + \sin(\omega TW_l)\big) \\ C_{lm}(\omega) &= \frac{1}{W_l Z_{0max}}\frac{1}{2}\big(\sinh(\omega TW_l) - \sin(\omega TW_l)\big) \end{aligned} \tag{5.39}$$

so that,

$$H_l(\omega) = \frac{Z_{0min}}{2W_l}\big(\sinh(\omega TW_l) + \sin(\omega TW_l)\big) + \frac{1}{2W_l Z_{0max}}\big(\sinh(\omega TW_l) - \sin(\omega TW_l)\big)Z_{01}Z_{02} \tag{5.40}$$

In a similar way J_u is given as:

$$J_u(\omega) = \frac{Z_{0max}}{2W_u}\big(\sinh(\omega TW_u) - \sin(\omega TW_u)\big) + \frac{1}{2W_u Z_{0min}}\big(\sinh(\omega TW_u) + \sin(\omega TW_u)\big)Z_{01}Z_{02} \tag{5.41}$$

5.3.3 Length Limits

All of the quantities needed for obtaining the upper and lower limits for solutions of (5.12) and (5.13) have been defined. The conditions which define a matched condition must allow for both $M = 0$ and $P = 0$. If F_l and G_u are known, the equations can be applied to impedance matching cases to see what limits can be produced.

Figures 5.5 - 5.7, show line length limiting cases under three sample conditions for 10:1 impedance transformers. The length limits are created by applying the Z_{0min} and Z_{0max} characteristics to the coefficients of A_n, B_n, C_n, and D_n as outlined above.

Figure 5.5 shows the unique conditions for the quarter-wave transformer. In the case when $Z_{0min} = Z_{0max}$, the F and G expressions determine M (5.12) are equal at lengths 0.25λ and odd multiples thereof. We view the zero-crossing closest to $\omega T = 0$ as a point below which a

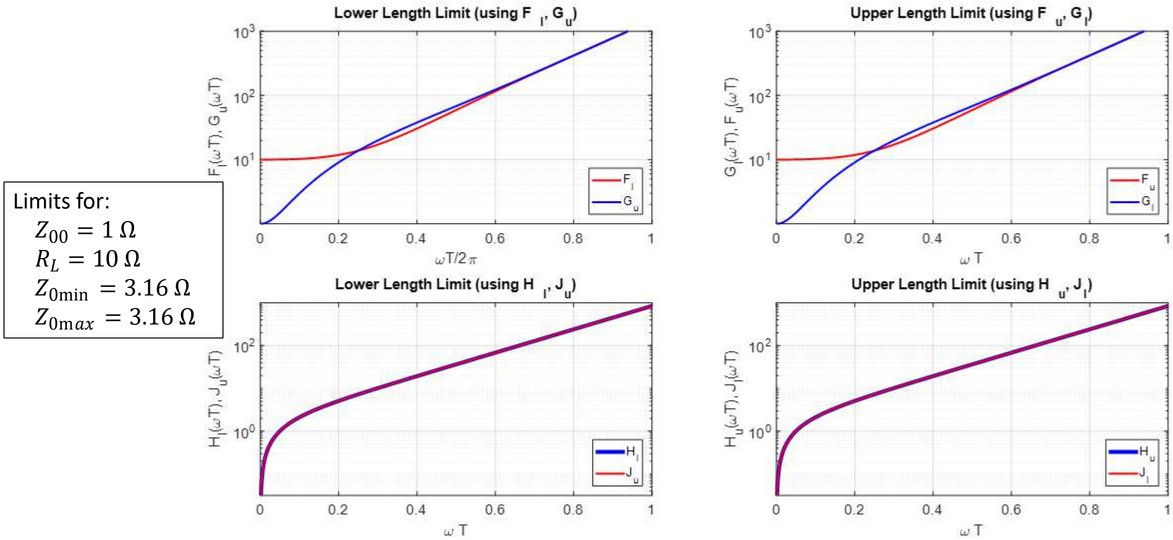

Figure 5.5: Lower and upper length limits for a 10:1 impedance transformer with $Z_{0min} = Z_{0max} = 3.16\,\Omega$.

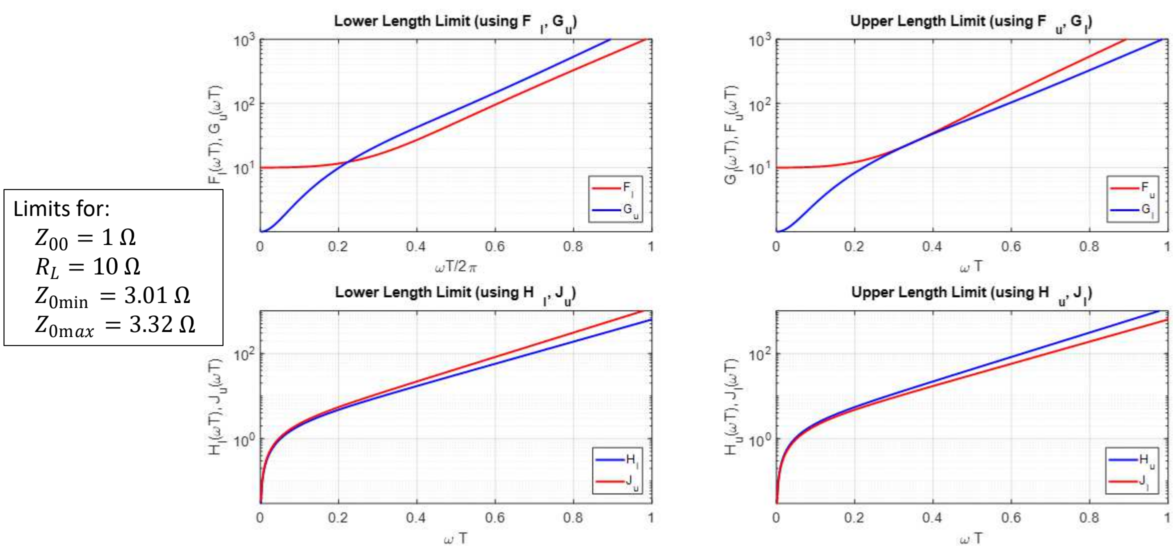

Figure 5.6: Lower and upper length limits for a 10:1 impedance transformer with $Z_{0min} = 3.01\,\Omega$ and $Z_{0max} = 3.32\,\Omega$.

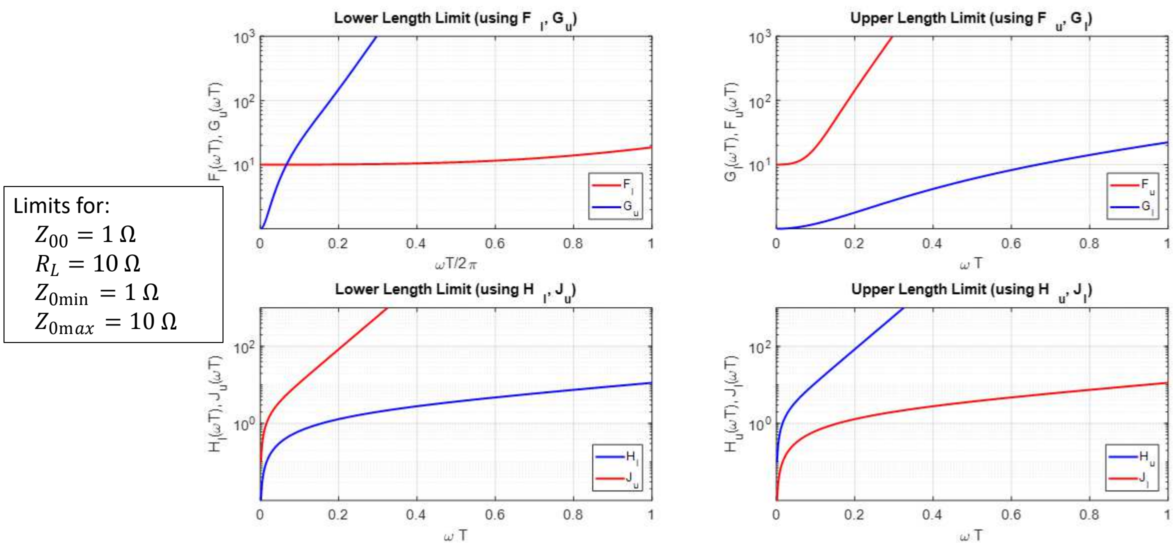

Figure 5.7: Lower and upper length limits for a 10:1 impedance transformer with $Z_{0min} = 1\,\Omega$ and $Z_{0max} = 3.16\,\Omega$.

perfect match will not occur (a lower length limit). If an intersection point existed for the H and J equations that determine P, the higher (larger) ωT value would be taken as the lower limit. The upper length limit indicates a point below which (lower ωt) the shortest match condition is expected.

The M condition requires the match to exist at 0.25λ since the lower length limit and upper length limit both appear at that length. The H and J equations that determine P, show an interesting condition in that they are equal at all frequency points (ωT). This means that although H_l and J_u indicate a match as low as ($\omega T = 0$), the higher ($\omega T = .25\lambda$) is the overall lower limit.

When the Z_{0min} and Z_{0max} conditions are allowed to separate a little as shown in Figure 5.6, the lower limit decreases (to $\omega T = 0.224$) as defined by F_l and G_u. There is an upper limit given by F_u and G_l at $\omega T = 0.335\lambda$, which indicates that the shortest length matching circuit for a 10:1 matching circuit with $Z_{0min} = 3.01\,\Omega$ and $Z_{0max} = 3.32\,\Omega$ will occur between $0.224\lambda \leq \omega T \leq 0.335\lambda$. The H_l, J_u crossing never happens, indicating that the F_l, G_u bound is the lowest length bound. Likewise H_u and J_l do not cross, and provide no additional information on a upper length bound.

A more extreme case of impedance deviation is considered when $Z_{0min} = 1\,\Omega$ and $Z_{0max} = 10\,\Omega$ (see Figure 5.7). Here the lower bound defined by F_l and G_u is found at a lower frequency (ωT), and no upper bounds are present. In fact for any case other than $Z_{0min} = Z_{0max}$, the H_l, J_u crossing never happens, and can be discarded as a useful result for the limits created by the approach in Chapter 5. The one consistently useful comparison is the lower bound created by the F_l and G_u equality. For any condition of Z_{0min} and Z_{0max} impedance parameters, there appears to be a length with respect to frequency where an equality of the positive and negative terms of (5.12) exist indicating a lower length bound. Some further examples of the lower length limit found using this information can be found in Section 5.4 below.

5.4 Conclusion

Limits for the length of a nonuniform transmission line being used as an impedance matching circuit are found by using the minimum and maximum characteristic impedance values of the transmission line. Figures 5.8 through 5.11 show plots of F_l and G_u for several different specific matching circuits. The intersection points of these two lines indicate the spot where these two equations are equal. Lengths (with respect to frequency, ωT), below these intersection points will not allow a matching solution for the Z_{0min} and Z_{0max} selected. The Bramham circuit uses the minimum and maximum impedances equal to the input and load impedances of the system. Using these values for minimum and maximum and a comparison has been made representing the limit found above and the known length of the Bramham circuit (see Figure 5.12). Expanding on the data presented in Chapter 3, Table 5.1 shows how the limits found in this chapter can be compared for exponential lines and other matching circuits. For the quarter-wave transformer, the limit computed is 0.25λ. For transmission lines shorter than the quarter-wave transformer as shown in Table 5.1, the length limit decreases more rapidly than the length of the circuit itself making the bound less tight. Looking at exponential tapers longer than a quarter wave transformer, the length limit derived in this chapter also decreases since Z_{0min} and Z_{0max} are diverging, but this divergence does not create a shorter actual circuit, at least from the exponential family of tapers.

The results in Table 5.1 can be compared to those found in [12]. As shown in Figure 5.12, when $R_L/Z_{00} = 10$ and $Z_{0max}/Z_{0min} = 10$, the limit defined [12] gives a value of 0.05λ, while Table 5.1 shows a tighter bound of 0.067λ. Results for the length limit for the quarter-wave transformer can also be compared; in [12] a limit is found to be 0.21λ when $Z_{0min} = Z_{0max} = \sqrt{R_L Z_{00}}$, while in Table 5.1, this limit is exactly 0.25λ. In general, the bounds presented in this chapter are much better than those of [12]. The major difference between the two limits is that [12] allows matches for all complex s, while the method listed in this chapter replaces s with $j\omega$. The bounds found in this chapter maintain their validity as long as ω is restricted to only positive real values, which applies to most practical applications.

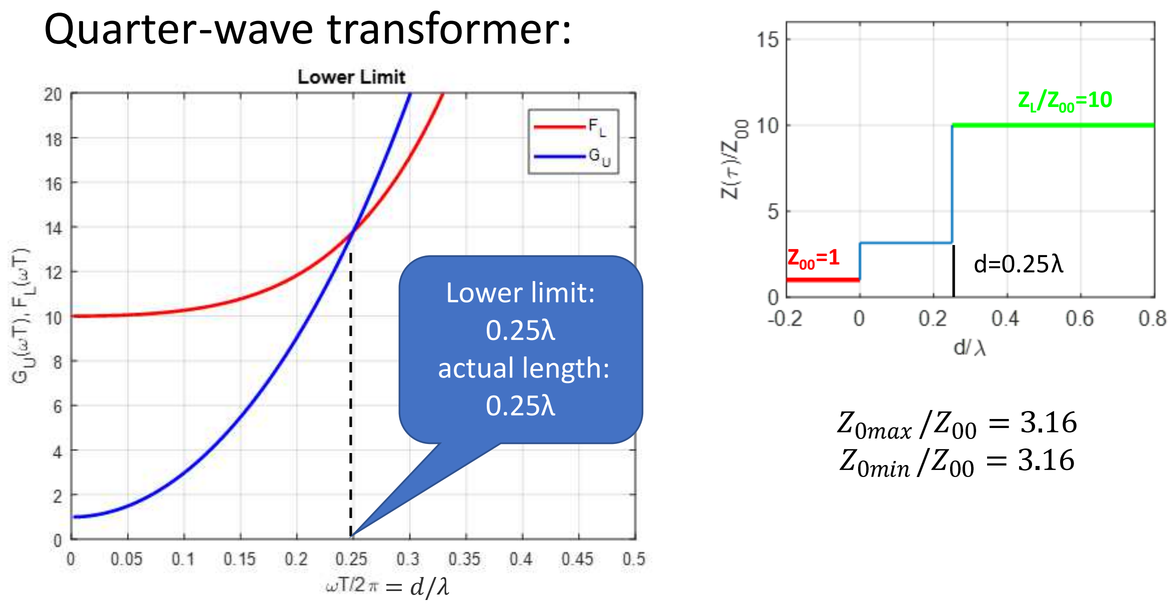

Figure 5.8: Limits for a 10:1 impedance discontinuity with $Z_{0max} = Z_{0min} = \sqrt{10 * 1}\,\Omega$

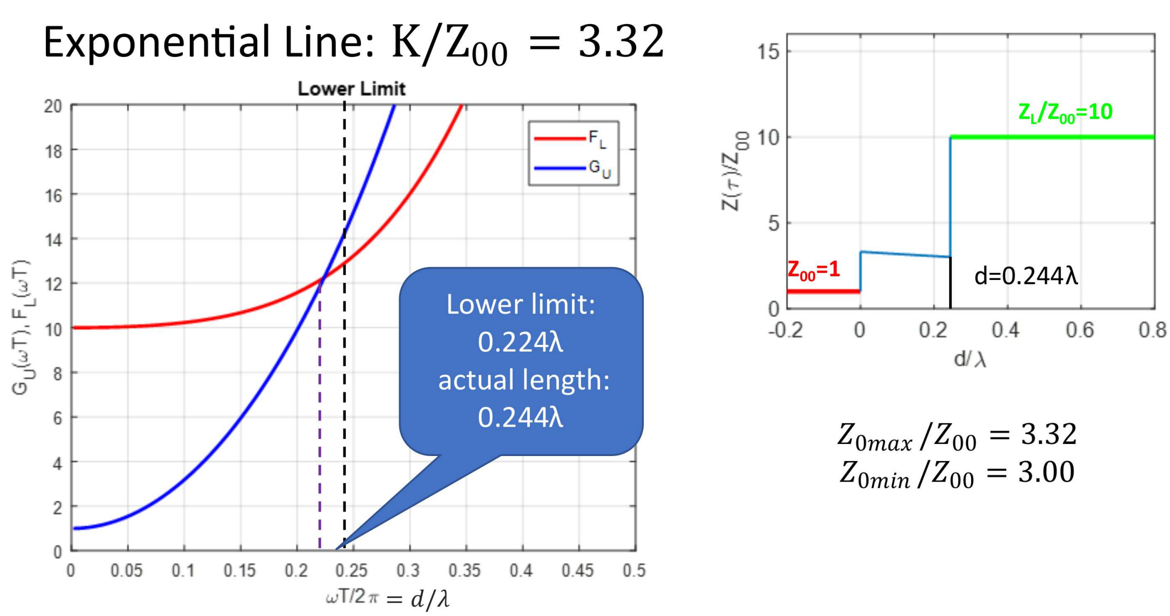

Figure 5.9: Limits for a 10:1 impedance discontinuity with $Z_{0max} = 3.32\,\Omega$ $Z_{0min} = 3.00\,\Omega$

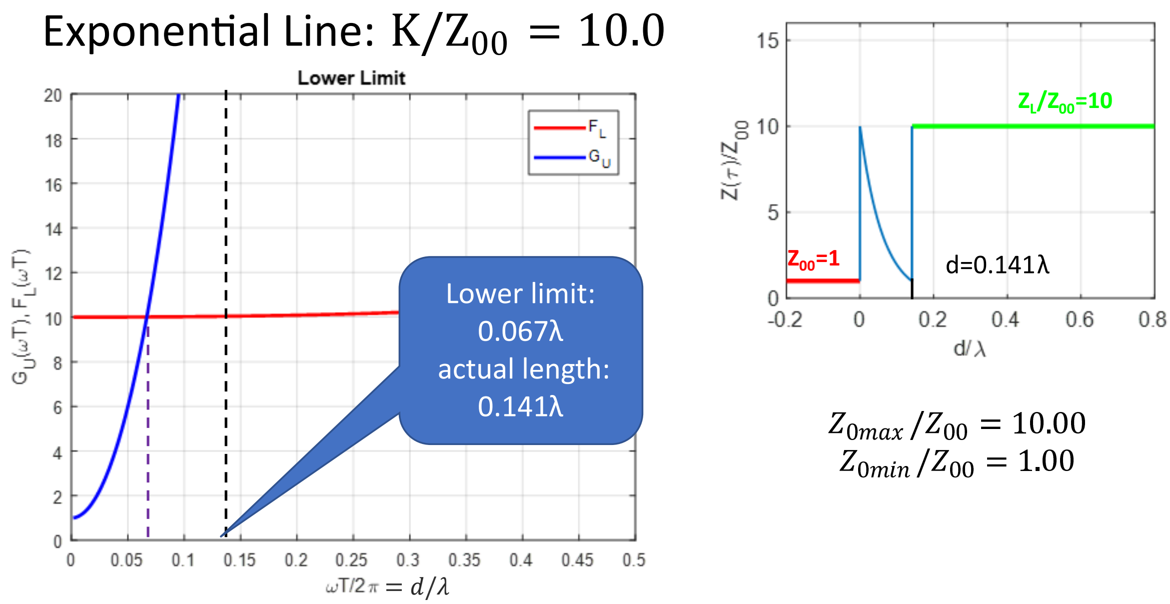

Figure 5.10: Limits for a 10:1 impedance discontinuity with $Z_{0max} = 10\,\Omega$ $Z_{0min} = 1\,\Omega$

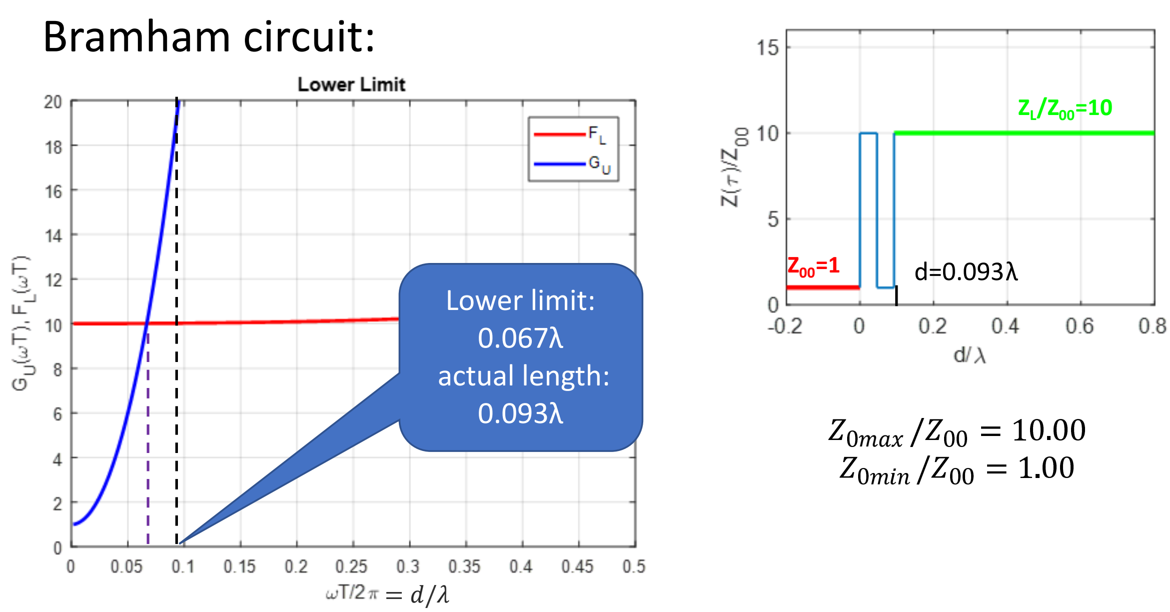

Figure 5.11: Limits for a 10:1 impedance discontinuity with $Z_{0max} = 10\,\Omega$ $Z_{0min} = 1\,\Omega$ Bramham configuration

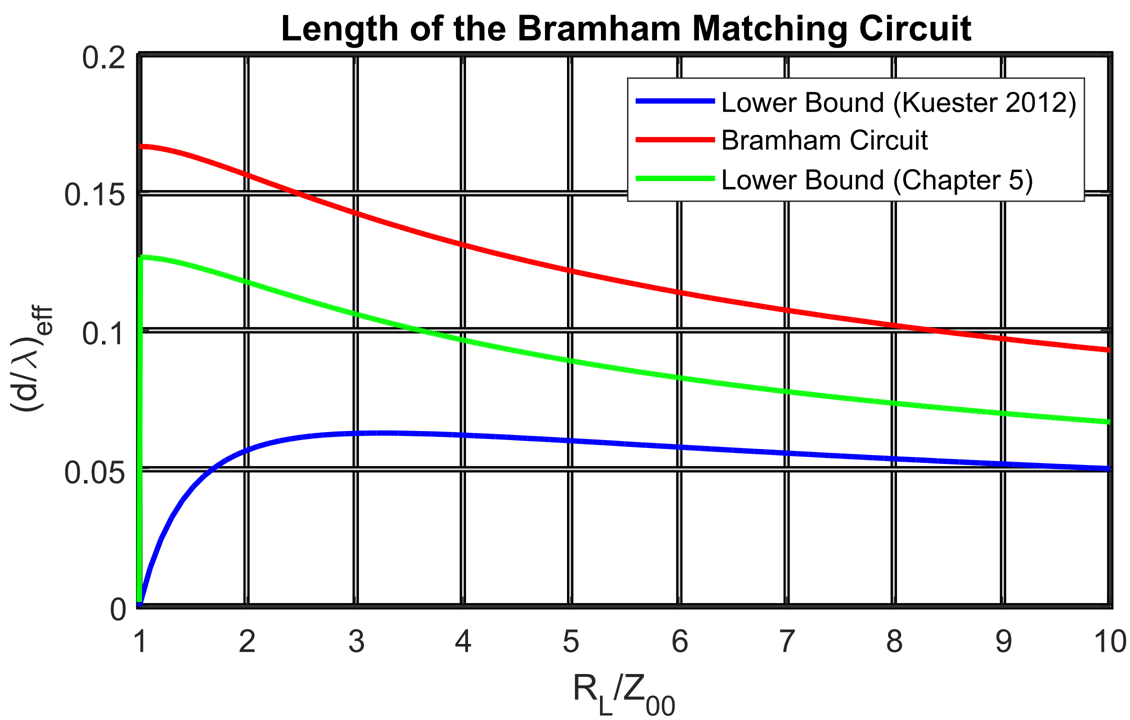

Figure 5.12: Limit found for the Bramham circuit by solving for ω from Equations (5.20) and (5.21

Transmission line	**Length Limit**	Actual Length	-20 dB Bandwidth
Exponential (K=1.0Ω)	**.067λ**	.533λ	15.7%
Exponential (K=1.105Ω)	**.072λ**	.487λ	15.1%
Exponential (K=1.5Ω)	**.100λ**	.381λ	12.0%
Exponential (K=3.16Ω) (λ/4)	**.250λ**	.250λ	9.0%
Exponential (K=Z_L=10Ω)	**.067λ**	.141λ	7.7%
Bramham	**.067λ**	.093λ	7.7%
Exponential (K=15Ω)	**.045λ**	.113λ	7.5%
Exponential (K=21Ω)	**.032λ**	.093λ	7.3%
Exponential (K=25Ω)	**.027λ**	.084λ	7.3%
Exponential (K=30Ω)	**.022λ**	.075λ	7.2%

Table 5.1: Length limits compared to examples of known length: Quarter-wave, Bramham and exponential tapers.

Chapter 6

Tighter Bounds Using a Bôcher Approach

The length limits presented in Chapter 5 make use of only Z_{0max} and Z_{0min}. In the case of the quarter-wave transformer ($Z_{0max} = Z_{0min}$) the shortest possible line length that will produce a match as predicted by the limit is exactly $\lambda/4$ (see Figure 5.8). For the more general case, when Z_{0max} and Z_{0min} deviate from each other, the lower bounds are not as tight. In this chapter, we search for a way to tighten the bound of Chapter 5 in the general case if more is known about the taper to be used. What we will call the Bôcher approach seeks to get tighter bounds on the length of matching transmission lines by using additional information (such as average impedance) to bound A_n, B_n, C_n, and D_n more tightly.

6.1 The Bôcher Approach to Bounding the ABCD Coefficients

The bounds on the coefficients of the series expansions used in Chapter 5 were essentially those of Peano [27] [28]. These bounds can be improved using a refinement suggested by the work of Bôcher [34] (see also Pease [35], who uses the nonuniform transmission line as an example), but will be modified somewhat to suit our needs. Beginning with the equation for A_n (5.7):

$$A_n = \int_0^T \frac{1}{Z_0(\tau_{2n})} \int_0^{\tau_{2n}} Z_0(\tau_{2n-1}) \cdots \int_0^{\tau_2} Z_0(\tau_1)\, d\tau_1 d\tau_2 \cdots d\tau_{2n} \tag{6.1}$$

let the constant $Z_{0\text{ref}}$ be an arbitrary positive real reference impedance. Equation (6.1) is rewritten as

$$A_n = \int_0^T \frac{Z_{0\text{ref}}}{Z_0(\tau_{2n})} \int_0^{\tau_{2n}} \frac{Z_0(\tau_{2n-1})}{Z_{0\text{ref}}} \cdots \int_0^{\tau_2} \frac{Z_0(\tau_1)}{Z_{0\text{ref}}}\, d\tau_1 d\tau_2 \cdots d\tau_{2n} \tag{6.2}$$

Next, define the (dimensionless) functions

$$\phi_{\max}(\tau) = \left\{ \begin{array}{ll} \dfrac{Z_0(\tau)}{Z_{0\mathrm{ref}}} & \text{if } Z_0(\tau) > Z_{0\mathrm{ref}} \\ \\ \dfrac{Z_{0\mathrm{ref}}}{Z_0(\tau)} & \text{if } Z_0(\tau) < Z_{0\mathrm{ref}} \\ \\ 1 & \text{if } Z_0(\tau) = Z_{0\mathrm{ref}} \end{array} \right\} = \max\left[\frac{Z_0(\tau)}{Z_{0\mathrm{ref}}}, \frac{Z_{0\mathrm{ref}}}{Z_0(\tau)}\right] \tag{6.3}$$

and

$$\phi_{\min}(\tau) = \left\{ \begin{array}{ll} \dfrac{Z_{0\mathrm{ref}}}{Z_0(\tau)} & \text{if } Z_0(\tau) > Z_{0\mathrm{ref}} \\ \\ \dfrac{Z_0(\tau)}{Z_{0\mathrm{ref}}} & \text{if } Z_0(\tau) < Z_{0\mathrm{ref}} \\ \\ 1 & \text{if } Z_0(\tau) = Z_{0\mathrm{ref}} \end{array} \right\} = \min\left[\frac{Z_0(\tau)}{Z_{0\mathrm{ref}}}, \frac{Z_{0\mathrm{ref}}}{Z_0(\tau)}\right] \tag{6.4}$$

Clearly, we have

$$\phi_{\min}(\tau) \le \frac{Z_{0\mathrm{ref}}}{Z_0(\tau)} \le \phi_{\max}(\tau), \quad \phi_{\min}(\tau) \le \frac{Z_0(\tau)}{Z_{0\mathrm{ref}}} \le \phi_{\max}(\tau), \quad \text{and} \quad \phi_{\min}(\tau) \le 1 \le \phi_{\max}(\tau) \tag{6.5}$$

for all τ.

From (6.5) and (6.2) then, we have

$$A_n \le \int_0^T \phi_{\max}(\tau_{2n}) \int_0^{\tau_{2n}} \phi_{\max}(\tau_{2n-1}) \cdots \int_0^{\tau_2} \phi_{\max}(\tau_1)\, d\tau_1 d\tau_2 \cdots d\tau_{2n} \tag{6.6}$$

The right side of (6.6) can now be evaluated using a lemma due to Cauchy [34] which will be the basis of the Bôcher approach. A lower bound for A_n can be computed in a similar way.

$$A_n \ge \int_0^T \phi_{\min}(\tau_{2n}) \int_0^{\tau_{2n}} \phi_{\min}(\tau_{2n-1}) \cdots \int_0^{\tau_2} \phi_{\min}(\tau_1)\, d\tau_1 d\tau_2 \cdots d\tau_{2n} \tag{6.7}$$

and will also be evaluated using Cauchy's lemma.

Cauchy Formula for Repeated Integration Let

$$q_k(\tau) \equiv \int_0^{\tau} q(\tau_k) \int_0^{\tau_k} q(\tau_{k-1}) \cdots \int_0^{\tau_2} q(\tau_1)\, d\tau_1 d\tau_2 \cdots d\tau_k$$

where $q(\tau)$ is a suitably integrable function. Then

$$q_k(\tau) = \frac{1}{k!} \left[\int_0^{\tau} q(\tau')\, d\tau' \right]^k = \frac{1}{k!} \left[q_1(\tau) \right]^k \tag{6.8}$$

where

$$q_1(\tau) = \int_0^{\tau} q(\tau')\, d\tau' \tag{6.9}$$

To prove (6.8), note that it is obviously true for $k = 1$, and that $q_1'(\tau) = q(\tau)$. Now suppose it is true for $k - 1$. We have

$$q_k(\tau) = \int_0^{\tau} q(\tau_k) q_{k-1}(\tau_k)\, d\tau_k = \int_0^{\tau} q_1'(\tau_k) \frac{1}{(k-1)!} \left[q_1(\tau_k) \right]^{k-1} d\tau_k = \frac{1}{(k-1)!} \int_0^{\tau} \frac{1}{k} \frac{d}{d\tau_k} \left[q_1(\tau_k) \right]^k d\tau_k$$

which is equivalent to (6.8).

Having shown that this lemma is applicable for all k, it can now be applied to the problem of finding limits on A_n by putting $q(\tau) = \phi_{\max}(\tau)$ in (6.8).

$$A_n \le \frac{1}{(2n)!} \left[\int_0^{T} \phi_{\max}(\tau)\, d\tau \right]^{2n} \tag{6.10}$$

In a similar way, using $q(\tau) = \phi_{\min}(\tau)$, we can show that

$$A_n \ge \frac{1}{(2n)!} \left[\int_0^{T} \phi_{\min}(\tau)\, d\tau \right]^{2n} \tag{6.11}$$

Similar bounds can be found for B_n, C_n and D_n by the same method; the bounds for D_n are identical to those in (6.10) and (6.11) for A_n. These bounds are sharp, with equality holding in the case $Z_0(\tau) = Z_{0\text{ref}} =$ constant. For suitable choices of $Z_{0\text{ref}}$, they seem likely to be tighter than the Peano bounds ([27]) and ([28]) that were used in [12]. In fact, if we put $Z_{0\text{ref}} = \sqrt{Z_{0\max} Z_{0\min}}$, then by (6.3), $\phi_{\max} \le \sqrt{Z_{0\max}/Z_{0\min}}$, while by (6.4), $\phi_{\min} \ge \sqrt{Z_{0\min}/Z_{0\max}}$ and thus

$$\int_0^{T} \phi_{\max}(\tau)\, d\tau \le T \sqrt{\frac{Z_{0\max}}{Z_{0\min}}}; \qquad \int_0^{T} \phi_{\min}(\tau)\, d\tau \ge T \sqrt{\frac{Z_{0\min}}{Z_{0\max}}} \tag{6.12}$$

which show that (6.10) and (6.11) are at least as tight as (5.11) for this choice of $Z_{0\text{ref}}$.

The bounds (6.10) and (6.11) can be written in various other ways. For instance,

$$\frac{T^{2n}}{(2n)!}\phi_l^{2n} \leq \left\{ \begin{array}{c} A_n \\ \\ D_n \end{array} \right\} \leq \frac{T^{2n}}{(2n)!}\phi_u^{2n} \tag{6.13}$$

where

$$\phi_u = \frac{1}{T}\int_0^T \phi_{\max}(\tau)\,d\tau \tag{6.14}$$

and

$$\phi_l = \frac{1}{T}\int_0^T \phi_{\min}(\tau)\,d\tau \tag{6.15}$$

Recall from (6.5) that

$$\phi_l \leq 1 \leq \phi_u$$

and therefore that the upper bounds are always $\geq T^{2n}/(2n)!$ while the lower bounds are $\leq T^{2n}/(2n)!$, as was the case for the Peano bounds (5.11). But as seen above, with an optimum choice of reference impedance the Bôcher bounds will be tighter than the Peano bounds.

In general, optimizing the choice of $Z_{0\text{ref}}$ can be a difficult task, and will not be attempted here. We might choose $Z_{0\text{ref}} = \sqrt{Z_{0\max}Z_{0\min}}$ (as performed in Appendix C for the exponential line), or instead proceed as follows. If $Z_{0\text{ref}} \geq Z_{0\max}$, then (6.14) and (6.15) become

$$\phi_u = \frac{Y_{0\text{av}}}{Y_{0\text{ref}}} > Z_{0\max}Y_{0\text{av}}; \qquad \phi_l = \frac{Z_{0\text{av}}}{Z_{0\text{ref}}} < \frac{Z_{0\text{av}}}{Z_{0\max}} \tag{6.16}$$

Where,

$$Z_{0\text{av}} = \frac{1}{T}\int_0^T Z_0(\tau)\,d\tau; \qquad Y_{0\text{av}} = \frac{1}{T}\int_0^T Y_0(\tau)\,d\tau \tag{6.17}$$

The smallest value our upper bound can take for such $Z_{0\text{ref}}$ is therefore achieved in the limit $Z_{0\text{ref}} \to Z_{0\max}$; the largest value of our lower bound is also attained under the same condition:

When Z_{0ref} gets even bigger than Z_{0max}, the bounds just get looser. For this reason, the best choice in this range is $Z_{0ref} = Z_{0max}$.

$$\phi_u = Z_{0\max}Y_{0\text{av}}; \qquad \phi_l = \frac{Z_{0\text{av}}}{Z_{0\max}} \tag{6.18}$$

In a similar way, if $Z_{0\text{ref}} \leq Z_{0\text{min}}$, the best bounds are achieved when $Z_{0\text{ref}} = Z_{0\text{min}}$:

$$\phi_u = \frac{Z_{0\text{av}}}{Z_{0\text{min}}}; \qquad \phi_l = Z_{0\text{min}} Y_{0\text{av}} \tag{6.19}$$

We conclude that the optimum choice of $Z_{0\text{ref}}$ to obtain the lowest value of ϕ_u will lie in the range $Z_{0\text{min}} \leq Z_{0\text{ref}} \leq Z_{0\text{max}}$, and may have to be determined by numerical experimentation in any particular case. An initial study of choices for $Z_{0\text{ref}}$ within this range is introduced in Appendix C.

6.1.1 Bounds on B_n and C_n

Bôcher-type bounds on B_n and C_n can be found in a similar way. The only complication is that not all the factors of $Z_{0\text{ref}}$ will cancel as they did for A_n and D_n. We have

$$Z_{0\text{ref}} \frac{T^{2n+1}}{(2n+1)!} \phi_l^{2n+1} \leq B_n \leq Z_{0\text{ref}} \frac{T^{2n+1}}{(2n+1)!} \phi_u^{2n+1} \tag{6.20}$$

$$\frac{1}{Z_{0\text{ref}}} \frac{T^{2n+1}}{(2n+1)!} \phi_l^{2n+1} \leq C_n \leq \frac{1}{Z_{0\text{ref}}} \frac{T^{2n+1}}{(2n+1)!} \phi_u^{2n+1} \tag{6.21}$$

If only bounds on products of terms like $B_n C_m$ are required, the reference impedance drops out and we have:

$$\frac{T^{2n+2m+2}}{(2n+1)!(2m+1)!} \phi_l^{2n+2m+2} \leq B_n C_m \leq \frac{T^{2n+2m+2}}{(2n+1)!(2m+1)!} \phi_u^{2n+2m+2} \tag{6.22}$$

But in (6.20) and (6.21), determination of the optimum choice of $Z_{0\text{ref}}$ is more complicated, and can be expected to give different results than was the case for A_n and D_n.

6.1.2 Summary of Bôcher bounds

To summarize these results, the optimum Bôcher-type bounds in (6.13), (6.20) and (6.21) are specified as follows:

Lower Bounds:

$$\phi_l = \frac{Z_{0\text{av}}}{Z_{0\text{max}}} \qquad \left(\text{if } \frac{Z_{0\text{av}}}{Z_{0\text{max}}} \geq \frac{Y_{0\text{av}}}{Y_{0\text{max}}} \right) \tag{6.23}$$

$$\phi_l = Z_{0\min} Y_{0\mathrm{av}} \qquad \left(\text{if } \frac{Z_{0\mathrm{av}}}{Z_{0\max}} \leq \frac{Y_{0\mathrm{av}}}{Y_{0\max}}\right) \tag{6.24}$$

Upper Bounds:

$$\phi_u = Z_{0\max} Y_{0\mathrm{av}} \qquad \left(\text{if } \frac{Z_{0\mathrm{av}}}{Z_{0\min}} \geq \frac{Y_{0\mathrm{av}}}{Y_{0\min}}\right) \tag{6.25}$$

$$\phi_u = \frac{Z_{0\mathrm{av}}}{Z_{0\min}} \qquad \left(\text{if } \frac{Z_{0\mathrm{av}}}{Z_{0\min}} \leq \frac{Y_{0\mathrm{av}}}{Y_{0\min}}\right) \tag{6.26}$$

6.2 Numerical Results for the Bramham Case

The Bôcher approach provides an opportunity to create tighter bounds on the coefficients A_n, B_n, C_n, and D_n, which in turn, can create tighter length limits for the matching circuits. The bounding technique is then the same as the one used in Chapter 5, but using the more defined coefficient bounds. The addition of $Z_{0\mathrm{ref}}$ as a parameter that can be optimized makes finding universal limits a bit more involved.

We have tried different values of $Z_{0\mathrm{ref}}$ for finding the coefficient bounds for the 10:1 Bramham circuit to compare to the bounds in Figure 5.11. For ϕ_u, the choice of $Z_{0\mathrm{ref}} = \sqrt{Z_{0\min} Z_{0\max}}$ gives the tightest bound.

$$W_u = \phi_u = \frac{\sqrt{Z_{0\max} Z_{0\min}}}{Z_{0\min}} = \sqrt{10} = 3.162 \tag{6.27}$$

These are the same as Peano bounds from Chapter 5, Although there is no advantage, the Peano bounds are never worse.

For ϕ_l, choosing either $Z_{0\mathrm{ref}} = Z_{0\max}$ or $Z_{0\mathrm{ref}} = Z_{0\min}$ produced the tightest bound so (6.25) or (6.25) could be used:

$$W_l = \phi_l = \frac{Z_{0\mathrm{av}}}{Z_{0\max}} = \frac{0.5(10+1)}{10} = 0.55 \tag{6.28}$$

In this case, the bounds for W_l are significantly different from that found in Chapter 5 using the Peano bounds. Looking at the resultant F_l and G_u plot in Figure 6.1, the F_l plot is significantly different, potentially producing tighter length limits. In this Bramham case, however, the F_l line is nearly horizontal in the region where the G_u line crosses, and only a very small change in the length limit is realized.

In Appendix C, we have presented Bôcher bounds for the case of the exponential line. In future developments of this work, a determination of length bounds for exponential lines may show more significant improvements of the Bôcher approach.

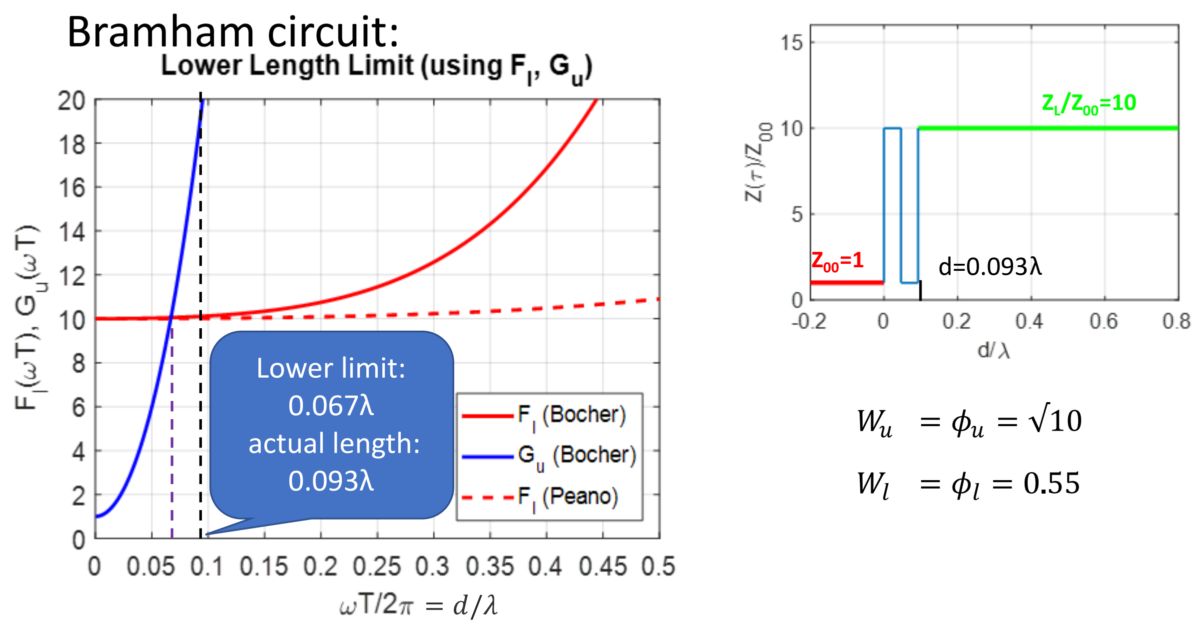

Figure 6.1: Limits for a 10:1 impedance discontinuity with $W_u = \phi_u = 3.162$ and $W_l = \phi_l = 0.55$ Bramham configuration

Chapter 7

Conclusion

7.1 Results

Nonuniform transmission lines are effective impedance transformers for broadband and narrowband applications. In this thesis, the trade-offs of performance and length have been demonstrated showing that electrically short impedance transformers can be realized when very large impedance variations are allowed. Practical limitations on the highest and lowest allowable impedance characteristics can be used to define a limit on the shortest possible length a transmission line can have to perform a match of a given impedance ratio. While much current design work is done in software analysis tools, a priori knowledge of possible solutions can speed development efforts by eliminating solution paths that will not give a possible solution.

A detailed investigation into the broad usage of exponentially tapered transmission lines has been demonstrated. A design procedure has been presented giving a choice of exponential line impedance matching solutions. The impedance matching response for an exponential line with impedance discontinuities at either end has been analytically computed, simulated, and manufactured. A comparison of the ideal and the manufactured exponential line impedance matching circuits revealed the sensitivity these circuits have to fabrication anomalies and the impacts of capacitive and inductive parasitics. In general, modest parasitics were observed which had the favorable impact of shortening the electrical length of the matching circuit while having minimal impact on the frequency bandwidth or quality of the match.

7.2 Future Work

In this thesis, only real load impedances have been considered. This research could be continued to include using nonuniform matching circuits for matching complex load impedances. In that case, the situation is additionally complicated by the frequency dependence of the load impedance, which will interact with that of the matching circuit in a nontrivial way. The parasitic effects of impedance discontinuities are one such type of frequency dependence; an analytical or numerical treatment of these could be used to reduce any design iterations required by adjusting the transmission line length in the original design. This study would be most useful if completed for different types of transmission lines in various dielectric media.

A limiting factor for the usefulness of nonuniform transmission lines can be their power handling capability. The narrowest line section in a nonuniform transmission line will limit the maximum power that the circuit will allow before melting the trace. A study of the power handling limitations of different substrates for these narrow transmission line sections can further define physical limitations for nonuniform transmission line impedance transformation.

Impedance tapers have potential applications in other ways besides impedance matching. The results of this thesis could be applied to the design of broadband coupling circuits such as quadrature and 180° hybrids. Power dividers, diplexers and antenna array feed networks could also benefit from the principles studied in this thesis.

Although the Chen-Hamid two-stage generalization of the Bramham matching circuit has been known for some time, it does not seem to have been thoroughly studied from the standpoint of optimization and compensation for parasitic effects. This would be a valuable extension of this thesis work, as would the treatment of circuits with more than two stages. Some classical work on this problem is well-known (Chebyshev, Butterworth and other types of stepped impedance filters, for example), but designs that focused on shortening the length of the circuit have been very little investigated.

Tighter limits than those found in Chapter 5 for the shortest possible nonuniform line matching circuits might also be found by further refining the bounds on the coefficients A_n, B_n, C_n and D_n. An in-depth study of many inequalities has been initiated, and some of its initial findings were presented in Chapter 6 and Appendix C. In some cases, as more information about a nonuniform transmission line (e. g., weighted averages or maximum rate of change of the characteristic impedance) is applied to the calculation of a length limit, a tighter bound on that limit should be possible to obtain. Since the bounds in this thesis are based on the series expansion of ABCD Parameters, the possibility can be explored to find tighter bounds by improving the limits on only some of the expansion coefficients rather than on the entire infinite series. Doing this for the coefficients of lowest order should be profitable, since we are interested in short length/low frequency situations where these coefficients are most important to the values of the chain parameters.

Bibliography

[1] Y.-W. Hsu, "Direct synthesis of passband impedance matching with non-uniform transmission lines," Ph.D. dissertation, Ph.D dissertation, Department of Electrical, Computer, and Energy Eng., University of Colorado - Boulder, 2005.

[2] A. T. N. A. for Amateur Radio, "RF cafe - February 1943 QST Cover," February 1943 QST Cover - Online, 03/20/2023, 1943. [Online]. Available: https://www.rfcafe.com/references/qst/impedance-matching-transformer-february-1943-qst.htm

[3] studylib.net, "Quarter wave transformers and how they are used in a 3dB T," Online, 03/20/2023, 2013. [Online]. Available: https://studylib.net/doc/18060094/

[4] P. Regtien and E. Dertien, Sensors for Mechatronics. Elsevier - Amsterdam, Netherlands, 2018.

[5] S. I. Technologie, "M9," Online, 03/20/2023. [Online]. Available: http://www.shreeimagingtechnologie.in/products/m9.php

[6] B. A. Bramham, "A convenient transformer for matching coaxial lines," Electron Eng., vol. Vol. 33, pp. 42–44, 1961.

[7] M. S. Wheeler, "Two-section transmission-line transformer," Wireless Eng., vol. 32, pp. 15–18, 1955.

[8] G. Chen and M. Hamid, "Two-section impedance transformer with arbitrary length," Electron. Eng., vol. Vol. 63, pp. 911–920, 1987.

[9] R. P. Arnold and W. L. Bailey, "Match impedances with tapered lines," Electron. Design, vol. 22, pp. 136–139, June 1974.

[10] R. K. Barik and S. S. Karthikeyan, "Design of dual/tri-frequency impedance transformer with ultra-high transforming ratio," Int. J. Micr. and Wireless Tech., vol. 9, pp. 1951–1960, 2017.

[11] R. J. Sprungle and E. F. Kuester, "Reflection and bandwidth limits for exponentially tapered transmission lines," National Radio Science Meeting, Boulder, Colorado, paper B7-1, 6-9 January 2016.

[12] E. F. Kuester, "A lower bound for the length of nonuniform transmission line matching sections," Int J Electron Commun (AEÜ), vol. 66, pp. 1011–1016, 2012.

[13] D. A. Frickey, "Conversions between S, Z, Y, h, ABCD, and T parameters which are valid for complex source and load impedances," IEEE Transactions on Microwave Theory and Techniques, vol. 42, pp. 205–211, 1994.

[14] L. R. Walker and N. Wax, "Non-uniform transmission lines and reflection coefficients," Journal of Applied Physics, vol. 17, pp. 1043–1045, 1946.

[15] E. F. Kuester, Theory of Waveguides and Transmission Lines. Boca Raton, FL: CRC Press, 2021.

[16] L. A. Pipes, "Direct computation of transmission matrices of electrical transmission lines," Journal of The Franklin Institute, vol. 281 Number 4, pp. 387–405, 1966.

[17] D. Das and O. Rustogi, "Uniform transmission line equivalence of cascaded exponential lines," IEEE Transactions on Microwave Theory and Techniques, vol. MTT-16 num 8, pp. 511–516, 1968.

[18] M. Kutta, "Beitrag zur näherungsweisen integration totaler differentialgleichungen." Zeitschrift für Mathematik und Physik, vol. 46, pp. 435–453, 1901.

[19] L. Rayleigh, "On the propagation of waves through a stratified medium, with special reference to the question of reflection," Proc. Roy. Soc. London A, vol. 86, no. 586, pp. 207–226, Feb. 1912.

[20] F. Bolinder, "Fourier transforms in the theory of inhomogeneous transmission lines," Proc. IRE, vol. 38, no. 11, p. 1354, Nov. 1950.

[21] H. Bremmer, "The W.K.B. approximation as the first term of a geometric-optical series," Commun. Pure Appl. Math., vol. 4, no. 1, pp. 105–115, Jun. 1951.

[22] F. Bolinder, "Fourier transforms in the theory of inhomogeneous transmission lines," Trans. Roy. Inst. Technol. Stockholm, vol. 48, pp. 1–84, Jan. 1951.

[23] ——, "Fourier transforms and tapered transmission lines," Proc. IRE, vol. 44, no. 4, p. 557, Apr. 1956.

[24] R. Ghose, Microwave Circuit Theory and Analysis. New York: McGraw-Hill, 1963.

[25] R. W. Klopfenstein, "A transmission line taper of improved design," Proceedings of the IRE, vol. 44, pp. 31–35, 1956.

[26] R. P. Hecken, "A near-optimum matching section without discontinuities," IEEE Trans. Microw. Theory Techn., vol. MTT-20, no. 11, pp. 734–739, Nov. 1972.

[27] G. Peano, "Integrazione per serie delle equazioni differenziali lineari," Atti Accad. Sci. Torino Cl. Sci. Fis. Mat. Nat., vol. 22, pp. 437–446, 1887 [English transl. in H. C. Kennedy, Selected Works of Giuseppe Peano. Toronto: University of Toronto Press, 1973, pp. 58-66].

[28] ——, "Integrazione per serie delle equazioni differenziali lineari," Math. Ann., vol. 32, pp. 450–456, 1888, English transl. in A Source Book in Classical Analysis (G. Birkhoff, ed.). Cambridge, MA: Harvard University Press, 1973, pp. 311-317.

[29] P. Drude, The Theory of Optics. New York: Longmans, Green and Co., 1902.

[30] L. A. Weinstein (Vainshtein), The Theory of Diffraction and the Factorization Method. Boulder, CO: Golem Press, 1969.

[31] R. J. Sprungle and E. F. Kuester, "Design trade-offs in the use of exponentially tapered transmission line segments for impedance transformation," IEEE Transactions on Microwave Theory and Techniques, vol. 70, no. 8, pp. 3862–3869, 2022.

[32] H. A. Wheeler, "Transmission-line properties of a strip line between parallel planes," IEEE Transactions on Microwave Theory and Techniques, vol. 26, Issue: 11, pp. 866 – 876, 1978.

[33] L. Zhu and W. Menzel, "Broad-band microstrip-to-CPW transition via frequency-dependent electromagnetic coupling," IEEE Trans. Microw. Theory Techn., vol. 52, no. 5, pp. 1517–1522, May 2004.

[34] M. Bocher, "On systems of linear differential equations of the first order," Amer. J. Math., vol. 24, pp. 311–318, 1902.

[35] M. C. Pease III, Methods of Matrix Algebra. New York: Academic Press, 1965.

[36] P. H. Smith, "Transmission line calculator," Electronics, vol. 12 number 1, pp. 29–31, 1939.

[37] ——, "An improved transmission line calculator," Electronics, vol. 17 number 1, p. 130, 1944.

[38] R. M. Redheffer, "Reflection and transmission equivalence of dielectric media," Proceedings of the IRE, vol. 39, p. 503, 1951.

[39] R. Direen, "Fundamental limitations on the terminal behavior of antennas and nonuniform transmission lines," Ph.D. dissertation, University of Colorado at Boulder, 2010.

[40] C. Chao and W. Ku, "A general expression of the reflection coefficients of an exponential transmission line," Proceedings of the IEEE, vol. 56,Issue 12, pp. 2199–2200, 1968.

[41] N. Younan, "An exponentially tapered transmission line antenna," IEEE Transactions on Electromagnetic Compatibility, vol. 36 No: 2, pp. 141 – 144, 1994.

[42] C. P. Womack, "The use of exponential transmission lines in microwave components," IRE Transactions on Microwave Theory and Techniques, vol. 10, Issue: 2, pp. 124 – 132, 1962.

Appendix A

Reflections from Continuous Transmission line with Discontinuities

Riccati Equation: The exact form of the transmission line equation can be expressed as:

$$\rho'(x) = 2j\beta\rho(x) - N(x)(1 - \rho^2(x)) \tag{A.1}$$

In the case when $\rho(x)$ is small, $\rho^2(x)$ can be neglected. This is called the WentzelKramersBrillouin (WKB) approximation:

$$\rho'(x) = 2j\beta\rho(x) - N(x) \tag{A.2}$$

While equation (A.1) can only be solved using numerical methods, equation (A.2) can be solved as follows. Define.

$$\rho(x) = e^{2j\beta x} f(x) \tag{A.3}$$

Therefore.

$$\rho'(x) = 2j\beta rho(x) + e^{2j\beta x} f'(x) \tag{A.4}$$

Substituting equation (A.2) for $\rho(x)$.

$$2j\beta f(x)e^{2j\beta x} + e^{2j\beta x} f'(x) = 2j\beta f(x)e^{2j\beta x} - N(x) \tag{A.5}$$

$$e^{2j\beta x} f'(x) = -N(x) \tag{A.6}$$

$$f'(x) = -N(x)e^{-2j\beta x} \tag{A.7}$$

$$\int_{x}^{d} -N(x)e^{-2j\beta x}dx' \tag{A.8}$$

$$f(d) - f(x) = -\int_{x}^{d} -N(x')e^{-2j\beta x'}dx' \tag{A.9}$$

$$f(x) = f(d) + \int_{x}^{d} -N(x')e^{-2j\beta x'}dx' \tag{A.10}$$

$$f(x) = f(d) + \int_{x}^{d} -N(x')e^{-2j\beta x'}dx' \tag{A.11}$$

Recall $\rho(x) = e^{2j\beta x}f(x)$.

$$\rho(x) = f(d)e^{2j\beta x} + \int_{x}^{d} -N(x')e^{2j\beta(x-x')}dx' \tag{A.12}$$

$$\rho(x) = \rho(d)e^{2j\beta(x-d)} + \int_{x}^{d} -N(x')e^{2j\beta(x-x')}dx' \tag{A.13}$$

Considering the return at the input end of the transmission line, $x = 0$.

$$\rho(0^{+}) = \rho(d)e^{-2j\beta d} + \int_{0}^{d} -N(x')e^{2j\beta(x')}dx' \tag{A.14}$$

$\rho(d)e^{-2j\beta d}$ indicates the reflection caused by a stepped impedance discontinuity between the load and the adjoining portion of the taper.

$\int_0^d -N(x')e^{2j\beta(x')}dx'$ accounts for the sum of reflections accumulated along the continuous portion of the impedance taper.

This derivation shows that all ways of solving the WKB equation (A.2), account for the reflection at the load end of a transmission line and the continuous reflections accumulated along the transmission line. An additional discontinuity at the source end of the transmission line can be accounted for by normalizing the entire system to the Z_{00} value at the input of the transmission line. There is an infinite series (citation required) of additional reflections between between the source and load end of the transmission line.

Appendix B

Types of Reflection Coefficients

Impedance matching using any technique is described in terms of reflection coefficient, and is often displayed on the Smith Chart. The insight from the looking at reflections on the Smith Chart allows the designer to see how a match is obtained and the characteristics of the match such as the bandwidth. In this appendix, the definition of reflection coefficient and its representation on the Smith Chart will be investigated to show what insights can be achieved.

B.1 Introduction

Between any two connected RF components a mismatch in their impedance will create a reflection. The reflection coefficient describes the magnitude and phase characteristics of the wave reflected from a load due to a wave incident from the source. A reflection coefficient is commonly used to describe impedance matching circuits. Figure B.1 describes a basic RF system with a resistive load, R_L, a transmission line of characteristic impedance Z_0, and a reference impedance Z_{00} which does not necessarily relate to any actual section of transmission line in the network.

Plotting this reflection coefficient on the complex plane in the form of a Smith chart [36] [37] gives insight into the character of the mismatch of a system. The Smith chart is often used as a convenient tool for displaying reflections due to mismatch and designing systems that work to minimize these reflections. Here we will examine two possible definitions for the reflection coefficient and how they can be used to gain insight into the matching process.

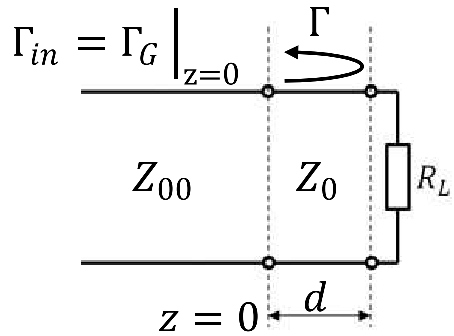

Figure B.1: The circuit model representation of an EM transmission line.

B.2 Global and Local Reflection Coefficients

B.2.1 Global

In Figure B.1, a basic model of a circuit with three impedances (Z_{00}, Z_0, and R_L) is shown. We define a global reflection coefficient Γ_G as the reflection along the transmission line as referenced to a hypothetical transmission line with a characteristic impedance of Z_{00} [38]:

$$\Gamma_G(z) = \frac{Z(z) - Z_{00}}{Z(z) + Z_{00}} \tag{B.1}$$

The reference impedance for this global reflection coefficient describing the reflection at the input of an RF system is often chosen to be the characteristic impedance of the input line, and in this case the resulting Γ_G is what is displayed when measurements are taken on a network analyzer. Such measurement devices often use $Z_{00} = 50\Omega$ for this reference impedance. At the load $Z(z = d) = Z_L$, which gives:

$$\Gamma_G(d) = \frac{R_L - Z_{00}}{R_L + Z_{00}} \tag{B.2}$$

At the input, $\Gamma_G(0) = \frac{Z(0)-Z_{00}}{Z(0)+Z_{00}}$; for a system that matches Z_L to Z_{00}, $\Gamma_G(0) = 0$.

Figure B.2 shows the global reflection coefficient Γ_G at a single frequency, plotted on a Smith chart for a 10:1 impedance mismatch, and also when a quarter-wave transformer is inserted to achieve a perfect match at the chosen frequency. This Smith chart is referenced to $Z_{00} = 1\Omega$.

When the reflection coefficient is measured on a network analyzer, it displays the global reflection coefficient with respect to $Z_{00} = 50\Omega$ (although this can be changed by the user if desired),

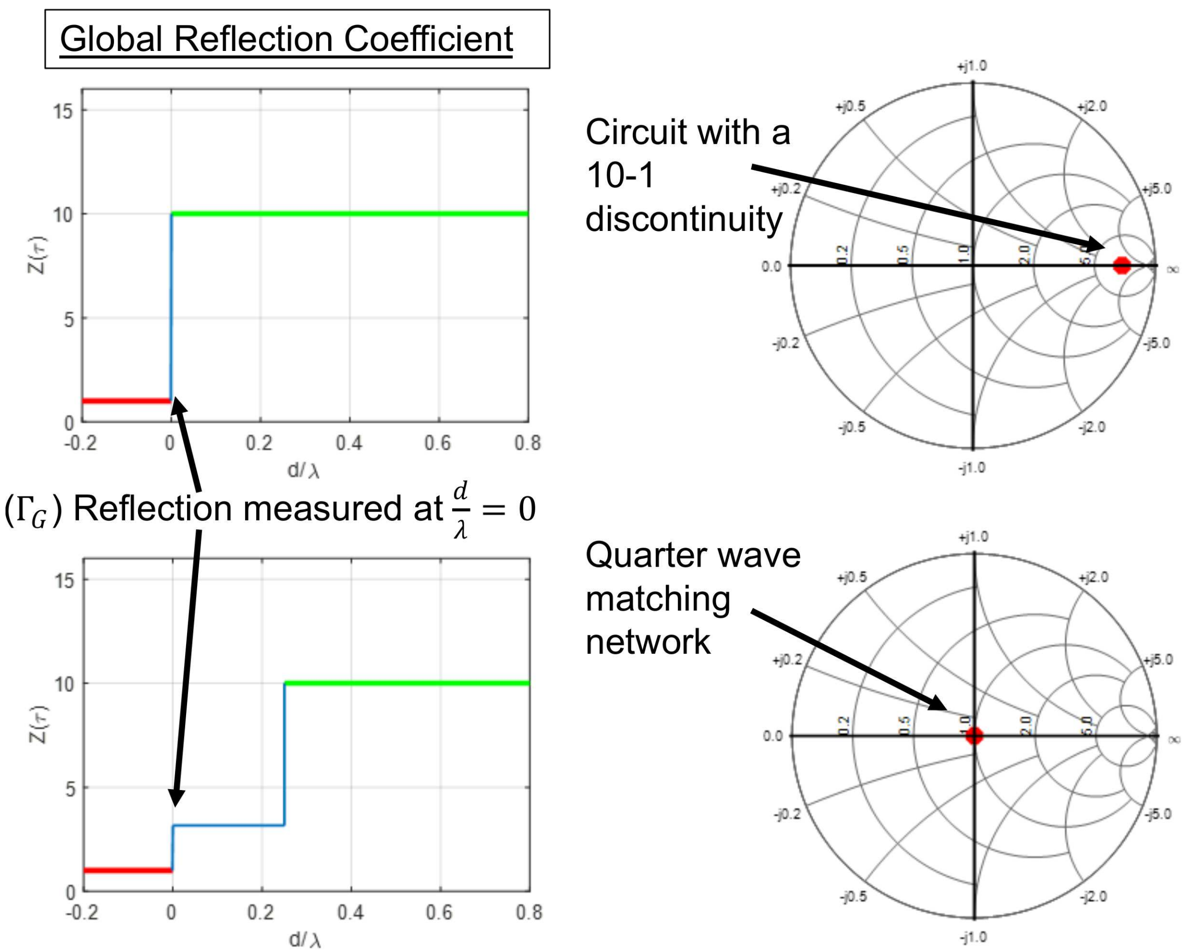

Figure B.2: Single point, single frequency global reflection coefficient, $\Gamma_G(0)$.

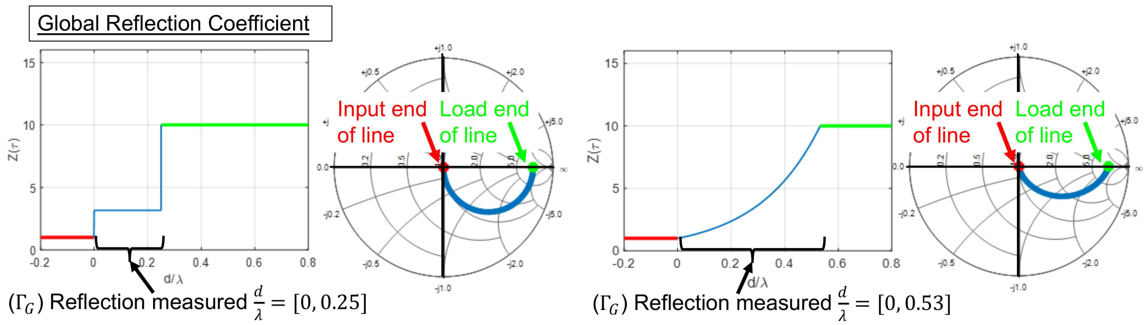

Figure B.3: Quarter-wave transformer and exponential line global reflection coefficient.

the trace following the variation of Γ_G with frequency at the fixed input position on the line. To gain insight into how matching circuits work, we study this spatial variation rather than frequency variation for two particular cases. Figure B.3 shows the variation of $\Gamma_G(z)$ along the transmission line from source to load, all referenced to the characteristic impedance Z_{00} of the input line. The global reflection coefficients for both a quarter-wave transformer and an exponentially tapered line are shown. Although both circuits differ greatly in length and in the method by which they match the load to the input impedance, the traces of their global reflection coefficients are rather similar.

B.2.1.1 Multiple Frequencies

Often when an antenna or RF circuit's reflection coefficient is measured on a network analyzer, a sweep of frequencies are collected. This allows the designer to see if a mismatch exists at a range around the design frequency. When network analyzers show reflection coefficient on a Smith Chart, the reference impedance is selected to match the ports of the analyzer (typically 50Ω). By using the constant external reference impedance, the network analyzer measurements are of global reflection coefficient. An example of a freqeuncy sweep is shown in Figure B.4.

B.2.2 Local

An alternative means to investigate how matching circuits operate, is to use a local reflection coefficient Γ. This quantity is defined by comparing the total impedance $Z(z)$ to the local characteristic impedance at the position z along the transmission line rather than to a fixed reference

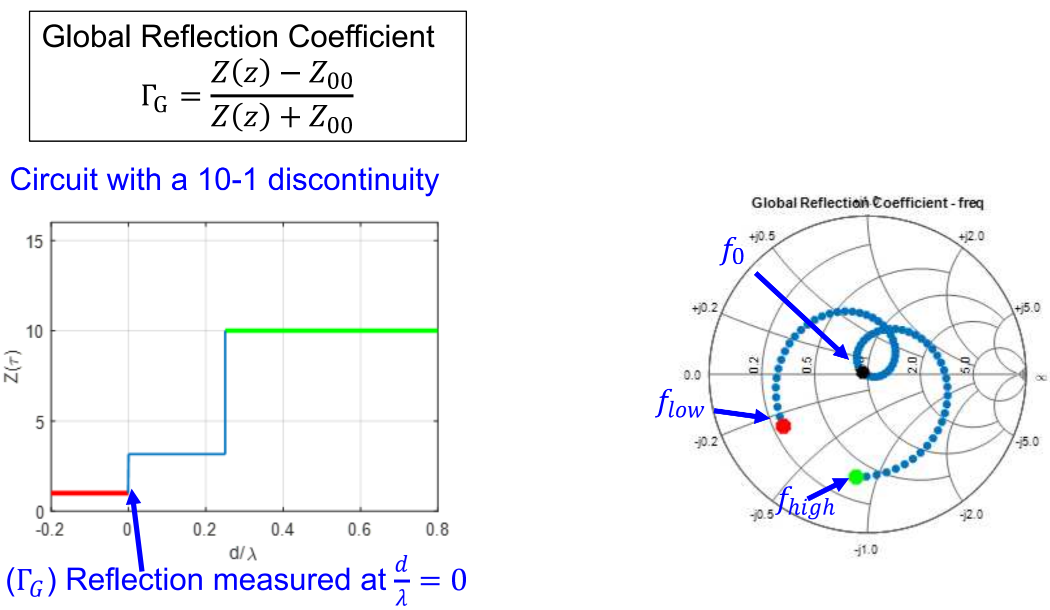

Figure B.4: Frequency Sweep of a Uniform line example.

impedance Z_{00} [14]:

$$\Gamma = \frac{Z(z) - Z_0(z)}{Z(z) + Z_0(z)} \tag{B.3}$$

By contrast with (B.1), Z and Z_0 are both functions of (z) in this case.

Since voltages and currents are continuous along a transmission line, $Z(z)$ will be continuous. This means that Γ_G will also be continuous, but Γ may not be since there can be step discontinuities in $Z_0(z)$. This behavior of Γ at discontinuities more dramatically points out the different ways by which the exponential line and the quarter-wave transformer achieve the impedance match than is done using plots of Γ_G.

The Riccati differential equations satisfied by $\Gamma_G(z)$ and $\Gamma(z)$ are also different [38], [14]. The Riccati equation for $\Gamma(z)$ contains a coefficient function $N(z) = Z_0'(z)/2Z_0(z)$, which is problematic from both the analytical and numerical points of view when Z_0 is discontinuous. The Riccati equation for Γ_G is easier to handle because it contains as coefficients only Z_0 but not Z_0'.

Figure B.5 shows the local reflection coefficients for the quarter-wave and exponential line matching circuits. In the case of the quarter-wave transformer, impedance discontinuities at the load and input ends show up as jumps in the Smith chart trace, while the quarter-wave section itself manifests as a semicircle about the center of the chart. Since there are no discontinuities at the load or source end for the exponential line, the ends of the path for Γ traced on the Smith chart are both located at 0. Some idea of the interpretation of the local reflection coefficient at interior points of the nonuniform line is conveyed by Figure B.6, which shows how $\Gamma(z)$ at a point in the middle of an exponential transmission line is what the reflection coefficient would be if the exponential taper were truncated at z and connected to a uniform transmission line at that point whose characteristic impedance had the constant value of $Z_0(z)$ at that position.

B.3 Use of Global and Local Reflection Coefficient

Since the local reflection coefficient Γ requires knowledge of the characteristic impedance along the length of the circuit being measured, it is less commonly used for measurements (the slotted

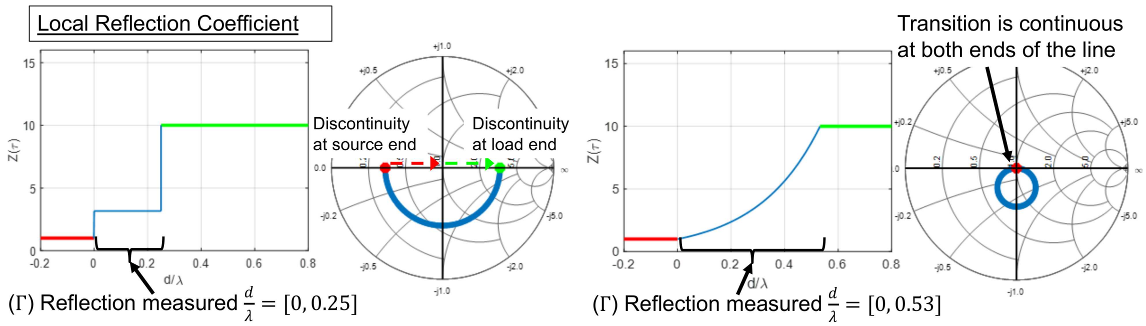

Figure B.5: Quarter-wave transformer and exponential line local reflection coefficient.

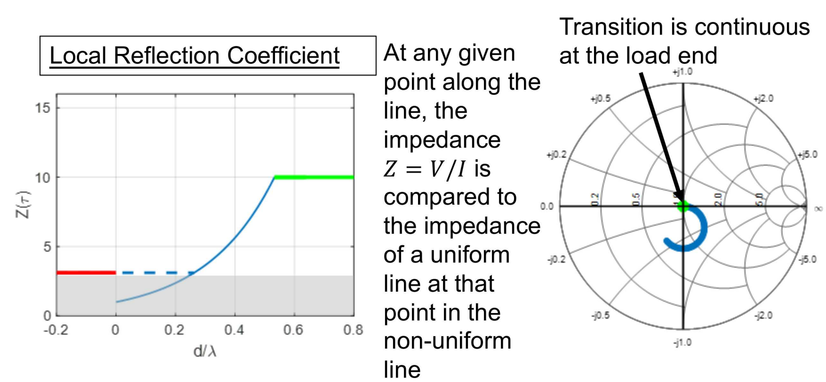

Figure B.6: Local reflection coefficient shown for a portion of an exponential line.

line, for example). The local reflection coefficient is, however, commonly used as a mathematical tool when computing reflections. Both Γ and Γ_G give insights into the matching and reflection properties of RF circuits. Figure B.3 showed relatively little difference for two different matching circuits by comparison with the results shown in Figure B.5. In this case, the local reflection coefficient gives greater insight into the operation of the two matching circuits. We have shown that both reflection coefficients provide insight into the understanding and design of nonuniform-line impedance matching circuits.

Appendix C

Reflections from Continuous Transmission line with Discontinuities

C.1 Introduction

In Chapter 6, bounds for the coefficients of the ABCD matrix were proposed using the Bôcher approach. The method required a $Z_{0\mathrm{ref}}$ to be chosen and it was found that the tightest bounds were found for all cases when $Z_{0\mathrm{min}} \leq Z_{0\mathrm{ref}} \leq Z_{0\mathrm{max}}$. For the general case, an optimum bound was not researched between Z_{0min} and Z_{0max}. This raises the question whether there is an optimum choice for Z_{0ref} for all nonuniform lines, or in any specific cases.

In this Appendix a small study comparing the effect of using different $Z_{0\mathrm{ref}}$ values for all cases of the exponential line (6.1) was carried out. The solution was done for two distinct cases as shown in Figure C.1 which both obey exponential lines of the form $Z_0(\tau) = Ke^{2N\tau}$. This is not an exhaustive study; only the first term $A_n = A_1$ was considered for short and long exponential lines to see if there are any differences at all in what Z_{0ref} is chosen within $Z_{0min} \leq Z_{0ref} \leq Z_{max}$.

The solutions for long and short exponential tapers each with three choices for the Z_{0ref} are shown in Table C.1. Following the table is the derivation of each of the formulas for A_1 limits. The take-away from this study is that there are some advantages to choosing one Z_{0ref} over another. It is likely that this will be the way that tighter bounds can be realized for longer circuits. Recall from Table 5.1, that longer broadband exponential tapers had the same length limits as the short narrowband tapers when only Z_{0min} and Z_{0min} were considered. In what follows, the intermediate value $Z_{middle} = \sqrt{Z_{0\mathrm{max}} Z_{0\mathrm{min}}} = Z_0(\frac{T}{2}) = Ke^{NT}$ was used. For all exponential lines that match two real impedances the Z_{middle} value will be found at the midpoint in electrical distance. The

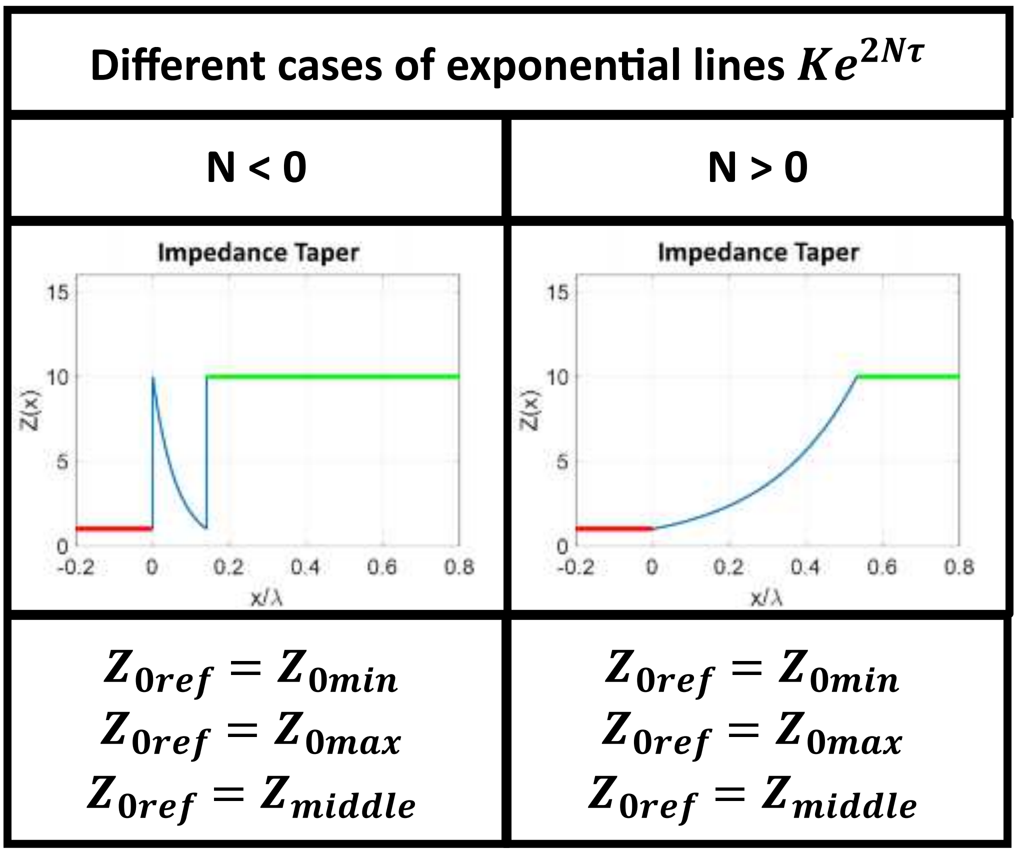

Figure C.1: Examples of the three cases of exponential impedance transformers defined by negative, zero, or positive slope of the curve.

Exponential Type	$Z_{0\mathrm{ref}}$ Choice	A_1 Bounds	Equation ref.
$N<0$	$Z_{0ref}=Z_{max}$ $Z_{0ref}=Z_{min}$	$\frac{1}{2}\left[\frac{e^{2NT}-1}{2N}\right]^2 \leq A_1 \leq \frac{1}{2}\left[-\frac{1-e^{-2NT}}{2N}\right]^2$	(C.8), (C.11) (C.16), (C.20)
	$Z_{0ref}=Z_{middle}$	$\frac{1}{2}\left(\frac{e^{NT}}{N}-\frac{1}{N}\right)^2 \leq A_1 \leq \frac{1}{2}\left(\frac{1}{N}-\frac{e^{-NT}}{N}\right)^2$	(C.48), (C.48)
$N>0$	$Z_{0ref}=Z_{max}$ $Z_{0ref}=Z_{min}$	$\frac{1}{2}\left[\frac{1-e^{-2NT}}{2N}\right]^2 \leq A_1 \leq \frac{1}{2}\left[\frac{e^{2NT}-1}{2N}\right]^2$	(C.26), (C.25) (C.35), (C.34)
	$Z_{0ref}=Z_{middle}$	$\frac{1}{2}\left(\frac{1}{N}-\frac{e^{-NT}}{N}\right)^2 \leq A_1 \leq \frac{1}{2}\left(\frac{e^{NT}}{N}-\frac{1}{N}\right)^2$	(C.61), (C.57)

Table C.1: Solutions for A_1 for exponential lines with different Z_0ref selections.

derivations are carried out without much comment.

C.2 $N<0$ case: $Z_{0max}=Z_{0\mathrm{ref}}$

$$Z_0 = Ke^{2N\tau} \tag{C.1}$$

$$Z_{0min} = Ke^{2NT} \tag{C.2}$$

$$Z_{0max} = K \tag{C.3}$$

$$\phi_{max} = \frac{Z_{0ref}}{Z_0(t)} = \frac{K}{Ke^{2N\tau}} = \frac{1}{e^{2N\tau}} \tag{C.4}$$

$$\phi_{min} = \frac{Z_0(t)}{Z_{0ref}} = \frac{Ke^{2N\tau}}{K} = e^{2N\tau} \tag{C.5}$$

$$A_n \leq \frac{1}{(2n)!}\left[\int_0^T \phi_{max}(\tau)d\tau\right]^{2n} = \frac{1}{(2n)!}\left[\int_0^T e^{-2N\tau}d\tau\right]^{2n} \tag{C.6}$$

$$A_1 \leq \frac{1}{2}\left[-\frac{e^{-2N\tau}}{2N}\Big|_0^T\right]^2 = \frac{1}{2}\left[-\frac{e^{-2NT}}{2N}+\frac{1}{2N}\right]^2 \tag{C.7}$$

Thus: A_{1max} (N < 0 case: $Z_{0max} = Z_{0ref}$) is

$$\boldsymbol{A_1 \leq \frac{1}{2}\left[\frac{1-e^{-2NT}}{2N}\right]^2} \tag{C.8}$$

Now solve for the lower bound.

$$A_n \geq \frac{1}{(2n)!}\left[\int_0^T \phi_{min}(\tau)d\tau\right]^{2n} = \frac{1}{(2n)!}\left[\int_0^T e^{2N\tau}d\tau\right]^{2n} \tag{C.9}$$

$$A_1 \geq \frac{1}{2}\left[\int_0^T e^{2N\tau}d\tau\right]^2 = \frac{1}{2}\left[\frac{e^{2NT}}{2N}\bigg|_0^T\right]^2 \tag{C.10}$$

Thus: A_{1min} (N < 0 case: $Z_{0max} = Z_{0ref}$) is

$$\boldsymbol{A_1 \geq \frac{1}{2}\left[\frac{e^{2NT}-1}{2N}\right]^2} \tag{C.11}$$

C.3 $N < 0$ case: $Z_{0min} = Z_{0ref}$

Equations (C.2) and (C.3) still apply

In this case, we have

$$\phi_{min} = \frac{Z_{0ref}}{Z_0(t)} = \frac{Ke^{2NT}}{Ke^{2N\tau}} = \frac{e^{2NT}}{e^{2N\tau}} \tag{C.12}$$

$$\phi_{max} = \frac{Z_0(t)}{Z_{0ref}} = \frac{Ke^{2N\tau}}{Ke^{2NT}} = \frac{e^{2N\tau}}{e^{2NT}} \tag{C.13}$$

$$A_n \leq \frac{1}{(2n)!}\left[\int_0^T \phi_{max}(\tau)d\tau\right]^{2n} = \frac{1}{(2n)!}\left[\int_0^T \frac{e^{2N\tau}}{e^{2NT}}d\tau\right]^{2n} \tag{C.14}$$

$$A_1 \leq \frac{1}{2}\left[\int_0^T \frac{e^{2N\tau}}{e^{2NT}}d\tau\right]^2 = \frac{1}{2e^{4NT}}\left[\frac{e^{2N\tau}}{2N}\bigg|_0^T\right]^2 = \frac{1}{2e^{4NT}}\left[\frac{e^{2NT}}{2N} - \frac{1}{2N}\right]^2 \tag{C.15}$$

Thus A_{1max} (N < 0 case: $Z_{0min} = Z_{0ref}$) is:

$$\boldsymbol{A_1 \leq \frac{1}{2e^{4NT}}\left[\frac{e^{2NT}-1}{2N}\right]^2 = \frac{1}{2}\left[\frac{1-e^{-2NT}}{2N}\right]^2} \tag{C.16}$$

This is identical to (C.8)

Now solve for the lower bound.

$$A_n \geq \frac{1}{(2n)!}\left[\int_0^T \phi_{min}(\tau)d\tau\right]^{2n} = \frac{1}{(2n)!}\left[\int_0^T \frac{e^{2NT}}{e^{2N\tau}}d\tau\right]^{2n} \tag{C.17}$$

$$A_n \geq \tag{C.18}$$

$$A_1 \geq \frac{1}{2}\left[\int_0^T \frac{e^{2NT}}{e^{2N\tau}}d\tau\right]^2 = \frac{e^{4NT}}{2}\left[-\frac{e^{-2NT}}{2N} + \frac{1}{2N}\right]^2 \tag{C.19}$$

Thus A_{1min} (N $<$ 0 case: $Z_{0min} = Z_{0ref}$) is:

$$\boldsymbol{A_1 \geq \frac{1}{2}\left[\frac{1 - e^{-2NT}}{2N}\right]^2} \tag{C.20}$$

This is identical to (C.11)

C.4 $N > 0$ **case:** $Z_{0min} = Z_{0ref}$

This section uses much of the math from the previous section applied to the corresponding conditions.

$$Z_{0min} = K \tag{C.21}$$

$$Z_{0max} = Ke^{2NT} \tag{C.22}$$

Since $Z_0(t) > Z_{0ref}$,

$$\phi_{min} = \frac{Z_{0ref}}{Z_0(t)} \tag{C.23}$$

$$\phi_{max} = \frac{Z_0(t)}{Z_{0ref}} \tag{C.24}$$

$$\boldsymbol{A_1 \leq \frac{1}{2}\left[\frac{e^{2NT} - 1}{2N}\right]^2} \tag{C.25}$$

$$\boldsymbol{A_1 \geq \frac{1}{2}\left[\frac{1-e^{-2NT}}{2N}\right]^2} \tag{C.26}$$

C.5 $N > 0$ case: $Z_{0max} = Z_{0ref}$

This section uses much of the math from the previous section applied to the corresponding conditions.

$$Z_{0min} = K \tag{C.27}$$

$$Z_{0max} = Ke^{2NT} \tag{C.28}$$

Then

$$\phi_{min} = \frac{Z_0(t)}{Z_{0ref}} \tag{C.29}$$

$$\phi_{max} = \frac{Z_{0ref}}{Z_0(t)} \tag{C.30}$$

$$\phi_{max} = \frac{Z_{0ref}}{Z_0(t)} = \frac{Ke^{2NT}}{Ke^{2N\tau}} = \frac{e^{2NT}}{e^{2N\tau}} \tag{C.31}$$

$$\phi_{min} = \frac{Z_0(t)}{Z_{0ref}} = \frac{Ke^{2N\tau}}{Ke^{2NT}} = \frac{e^{2N\tau}}{e^{2NT}} \tag{C.32}$$

$$A_n \leq \frac{1}{(2n)!}\left[\int_0^T \phi_{max}(\tau)d\tau\right]^{2n} = \frac{1}{(2n)!}\left[\int_0^T \frac{e^{2NT}}{e^{2N\tau}}(\tau)d\tau\right]^{2n} \tag{C.33}$$

Thus for $N > 0$ case: $Z_{0max} = Z_{0ref}$,

$$\boldsymbol{A_1 \leq \frac{1}{2}\left[\frac{1-e^{2NT}}{2N}\right]^2} \tag{C.34}$$

and

$$\boldsymbol{A_1 \geq \frac{1}{2}\left[\frac{1-e^{-2NT}}{2N}\right]^2} \tag{C.35}$$

These are the same as (C.25) and (C.26) respectively.

C.6 $N < 0$ case: $Z_{0middle} = Z_{0ref}$

$$Z_{0min} = Ke^{2NT} \tag{C.36}$$

$$Z_{0max} = K \tag{C.37}$$

$$Z_{0middle} = \sqrt{K * Ke^{2NT}} = Ke^{NT} \tag{C.38}$$

$$\phi_{max} = \begin{cases} \frac{Z_0(\tau)}{Z_{0ref}}, \text{if } \tau < \frac{T}{2} \\ \\ \frac{Z_{0ref}}{Z_0(\tau)}, \text{if } \tau > \frac{T}{2} \end{cases} = \begin{cases} \frac{Ke^{2N\tau}}{Ke^{NT}} = \frac{e^{2N\tau}}{e^{NT}}, \text{if } \tau < \frac{T}{2} \\ \\ \frac{Ke^{NT}}{Ke^{2N\tau}} = \frac{e^{NT}}{e^{2N\tau}}, \text{if } \tau > \frac{T}{2} \end{cases} \tag{C.39}$$

$$\phi_{min} = \begin{cases} \frac{Z_(0ref)}{Z_0(\tau)}, \text{if } \tau < \frac{T}{2} \\ \\ \frac{Z_0(\tau)}{Z_(0ref)}, \text{if } \tau > \frac{T}{2} \end{cases} = \begin{cases} \frac{Ke^{NT}}{Ke^{2N\tau}} = \frac{e^{NT}}{e^{2N\tau}}, \text{if } \tau < \frac{T}{2} \\ \\ \frac{Ke^{2N\tau}}{Ke^{NT}} = \frac{e^{2N\tau}}{e^{NT}}, \text{if } \tau > \frac{T}{2} \end{cases} \tag{C.40}$$

$$A_n \le \frac{1}{(2n)!} \left[\int_0^T \phi_{max}(\tau) d\tau \right]^{2n} = \frac{1}{(2n)!} \left[\int_0^{\frac{T}{2}} \frac{e^{2N\tau}}{e^{NT}} d\tau + \int_{\frac{T}{2}}^T \frac{e^{NT}}{e^{2N\tau}} d\tau \right]^{2n} \tag{C.41}$$

$$A_1 \le \frac{1}{2} \left[e^{-NT} \int_0^{\frac{T}{2}} e^{2N\tau} d\tau + e^{NT} \int_{\frac{T}{2}}^T e^{-2N\tau} d\tau \right]^2 = \frac{1}{2} \left[e^{-NT} \left(\frac{e^{2N\tau}}{2N} \right) \Bigg|_0^{\frac{T}{2}} + e^{NT} \left(\frac{e^{-2N\tau}}{-2N} \right) \Bigg|_{\frac{T}{2}}^T \right]^2 \tag{C.42}$$

$$A_1 \le \frac{1}{2} \left[\left(\frac{1}{2N} - \frac{e^{-NT}}{2N} \right) - \left(\frac{e^{-NT}}{2N} - \frac{1}{2N} \right) \right]^2 = \frac{1}{2} \left(\frac{1}{2N} - \frac{e^{-NT}}{2N} - \frac{e^{-NT}}{2N} + \frac{1}{2N} \right)^2 \tag{C.43}$$

$$\boldsymbol{A_1 \le \frac{1}{2} \left(\frac{1}{N} - \frac{e^{-NT}}{N} \right)^2} \tag{C.44}$$

Likewise,

$$A_n \geq \frac{1}{(2n)!}\left[\int_0^T \phi_{min}(\tau)d\tau\right]^{2n} = \frac{1}{(2n)!}\left[\int_0^{\frac{T}{2}} \frac{e^{NT}}{e^{2N\tau}}d\tau + \int_{\frac{T}{2}}^{T} \frac{e^{2N\tau}}{e^{NT}}d\tau\right]^{2n} \tag{C.45}$$

$$A_1 \geq \frac{1}{2}\left[e^{NT}\int_0^{\frac{T}{2}} e^{-2N\tau}d\tau + e^{-NT}\int_{\frac{T}{2}}^{T} e^{2N\tau}d\tau\right]^2 = \frac{1}{2}\left[e^{NT}\left(\frac{e^{-2N\tau}}{-2N}\right)\Bigg|_0^{\frac{T}{2}} + e^{-NT}\left(\frac{e^{2N\tau}}{2N}\right)\Bigg|_{\frac{T}{2}}^{T}\right]^2 \tag{C.46}$$

$$A_1 \geq \frac{1}{2}\left[\left(\frac{1}{-2N} - \frac{e^{NT}}{-2N}\right) + \left(\frac{e^{NT}}{2N} - \frac{1}{2N}\right)\right]^2 = \frac{1}{2}\left(\frac{-1}{2N} + \frac{e^{NT}}{2N} + \frac{e^{NT}}{2N} - \frac{1}{2N}\right)^2 \tag{C.47}$$

$$\boldsymbol{A_1 \geq \frac{1}{2}\left(\frac{e^{NT}}{N} - \frac{1}{N}\right)^2} \tag{C.48}$$

A little algebra (or numerical testing) will show that (C.44) is always tighter than (C.8), and (C.48) is always tighter than (C.11)

C.7 $N > 0$ case: $Z_{0middle} = Z_{0ref}$

$$Z_{0min} = K \tag{C.49}$$

$$Z_{0max} = Ke^{2NT} \tag{C.50}$$

$$Z_{0middle} = Ke^{NT} \tag{C.51}$$

$$\phi_{max} = \begin{cases} \frac{Z_(0ref)}{Z_0(\tau)}, \text{if } \tau < \frac{T}{2} \\ \frac{Z_0(\tau)}{Z_(0ref)}, \text{if } \tau > \frac{T}{2} \end{cases} = \begin{cases} \frac{Ke^{NT}}{Ke^{2N\tau}} = \frac{e^{NT}}{e^{2N\tau}}, \text{if } \tau < \frac{T}{2} \\ \frac{Ke^{2N\tau}}{Ke^{NT}} = \frac{e^{2N\tau}}{e^{NT})}, \text{if } \tau > \frac{T}{2} \end{cases} \tag{C.52}$$

$$\phi_{min} = \begin{cases} \frac{Z_0(\tau)}{Z_(0ref)}, \text{if } \tau < \frac{T}{2} \\ \frac{Z_(0ref)}{Z_0(\tau)}, \text{if } \tau > \frac{T}{2} \end{cases} = \begin{cases} \frac{Ke^{2N\tau}}{Ke^{NT}} = \frac{e^{2N\tau}}{e^{NT})}, \text{if } \tau < \frac{T}{2} \\ \frac{Ke^{NT}}{Ke^{2N\tau}} = \frac{e^{NT}}{e^{2N\tau}}, \text{if } \tau > \frac{T}{2} \end{cases} \tag{C.53}$$

$$A_n \leq \frac{1}{(2n)!} \left[\int_0^T \phi_{max}(\tau) d\tau \right]^{2n} = \frac{1}{(2n)!} \left[\int_0^{\frac{T}{2}} \frac{e^{NT}}{e^{2N\tau}} d\tau + \int_{\frac{T}{2}}^T \frac{e^{2N\tau}}{e^{NT}} d\tau \right]^{2n} \tag{C.54}$$

$$A_1 \leq \frac{1}{2} \left[e^{NT} \int_0^{\frac{T}{2}} e^{-2N\tau} d\tau + e^{-NT} \int_{\frac{T}{2}}^T e^{2N\tau} d\tau \right]^2 = \frac{1}{2} \left[e^{NT} \left(\frac{e^{-2N\tau}}{-2N} \right) \Big|_0^{\frac{T}{2}} + e^{-NT} \left(\frac{e^{2N\tau}}{2N} \right) \Big|_{\frac{T}{2}}^T \right]^2 \tag{C.55}$$

$$A_1 \leq \frac{1}{2} \left[\left(\frac{1}{-2N} - \frac{e^{NT}}{-2N} \right) + \left(\frac{e^{NT}}{2N} - \frac{1}{2N} \right) \right]^2 = \frac{1}{2} \left(\frac{-1}{2N} + \frac{e^{NT}}{2N} + \frac{e^{NT}}{2N} - \frac{1}{2N} \right)^2 \tag{C.56}$$

$$\boldsymbol{A_1 \leq \frac{1}{2} \left(\frac{e^{NT}}{N} - \frac{1}{N} \right)^2} \tag{C.57}$$

Likewise,

$$A_n \geq \frac{1}{(2n)!} \left[\int_0^T \phi_{min}(\tau) d\tau \right]^{2n} = \frac{1}{(2n)!} \left[\int_0^{\frac{T}{2}} \frac{e^{2N\tau}}{e^{NT}} d\tau + \int_{\frac{T}{2}}^T \frac{e^{NT}}{e^{2N\tau}} d\tau \right]^{2n} \tag{C.58}$$

$$A_1 \geq \frac{1}{2} \left[e^{-NT} \int_0^{\frac{T}{2}} e^{2N\tau} d\tau + e^{NT} \int_{\frac{T}{2}}^T e^{-2N\tau} d\tau \right]^2 = \frac{1}{2} \left[e^{-NT} \left(\frac{e^{2N\tau}}{2N} \right) \Big|_0^{\frac{T}{2}} + e^{NT} \left(\frac{e^{-2N\tau}}{-2N} \right) \Big|_{\frac{T}{2}}^T \right]^2 \tag{C.59}$$

$$A_1 \geq \frac{1}{2} \left[\left(\frac{1}{2N} - \frac{e^{-NT}}{2N} \right) - \left(\frac{e^{-NT}}{2N} - \frac{1}{2N} \right) \right]^2 = \frac{1}{2} \left(\frac{1}{2N} - \frac{e^{-NT}}{2N} - \frac{e^{-NT}}{2N} + \frac{1}{2N} \right)^2 \tag{C.60}$$

$$\boldsymbol{A_1 \geq \frac{1}{2} \left(\frac{1}{N} - \frac{e^{-NT}}{N} \right)^2} \tag{C.61}$$

C.8 Conclusion

The bounds shown in (C.44) and (C.57) are different than (C.8) and those shown in (C.48) and (C.61) are different than (C.11). This difference indicates there can be an optimal choice. It has not been proven in this Appendix what the selection of Z_{0ref} will give the tightest bounds, but it has been shown that improved bounds can be found by properly selecting Z_{0ref}.